

# Chapter 1

## 7 TeV and 8 TeV Differential Cross Section Measurement: Fitting, Unfolding and Measurement

### 1.1 Data-MC Comparison

Following the full event selection, the simulated events are scaled to match the luminosity of the data using the following scale factor:

$$S = \frac{\mathcal{L} \times \sigma}{N_{\text{processed}}} \quad (1.1)$$

where  $N_{\text{processed}}$  is the total number of events processed for each Monte Carlo sample and  $\sigma$  is the production cross section of each process. The numbers of events passing each selection step in data and in Monte Carlo simulation are shown in Tables 1.1 and 1.2 for the electron and muon channels respectively at  $\sqrt{s} = 7 \text{ TeV}$ , and in Tables 1.3 and 1.4 for the electron and muon channels respectively at  $\sqrt{s} = 8 \text{ TeV}$ .

The distributions of the primary variables  $E_{\text{T}}^{\text{miss}}$ ,  $H_{\text{T}}$ ,  $S_{\text{T}}$ ,  $p_{\text{T}}^{\text{W}}$  and  $M_{\text{T}}^{\text{W}}$  after the full selection requirements are applied are shown in Figures 1.1 and 1.2 for the electron and muon channels respectively at  $\sqrt{s} = 7 \text{ TeV}$ ; and in Figures 1.3 and 1.4 respectively at  $\sqrt{s} = 8 \text{ TeV}$ . The normalisations and shapes are all obtained from simulation except in the case of QCD which is taken from data: the conversion region is used in the electron channel and the non-isolated region is used in the muon channel. In general, the agreement between data and simulation is good, with the distributions simulation peaking at slightly higher energies because event reweighting to account for the  $p_{\text{T}}$  mismodelling of the top quark in simulation has not yet

Table 1.1: Expected and observed event yields at several stages of the electron-plus-jets selection. The figures in italics are data-driven estimates of QCD background.

Selection step	$t\bar{t}$	W + Jets	Z + Jets	Single-top	QCD	Sum MC	Data
	Multijet						
Skim							
Cleaning and HLT							
one isolated $e$							
loose $e$ veto							
loose $\mu$ veto							
conversion veto							
$\geq 1$ jets							
$\geq 2$ jets							
$\geq 3$ jets							
$\geq 4$ jets							
$\geq 1$ CSV b-tag							
$\geq 2$ CSV b-tag							

Table 1.2: Expected and observed event yields at several stages of the electron-plus-jets selection. The figures in italics are data-driven estimates of QCD background.

Selection step	$t\bar{t}$	W + Jets	Z + Jets	Single-top	QCD	Sum MC	Data
	Multijet						
Skim							
Cleaning and HLT							
one isolated $\mu$							
loose $\mu$ veto							
loose $e$ veto							
$\geq 1$ jets							
$\geq 2$ jets							
$\geq 3$ jets							
$\geq 4$ jets							
$\geq 1$ CSV b-tag							
$\geq 2$ CSV b-tag							

Table 1.3: Expected and observed event yields at several stages of the electron-plus-jets selection. The figures in italics are data-driven estimates of QCD background.

Selection step	$t\bar{t}$	W + Jets	Z + Jets	Single-top	QCD	Sum MC	Data
	Multijet						
Skim							
Cleaning and HLT							
one isolated $e$							
loose $e$ veto							
loose $\mu$ veto							
conversion veto							
$\geq 1$ jets							
$\geq 2$ jets							
$\geq 3$ jets							
$\geq 4$ jets							
$\geq 1$ CSV b-tag							
$\geq 2$ CSV b-tag							

Table 1.4: Expected and observed event yields at several stages of the electron-plus-jets selection. The figures in italics are data-driven estimates of QCD background.

Selection step	$t\bar{t}$	W + Jets	Z + Jets	Single-top	QCD	Sum MC	Data
	Multijet						
Skim							
Cleaning and HLT							
one isolated							
loose $\mu$ veto							
loose $e$ veto							
$\geq 1$ jets							
$\geq 2$ jets							
$\geq 3$ jets							
$\geq 4$ jets							
$\geq 1$ CSV b-tag							
$\geq 2$ CSV b-tag							

been carried out at this stage.

A comparison between data and simulation in the electron+jets QCD selections is shown in Figure 1.5. There is reasonably good agreement between the data and simulation in the conversion selection but low statistics in the  $\sqrt{s} = 8$  TeV simulation lead to some events with large weights, leading to peaks in the distribution. It can also be seen that there are more conversion events in the regions of the endcaps, where the larger amount of detector material for electrons to traverse leads to a higher number of conversions. The non-isolated QCD selection shows more discrepancies between the simulation and data, but it should be noted that at  $\sqrt{s} = 7$  TeV the simulation does not contain the triggers used in this analysis, unlike at  $\sqrt{s} = 8$  TeV, therefore the simulation distribution at  $\sqrt{s} = 7$  TeV is not affected by the trigger isolation requirements.

The true QCD background distribution is a mixture of the conversion and non-isolated distributions. A comparison of the two QCD background selections at  $\sqrt{s} = 7$  TeV and  $\sqrt{s} = 8$  TeV is also shown in the lower plots in Figure 1.5. Background events in which electrons come from jets misreconstructed as electrons or from b-quark or c-quark decays will pass the non-isolated selection, whereas conversion events in which the second electron is not rejected by the electron veto will pass the conversion selection. Another point to note is that, while the general shape of the conversion selection is expected to be the same in both signal and QCD background selections, the same may not be true of the non-isolated selection due to the isolation requirement in the signal selection. In addition, the number of events passing the QCD background selections will be very small compared to the number of events passing the signal selection, so the effect of even large uncertainties in the QCD background on the total number of events will be minimal.

In the muon+jets channel, again it is clear that the data and simulation are not in agreement and that there is a low amount of statistics available in simulation.

## 1.2 Binning Choice

The bin boundaries in the primary variable distributions is important because events generated in one bin can migrate to another bin after reconstruction due to the finite resolution of the detector. This altering of the number of events, either as a result of events moving into, or out of, a bin is important to understand so that the final reconstructed distribution can be deconvoluted (unfolded) to the true distribution.

In light of this, the binning choice is made based on two variables defined as purity ( $p^k$ ) and stability ( $s^k$ ):

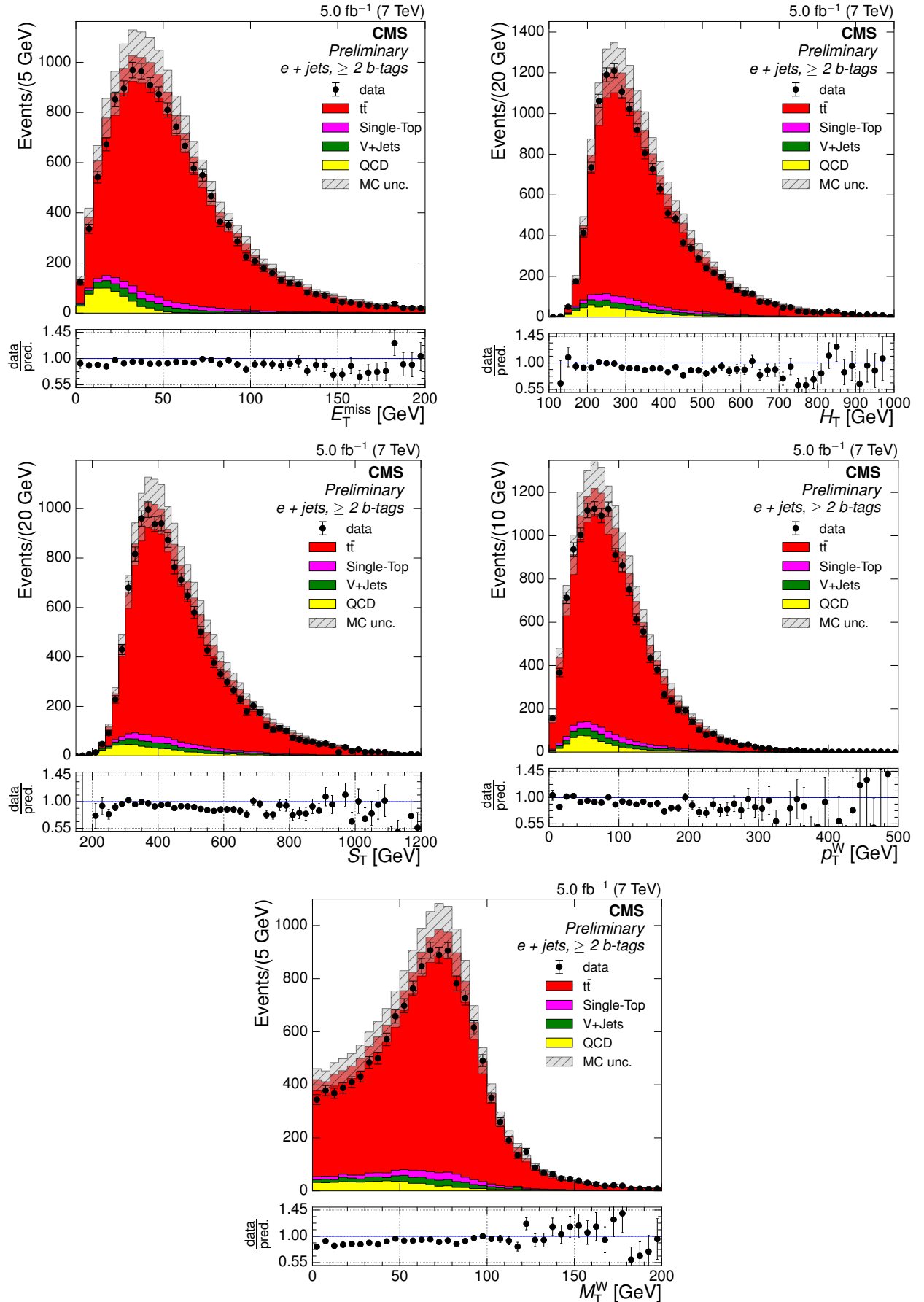


Figure 1.1: Comparison of Monte Carlo simulation to data in the electron+jets channel after final selection at  $\sqrt{s} = 7 \text{ TeV}$ .

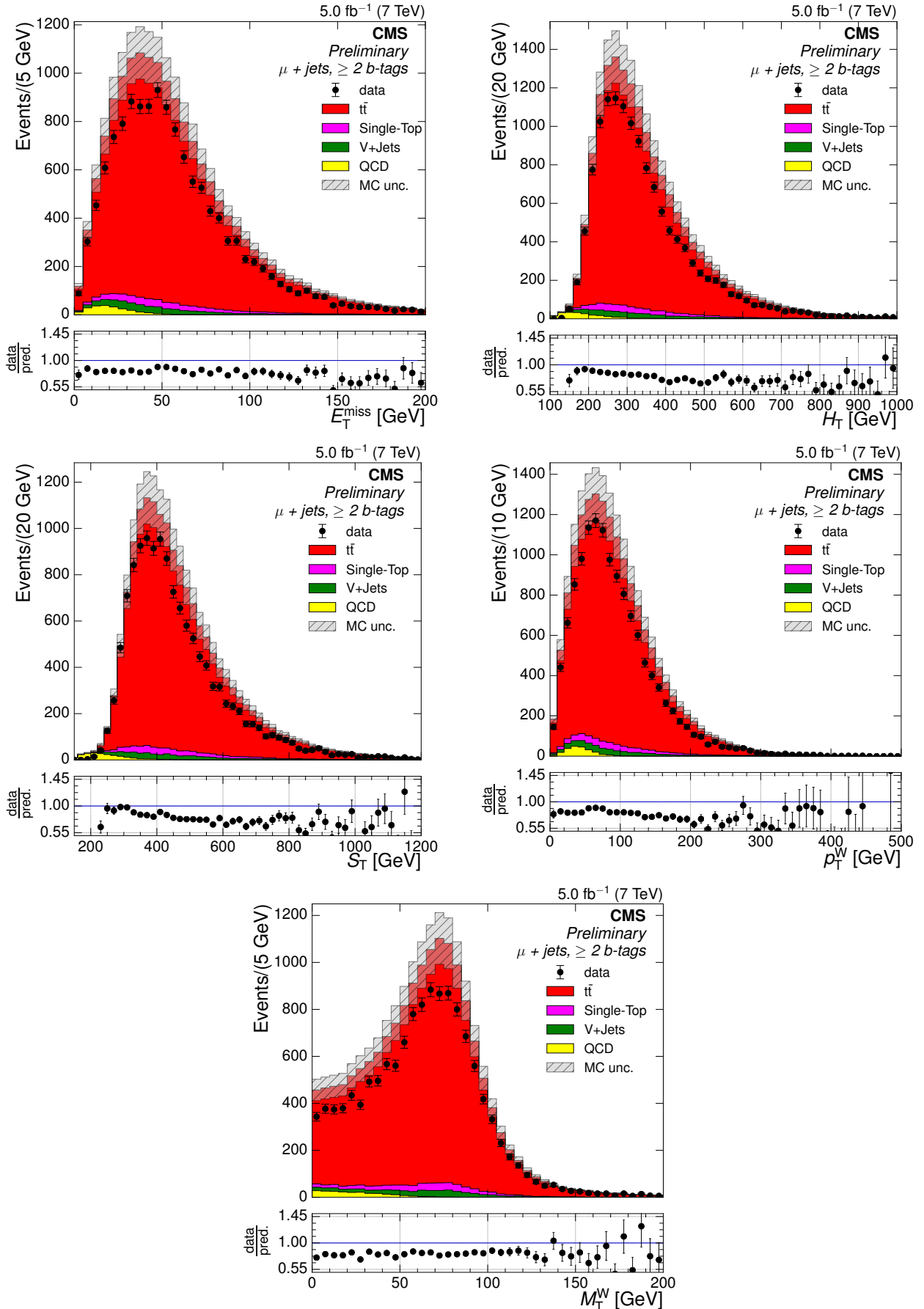


Figure 1.2: Comparison of Monte Carlo simulation to data in the muon+jets channel after final selection at  $\sqrt{s} = 7 \text{ TeV}$ .

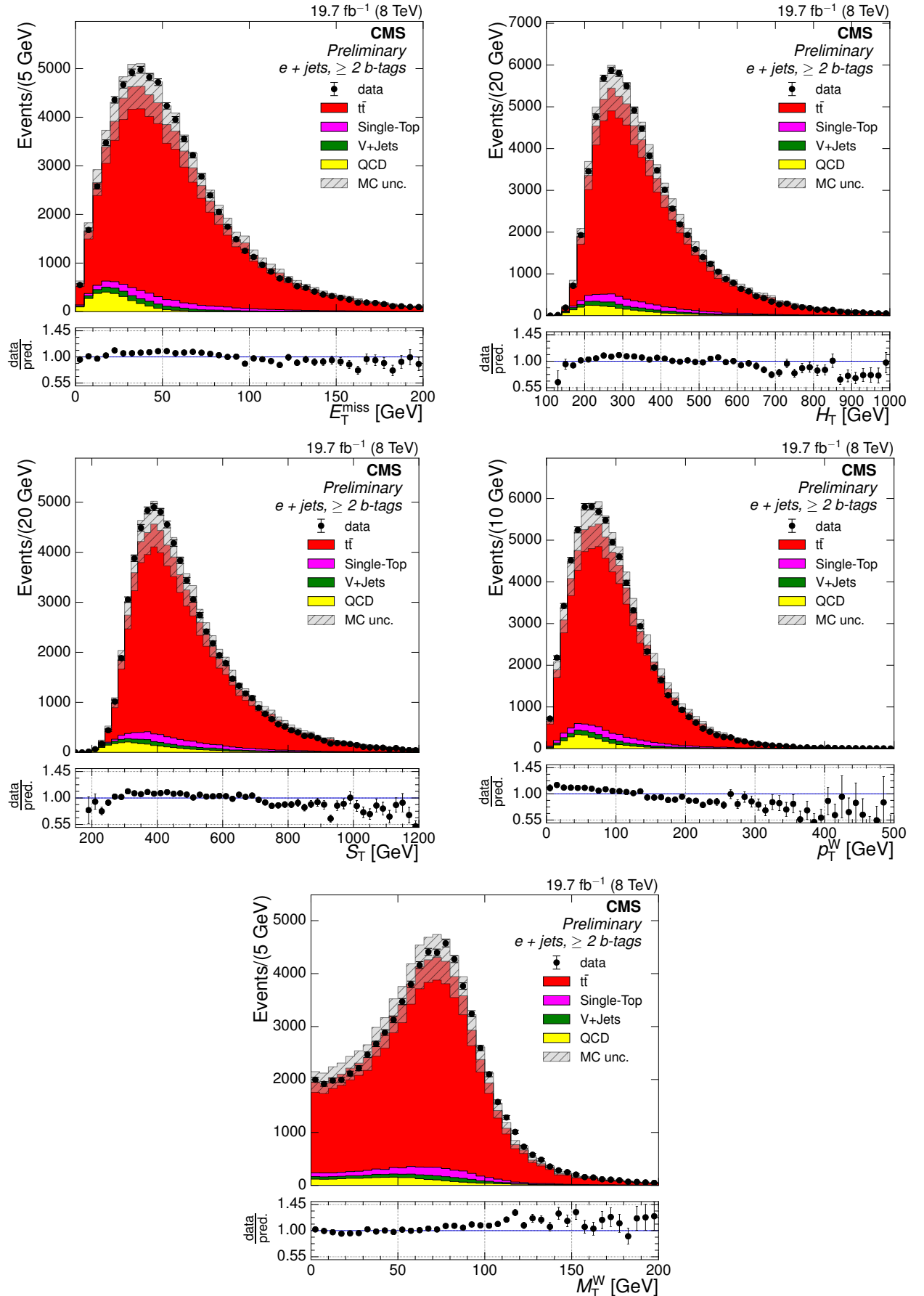


Figure 1.3: Comparison of Monte Carlo simulation to data in the electron+jets channel after final selection at  $\sqrt{s} = 8 \text{ TeV}$ .

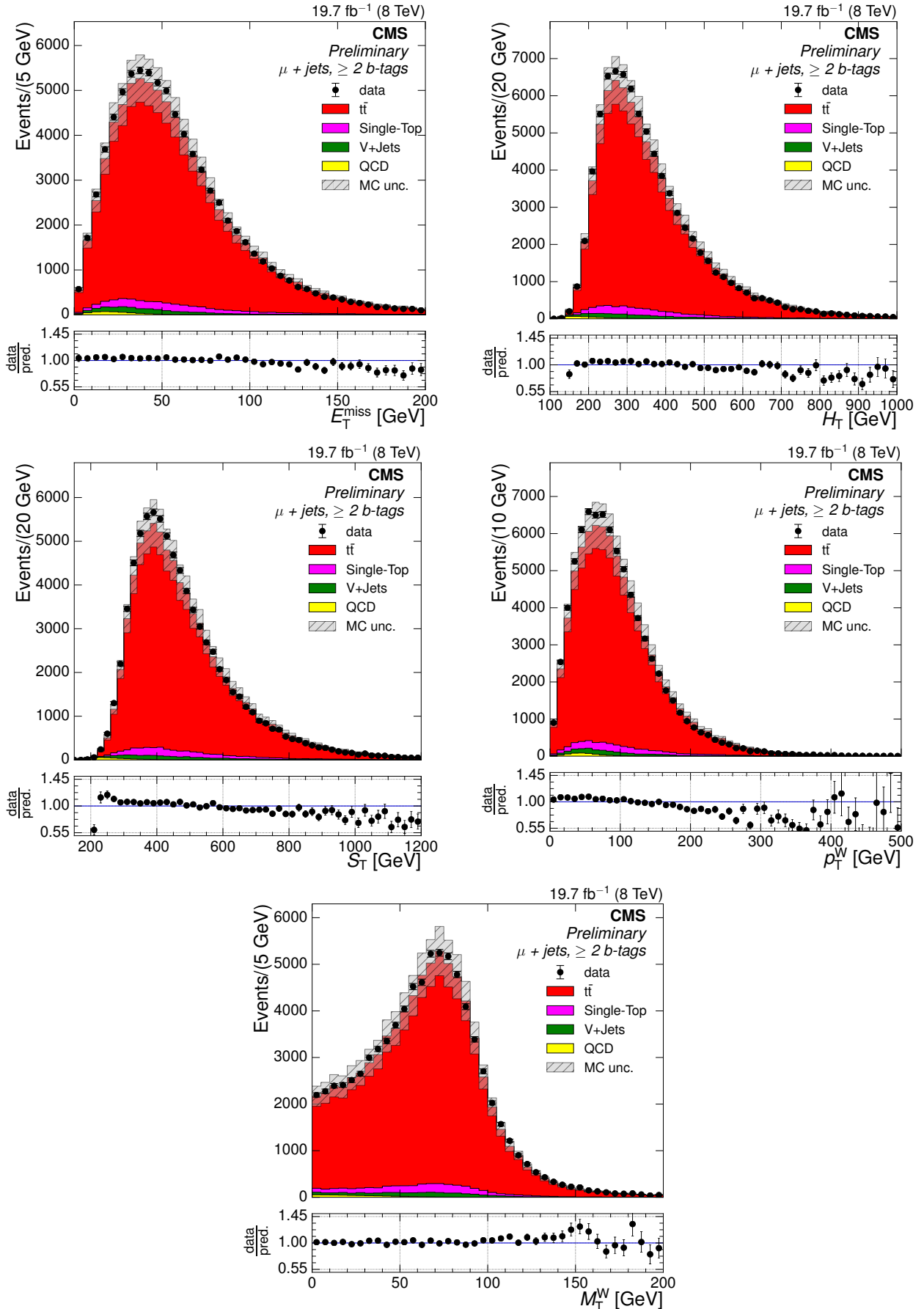


Figure 1.4: Comparison of Monte Carlo simulation to data in the muon+jets channel after final selection at  $\sqrt{s} = 8 \text{ TeV}$ .



Figure 1.5: Comparison of QCD selections in the electron+jets channel at  $\sqrt{s} = 7 \text{ TeV}$  on the left and at  $\sqrt{s} = 8 \text{ TeV}$  on the right. Conversion region is shown at the top, non-isolated selection in the middle and a comparison of the two selections in data (TODO:CHECK THIS, AND INSERT THE PLOTS IN THE FIRST PLACE!) is shown in the lower plots.

$$p^k = \frac{N_{\text{rec\&gen}}^k}{N_{\text{rec}}^k} s^k = \frac{N_{\text{rec\&gen}}^k}{N_{\text{gen}}^k}, \quad (1.2)$$

$N_{\text{rec\&gen}}^k$  is the number of events generated and reconstructed in bin  $k$ ,  $N_{\text{rec}}^k$  is the number of events reconstructed in bin  $k$  and  $N_{\text{gen}}^k$  is the number of events generated in bin  $k$ . The stability of a bin is sensitive to the migration of events out of a bin, while the purity is sensitive to the migration of events into a bin (see Figure 1.6).

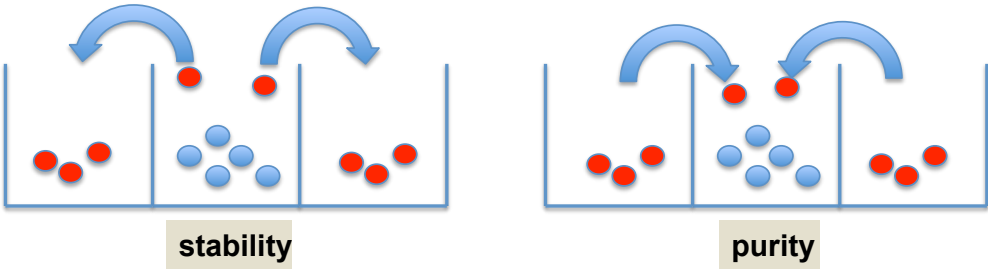


Figure 1.6: Stability quantifies the migration of events out of a bin while purity quantifies the migration of events into a bin. Both quantities compare the variable range (bin) in which an event is generated to the range in which they are reconstructed.

In this analysis, the bins for each primary variable distribution were chosen such that all bins have purity and stability values of 0.5 or greater, meaning that at least half of the events generated in a bin remain in that bin after reconstruction, and that at least half of the events reconstructed in a bin were generated in that bin. In order to avoid very small bins, a requirement that all bins have at least 100 events is also enforced.

The determination of the bin boundaries following these criteria is carried out simultaneously in (and therefore the binning is identical in) both centre of mass energies and both the electron+jets and muon+jets channel.

Plots of generated versus reconstructed events for all primary variables are shown in the electron+jets channel in Figure 1.7 for  $\sqrt{s} = 7$  TeV and in Figure 1.8 for  $\sqrt{s} = 8$  TeV. The corresponding plots in the muon+jets are shown in Figures 20 and 21 in Appendix .1. The purity and stability values of the chosen bins are shown in Appendix .2.

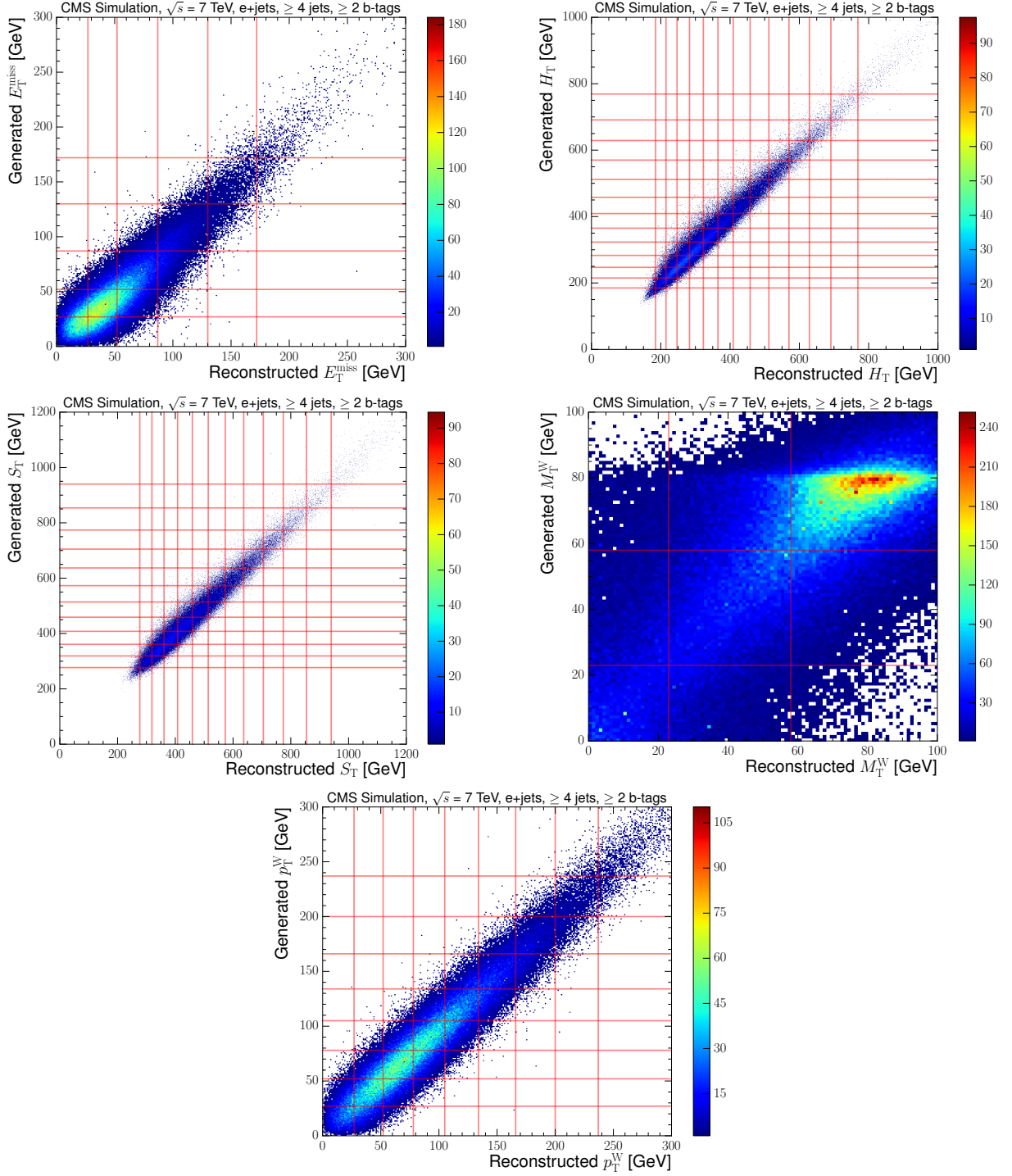


Figure 1.7: Generated versus reconstructed distributions of the primary variables  $E_T^{\text{miss}}$  (upper left),  $H_T$  (upper right),  $S_T$  (middle left),  $M_T^W$  (middle right) and  $p_T^W$  (lower) with horizontal and vertical lines representing the boundaries of the selected bins at  $\sqrt{s} = 7$  TeV in the electron+ jets channel. These distributions are obtained using  $t\bar{t}$  Monte Carlo simulation.

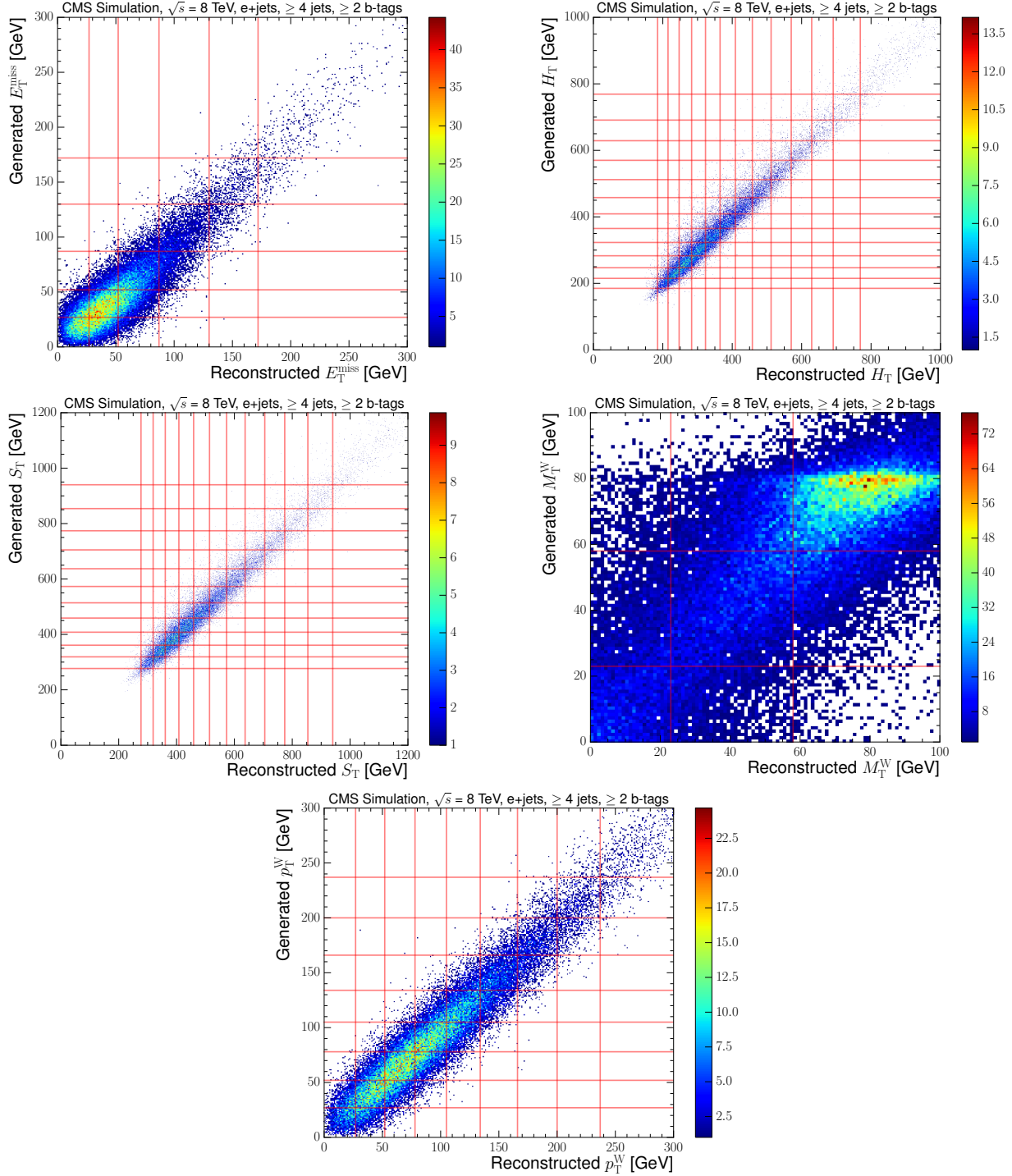


Figure 1.8: Generated versus reconstructed distributions of the primary variables  $E_T^{\text{miss}}$  (upper left),  $H_T$  (upper right),  $S_T$  (middle left),  $M_T^W$  (middle right) and  $p_T^W$  (lower) with horizontal and vertical lines representing the boundaries of the selected bins at  $\sqrt{s} = 8$  TeV in the electron+ jets channel. These distributions are obtained using  $t\bar{t}$  Monte Carlo simulation.

### 1.3 Maximum Likelihood Fit

A maximum log likelihood fit of four templates to data in each bin of the primary variables is used to obtain the number of events in each bin. The four templates used are  $t\bar{t}$ , single top,  $V+Jets$  (a combination of  $W+Jets$  and  $Z+Jets$  events) and QCD. The template distributions are obtained from the following three variables: the absolute pseudorapidity of the lepton ( $|\eta|$ ), the three-dimensional angle between the lepton and the nearest b-jet ( $\alpha$ ), and the invariant mass of the three jets with the highest  $p_T$  sum ( $M3$ ).

The fit is carried out by maximising the log of the likelihood function (LL):

$$LL(x_i, d_i) = -2 \log \prod_i \frac{x_i^{d_i} \cdot e^{-x_i}}{d_i!} = -2 \sum_i \log \left( \frac{x_i^{d_i} \cdot e^{-x_i}}{d_i!} \right). \quad (1.3)$$

where  $i$  is the bin index in the template,  $x_i$  is the total of all the templates in bin  $i$ , and  $d_i$  is the observed number of data events in bin  $i$ .  $x_i$  is defined to be

$$x_i = \sum_j N_j x_{ij}, \text{ with } \sum_i \theta_{ij} = 1 \text{ foreach process.} \quad (1.4)$$

where  $\theta_{ij}$  represents the templates and  $N_j$  represents the normalisations of the templates. Fitting using more than one fitting variable (the three aforementioned fitting variables), the log likelihoods are summed:

$$LL(x, d) = -\frac{2}{k} \sum_k \log L_k \quad (1.5)$$

where  $L_k$  is the likelihood function of each of the different fit variables. Here the division by  $k$  accounts for the fact that the same information is used in all three fit variables, and provides a conservative estimate of the uncertainties in the resulting fitted parameters. The fit functions by adjusting the normalisation of each template with the aim of equating  $x_i$  and  $d_i$  in each bin of each template. The starting normalisations in the templates are obtained from simulation after the full selection has been applied (this includes the QCD template, although the shape for this is obtained from data).

### 1.3.1 Choice of templates

Three fitting variables are used because no individual fit variable is able to distinguish between all four templates used in the fit:

- $t\bar{t}$
- single-top
- V+jets (W+jets + Z+jets)
- QCD multi-jet

$t\bar{t}$ , single-top and V+jets templates are taken from simulation, while the QCD template is extracted from data as described in Section ???. The W+jets and Z+jets templates are combined firstly due to the similar shapes of the distributions in these two background processes, and secondly due to limited statistics available in simulation. The four template shapes in each of the three fitting variables are shown in Figures 1.9 and 1.10 for  $\sqrt{s} = 7 \text{ TeV}$  and  $\sqrt{s} = 8 \text{ TeV}$  respectively. This combination of fitting variables was selected because they are uncorrelated to the primary variables under investigation, and they show good discrimination between the four templates. Single top events have similar signatures to  $t\bar{t}$  events, with a central lepton from the decay of the single top, leading to a single top template that is similar to the  $t\bar{t}$  template in the electron  $|\eta|$  and muon  $|\eta|$  distributions. In the  $\alpha$  distribution, the similarity is attributable to the fact that the average boost for single top events is lower than in  $t\bar{t}$  events, leading to a wider single top template. The M3 variable will be a combination of the jets from the hadronically decaying t-quark (a b-jet and two other jets from the W-boson) in  $t\bar{t}$  events, whereas in the other templates, M3 will simply correspond to some random combination of jets in the event. Hence, M3 shows the best discrimination between the single top and  $t\bar{t}$  templates.

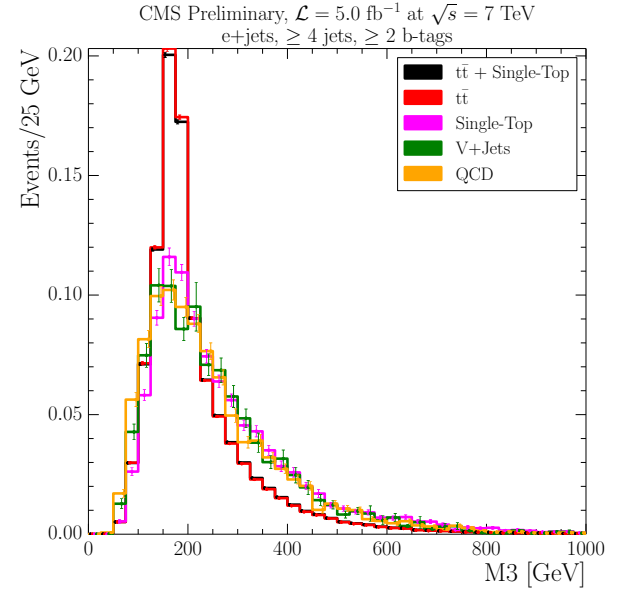
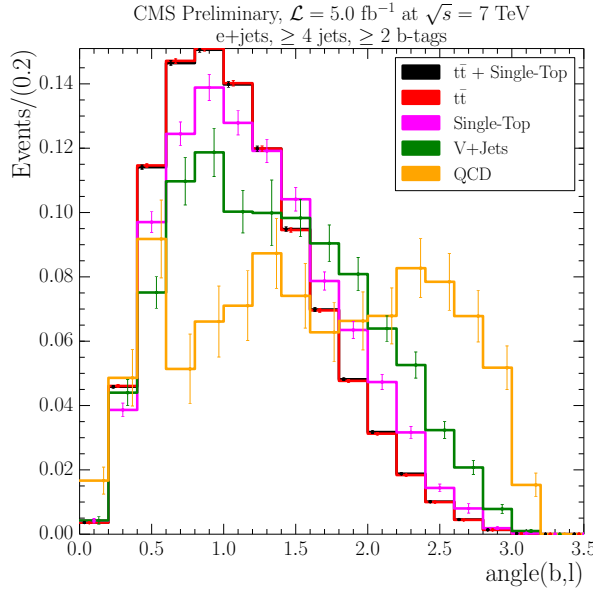
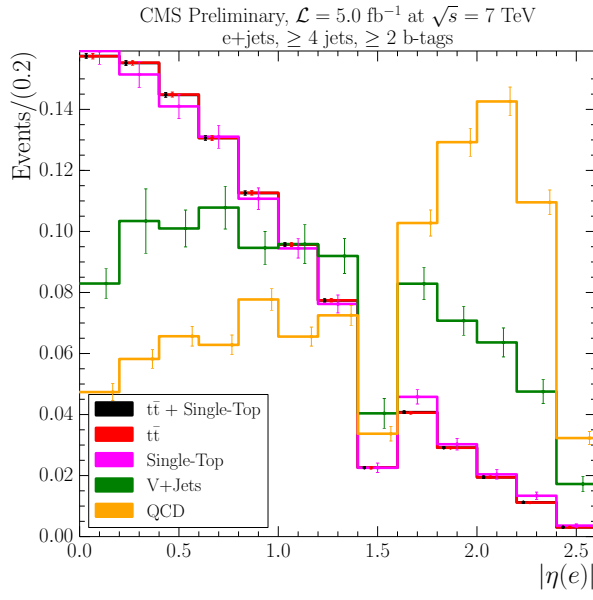


Figure 1.9: Normalised distributions of the four templates for the three fit variables at  $\sqrt{s} = 7 \text{ TeV}$ , inclusive across all primary variable bins: electron  $|\eta|$  (upper left), muon  $|\eta|$  (upper right),  $\alpha$  (lower left) and  $M3$  (lower right).

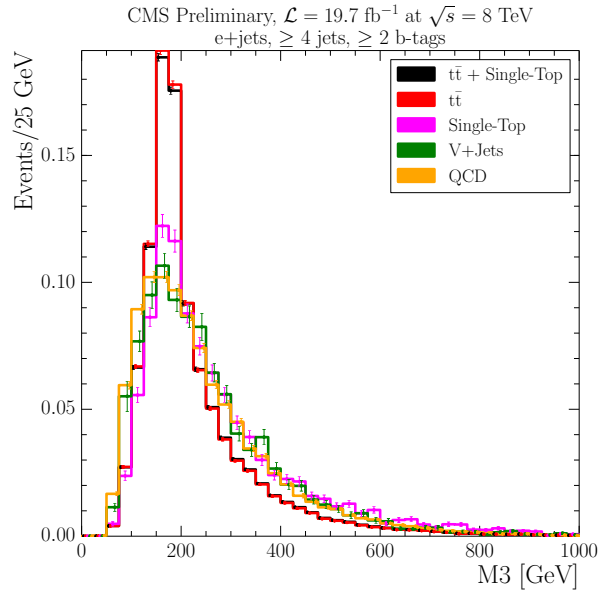
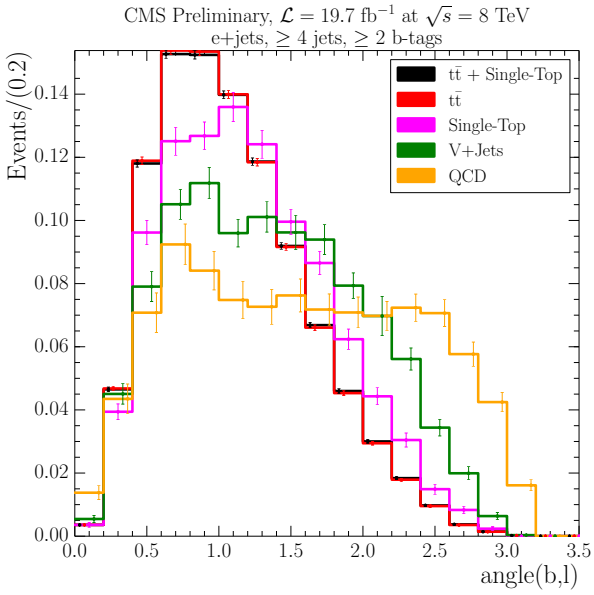
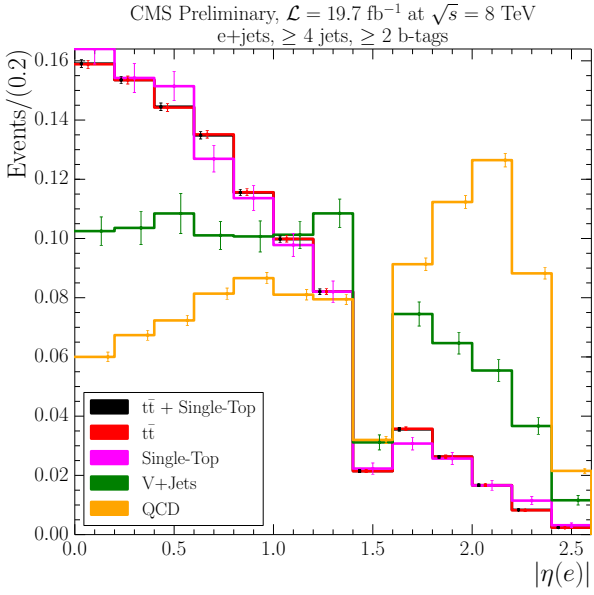


Figure 1.10: Normalised distributions of the four templates for the three fit variables at  $\sqrt{s} = 8 \text{ TeV}$ , inclusive across all primary variable bins: electron  $|\eta|$  (upper left), muon  $|\eta|$  (upper right),  $\alpha$  (lower left) and  $M_3$  (lower right).

The QCD templates inclusive across all bins of the primary variables are used because of low statistics in the QCD background selection in higher bins. Figure 1.11 shows a comparison between QCD templates at  $\sqrt{s} = 8$  TeV in the lowest three bins of the  $E_T^{\text{miss}}$  variable and also the inclusive  $E_T^{\text{miss}}$  QCD template. It can be seen that the third  $E_T^{\text{miss}}$  bin already shows low numbers of events, meaning the inclusive template is largely shaped by events in the first two bins. Therefore, the inclusive QCD template is used rather than those in individual bins. Similar plots showing the same behaviour for the other primary variables are shown in Appendix .3.

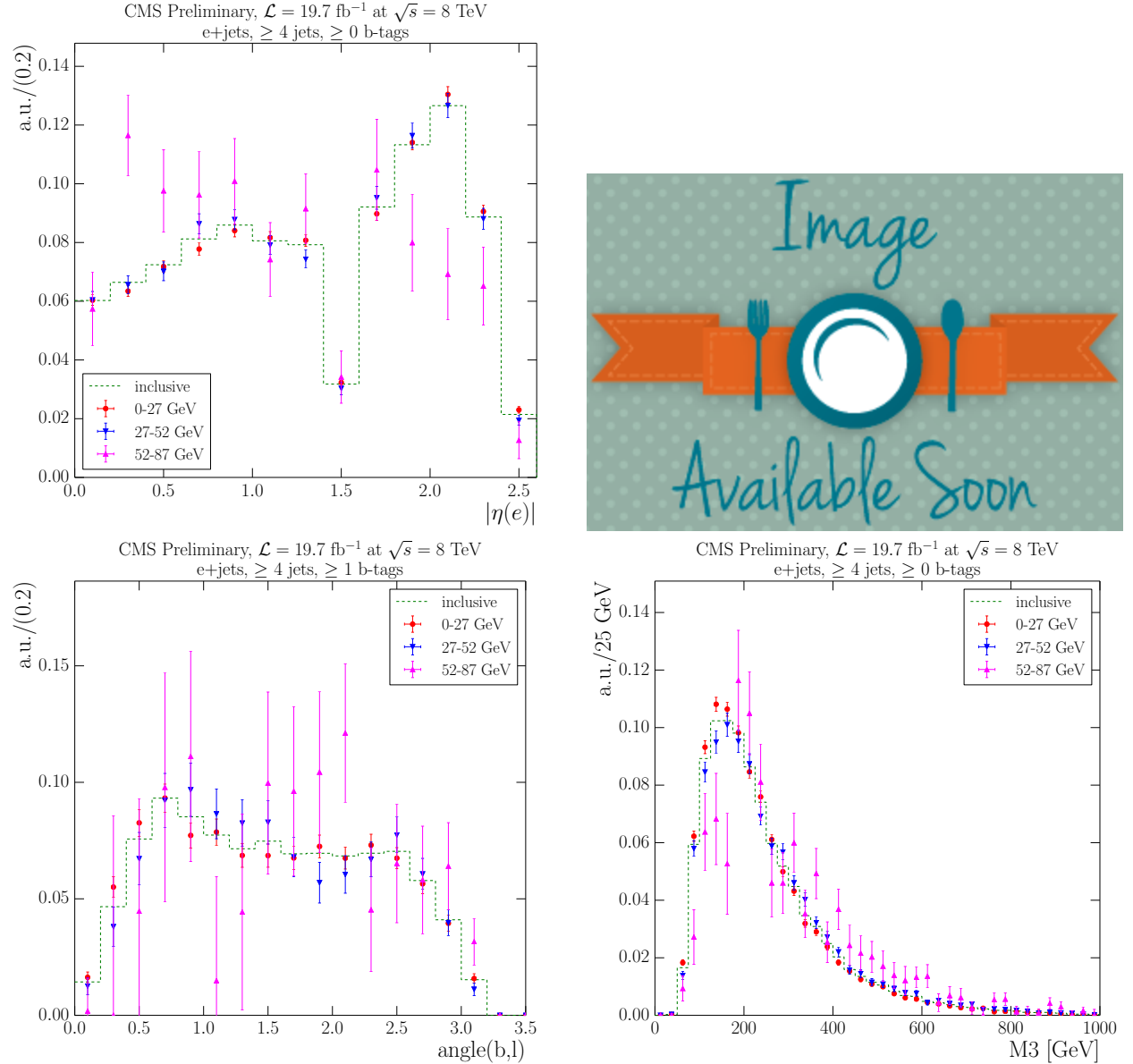


Figure 1.11: Normalised distributions of the QCD templates for the three fit variables at  $\sqrt{s} = 8$  TeV inclusive across all  $E_T^{\text{miss}}$  bins and for the lowest three  $E_T^{\text{miss}}$  bins: electron  $|\eta|$  (upper left), muon  $|\eta|$  (upper right),  $\alpha$  (lower left) and  $M_3$  (lower right).

An inclusive template is also used in the V+jets (W+jets + Z+jets template) for the same reason. Figure 1.12 shows a comparison between the V+jets templates at  $\sqrt{s} = 8$  TeV in each  $E_T^{\text{miss}}$  bin and also the inclusive  $E_T^{\text{miss}}$  V+jets template. As is the case for the QCD background template, it can be seen in the V+jets templates that there are diminished statistics available in higher bins, and the inclusive template shape is largely governed by the lower bins. Similar plots demonstrating the same behaviour for the other primary variables are shown in Appendix 4.

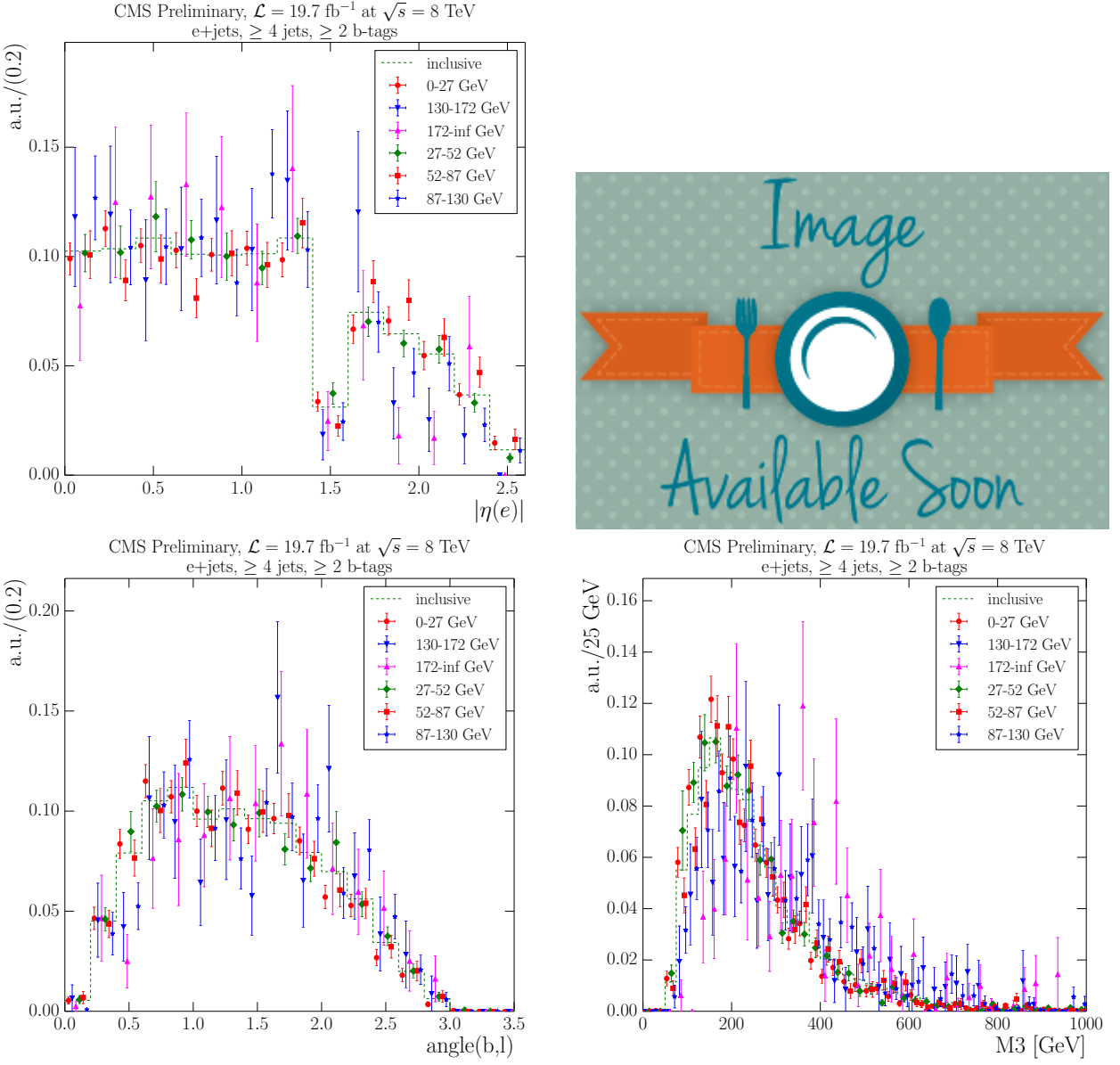


Figure 1.12: Normalised distributions of the V+jets templates for the three fit variables at  $\sqrt{s} = 8$  TeV inclusive across all  $E_T^{\text{miss}}$  bins and for the lowest three  $E_T^{\text{miss}}$  bins: electron  $|\eta|$  (upper left), muon  $|\eta|$  (upper right),  $\alpha$  (lower left) and  $M_3$  (lower right).

### 1.3.2 7TeV V+Jets theory systematic template

Unfortunately, Monte Carlo simulation at  $\sqrt{s} = 7$  TeV for theoretical systematic uncertainties have not been made available for W+jets and Z+jets processes. However, it can be seen in Figure 1.13 that the W+jets template shapes at  $\sqrt{s} = 7$  TeV and  $\sqrt{s} = 8$  TeV are similar. The V+jets template shapes used to evaluate these theoretical systematics are therefore obtained from  $\sqrt{s} = 8$  TeV theoretical systematic datasets, and then scaled to the normalisation in the nominal sample at  $\sqrt{s} = 7$  TeV.

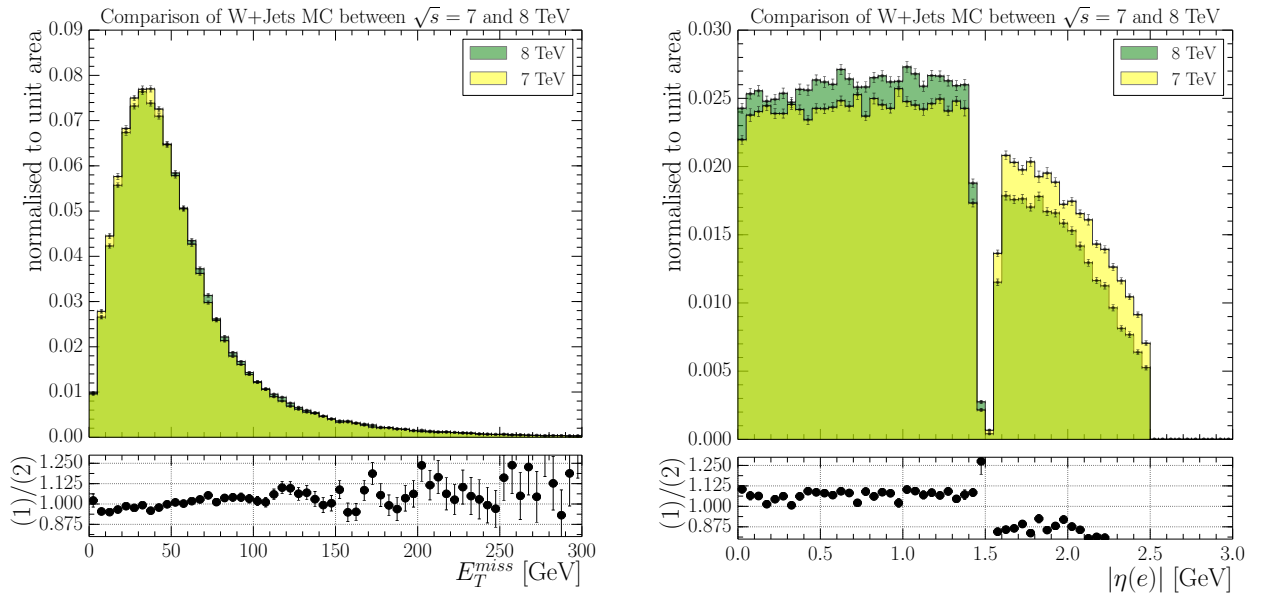


Figure 1.13: Shape comparison of W+jets templates in  $\sqrt{s} = 7$  TeV and  $\sqrt{s} = 8$  TeV Monte Carlo simulation for  $E_T^{\text{miss}}$  (left) and electron  $|\eta|$  (right) in the electron channel.

TODO: Insert Fit Template Plots

### 1.3.3 Fit Results

The results from the fit are shown in Figures 1.14 and 1.15 for the electron and muon channels respectively at  $\sqrt{s} = 7$  TeV, and in Figures 1.16 and 1.17 for the electron and muon channels at  $\sqrt{s} = 8$  TeV. The corresponding numerical values from the fit can be found in Appendix .5. Overall, the agreement within the data and the simulation is within the fit uncertainty.

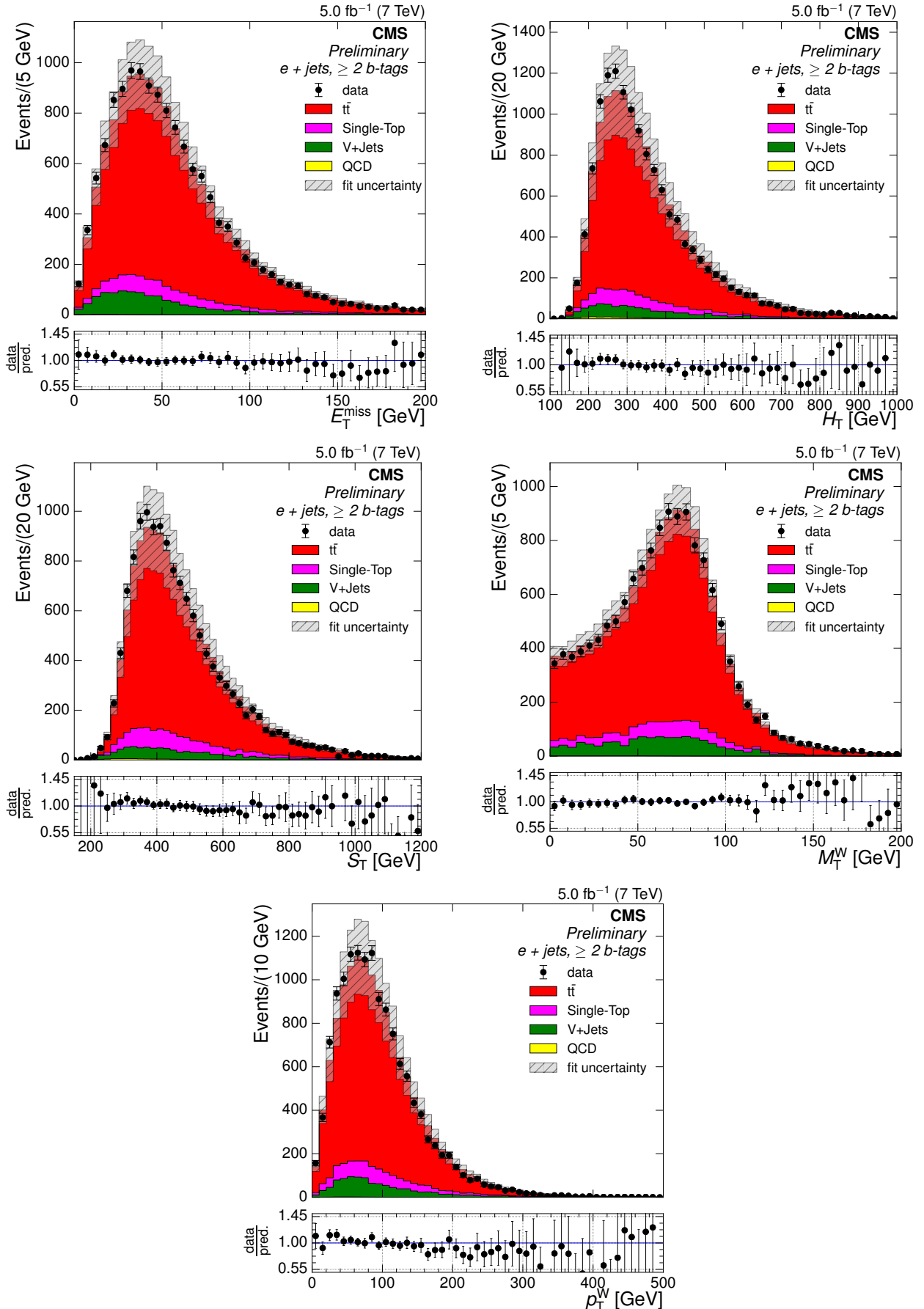


Figure 1.14: Comparison of Monte Carlo simulation to data in the electron+jets channel after fitting at  $\sqrt{s} = 7$  TeV.

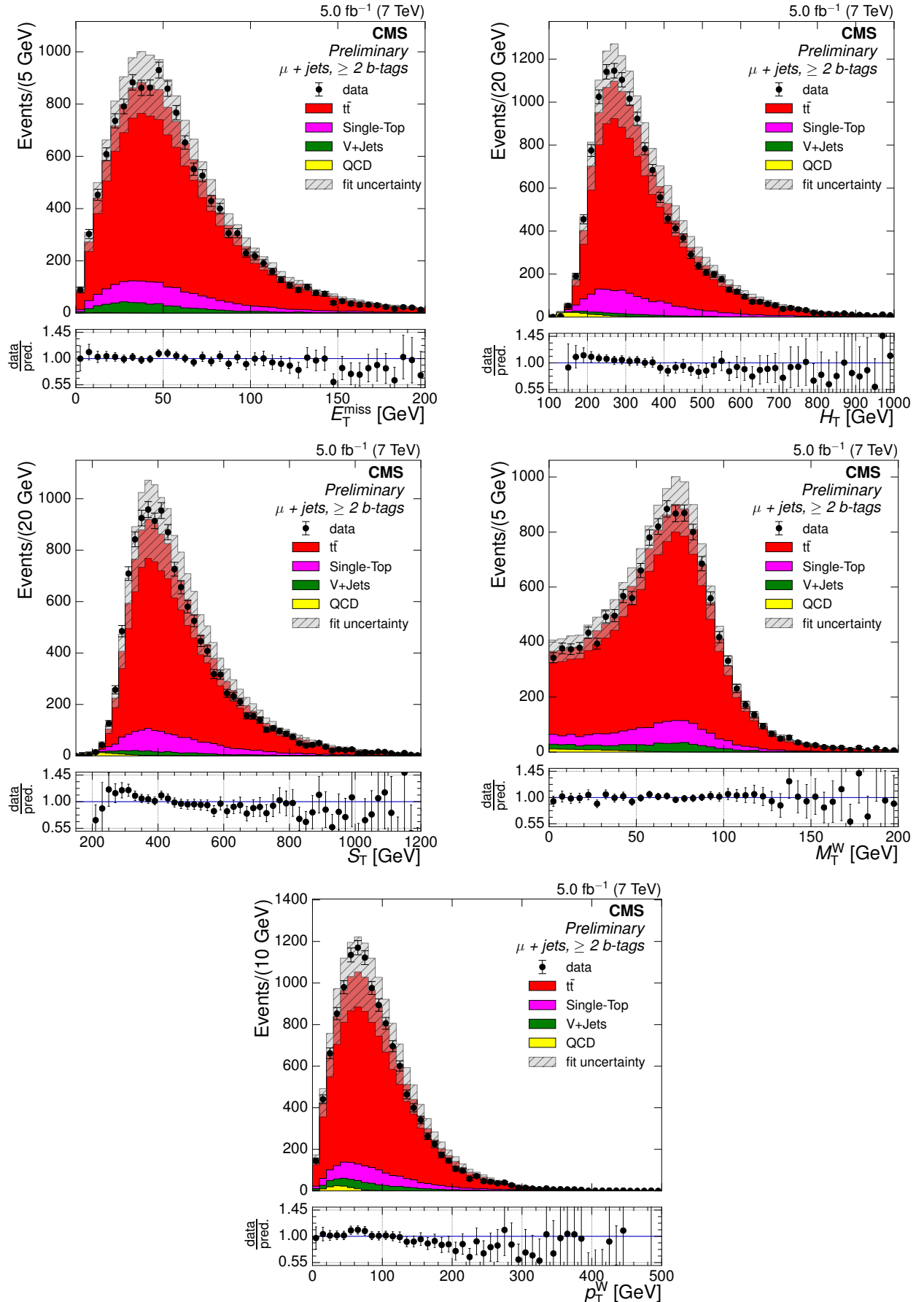


Figure 1.15: Comparison of Monte Carlo simulation to data in the muon+jets channel after fitting at  $\sqrt{s} = 7 \text{ TeV}$ .

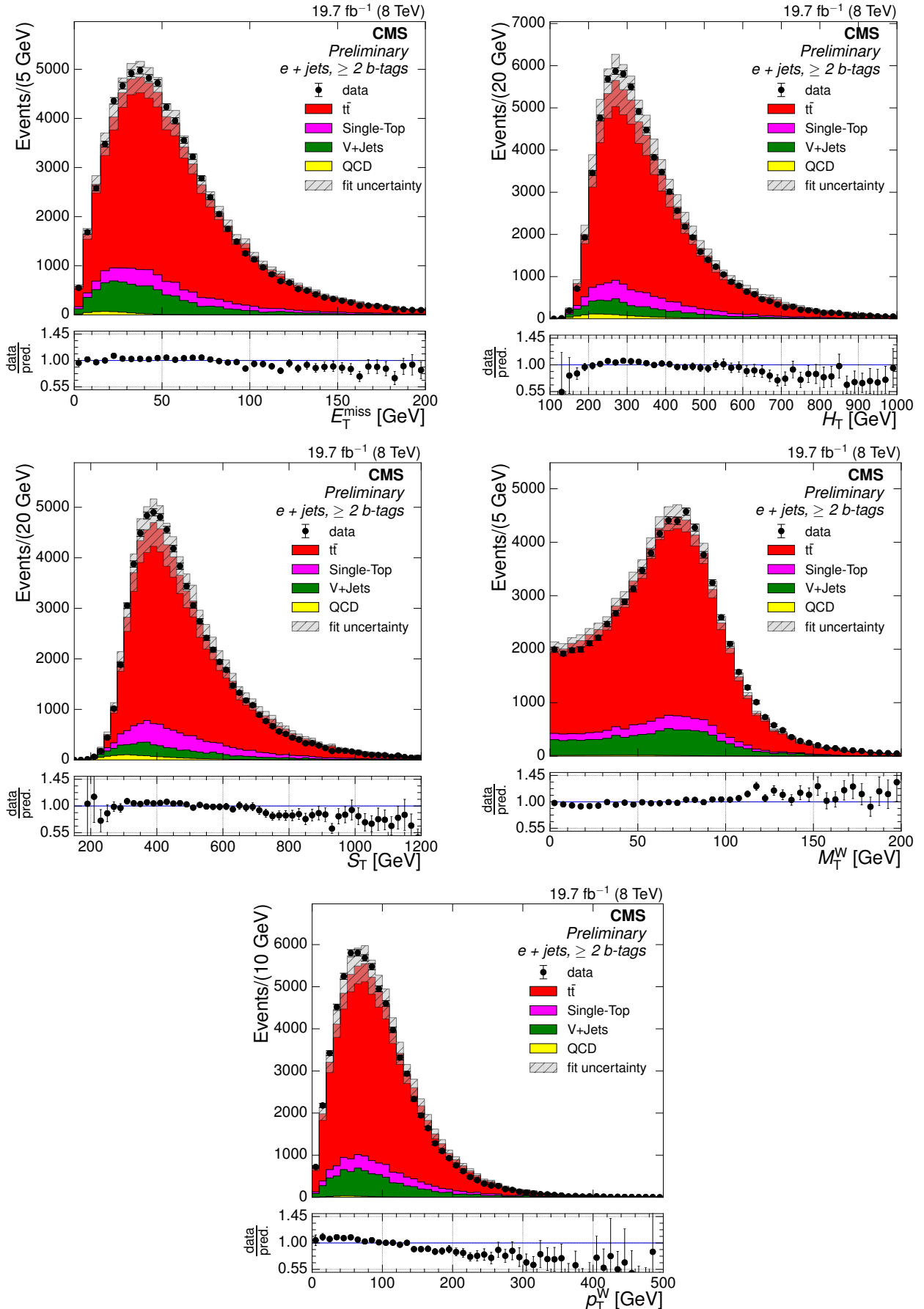


Figure 1.16: Comparison of Monte Carlo simulation to data in the electron+jets channel after fitting at  $\sqrt{s} = 8 \text{ TeV}$ .

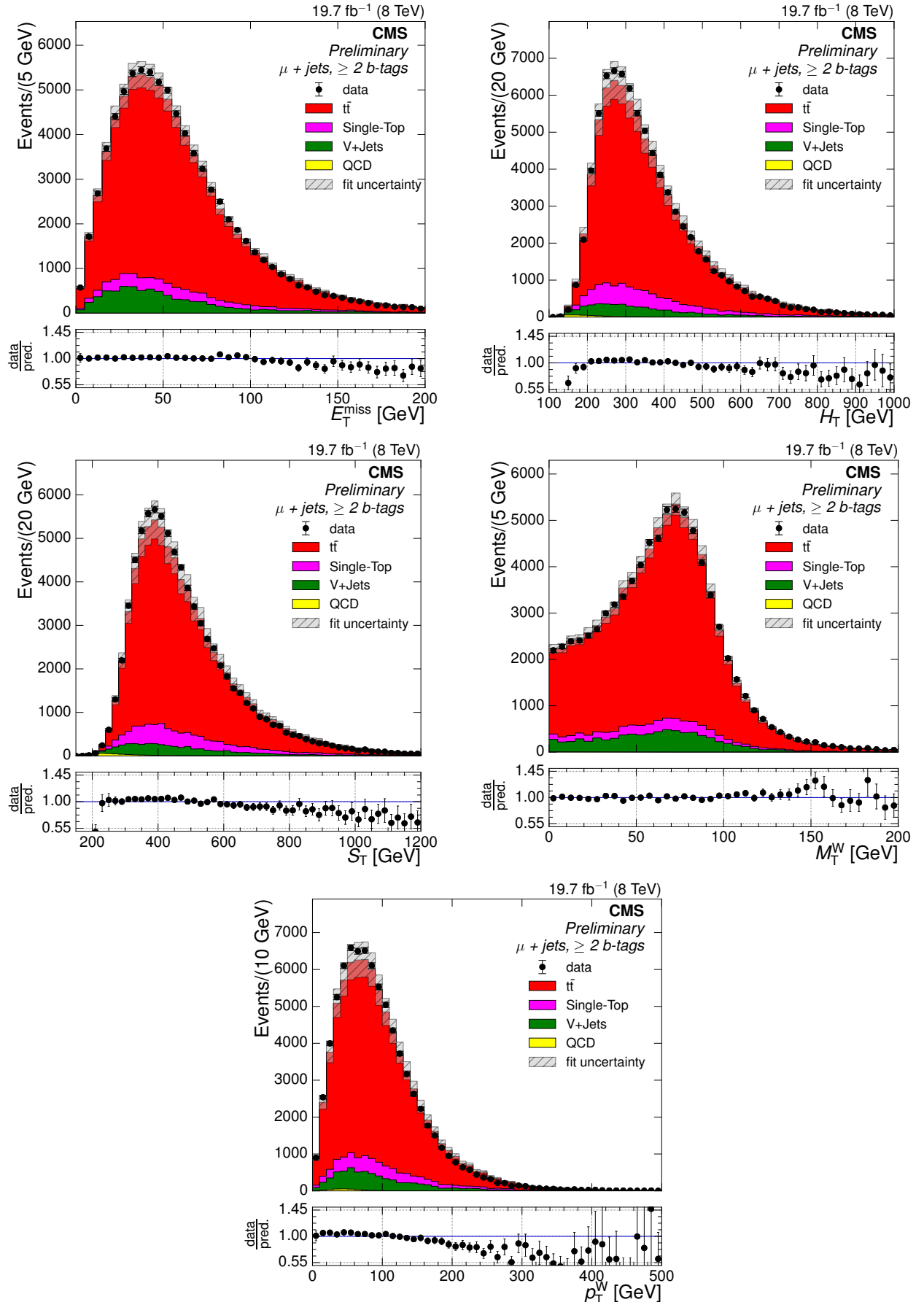


Figure 1.17: Comparison of Monte Carlo simulation to data in the muon+jets channel after fitting at  $\sqrt{s} = 8 \text{ TeV}$ .

## 1.4 Unfolding

The measurement of the differential cross section will be limited by the finite resolution of the detector, detector acceptance and selection efficiency. In order to allow later comparison of results with theory predictions and with measurements from other experiments, deconvolution, or unfolding, is employed to provide an estimate of the true distributions of the measured variables.

Generally speaking, some variable can be simulated to produce a true distribution, denoted by a vector  $x_0$ , and after performing the reconstruction algorithms on this, a corresponding measured distribution in simulation,  $b_0$ . These are related by

$$\hat{A}x_0 = b_0. \quad (1.6)$$

where  $\hat{A}$  is the response matrix, containing information about how the true distribution is reconstructed and measured as the distribution obtained in the real world. The variable in question is then measured in reality to have some distribution,  $b$ , which is then related to the true distribution by

$$\hat{A}x = b. \quad (1.7)$$

Directly inverting the response matrix results in rapidly oscillating solutions [2]. Therefore, in this analysis, the system is solved to identify the true underlying distribution,  $x$ , using Singular Value Decomposition (SVD) [2] of the response matrix, with the RooUnfold package [1]. In SVD unfolding, the response matrix is factorised as follows:

$$\hat{A} = USV^T. \quad (1.8)$$

$S$  is a diagonal matrix with non-negative diagonal elements of dimensions  $m \times n$ , and  $U$  and  $V$  are orthogonal matrices of dimensions  $m \times m$  and  $n \times n$  respectively. The diagonal elements of  $S$  are called *singular values* of the matrix  $A$  and the columns of  $U$  and  $V$  are called the left and right *singular vectors*. The inverse of the response matrix can then be stated as

$$\hat{A}^{-1} = VS^{-1}U^T. \quad (1.9)$$

In systems with a full rank response matrix and statistical errors in the bins of the distribution are small, the problem can be solved simply using the inverted response matrix  $\hat{A}^{-1}$ . However,

in ill-defined systems, the response matrix  $A$  is almost degenerate and has singular values near zero and in cases where the measurement has significant statistical errors, the problem produces an oscillating solution of no meaning, since random components will be amplified [2]. Regularisation is used in the SVD unfolding method to help overcome this problem.

Considering a measured variable that follows a smooth distribution, only the first few bins are expected to be significant, with following bins expected to be compatible with zero. Using  $d$ , a vector obtained by rotating the measured distribution

$$d = U^T \times b, \quad (1.10)$$

a plot of  $\log|d_i|$  versus  $i$  can be plotted, where the bin number is represented by  $i$ . This will show  $d_i$  as being statistically significant for small  $i$ , and falling exponentially to a random Gaussian distribution for larger  $i$ . A falling exponential function plus a flat line is fitted to this distribution, and the value of  $i$  at which the  $d_i$  changes from exponentially falling to within 10% of the flat component is taken as the value of the regularisation parameter,  $k$ , which represents the number of significant bins in the distribution [2].

The value of  $k$  should be between 2 and the number of bins in the distribution, and aims to prevent statistical fluctuations in the distribution being interpreted as real variations in the true data. A low value of  $k$  favours the Monte Carlo truth input, while a high value of  $k$  favours the measured data which is required to be unfolded. The  $\log|d_i|$  plots for  $E_T^{\text{miss}}$  variable at  $\sqrt{s} = 7 \text{ TeV}$  is shown in Figure 1.18. The resulting  $k$  values for both channels and both centre of mass energies are shown in Table 1.5.

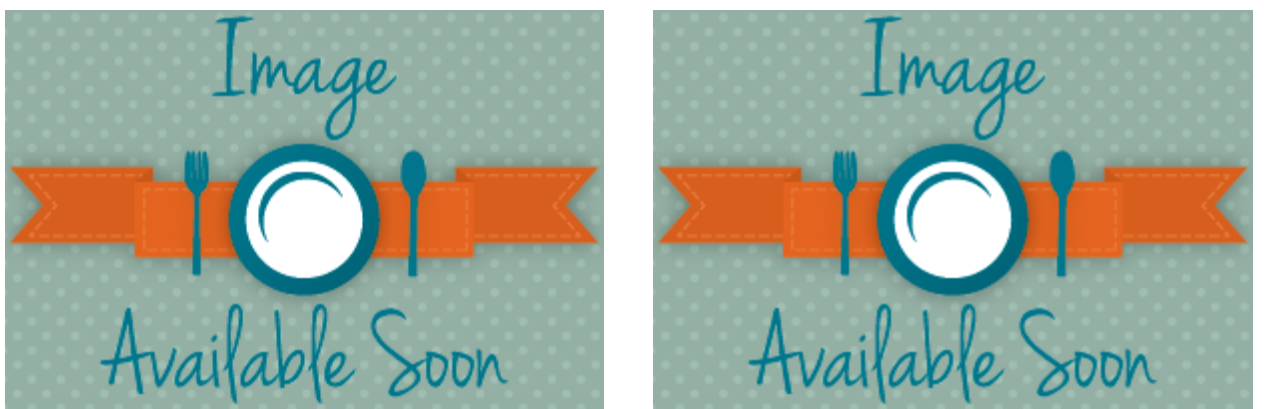


Figure 1.18:  $\log|d_i|$  plots at  $\sqrt{s} = 7 \text{ TeV}$  for the electron+jets channel (left) and the muon+jets channel (right). TODO:  $D_i$  PLOTS

In summary, the required inputs to unfolding are the Monte Carlo simulated true distributions before selection, the Monte Carlo simulated reconstructed distribution after selection, and the two-dimensional reconstruction matrix of the true variables after selection versus the

variable	k-value (electron)	k-value (muon)
$\sqrt{s} = 7 \text{ TeV}$		
$E_T^{\text{miss}}$	2	2
$H_T$	3	3
$S_T$	3	3
$M_T^W$	2	2
$p_T^W$	3	3
$\sqrt{s} = 8 \text{ TeV}$		
$E_T^{\text{miss}}$	3	3
$H_T$	3	3
$S_T$	4	4
$M_T^W$	2	2
$p_T^W$	3	3

Table 1.5: Optimal  $k$ -values for all primary variables at both 7 and 8 TeV.

measured distributions after selection. These are all obtained from Monte Carlo simulations of  $t\bar{t}$  events.

Unfolding is carried out to the semi-leptonic phase space, where the lepton is either an electron or a muon. In the cases of  $E_T^{\text{miss}}$ ,  $p_T^W$  and  $M_T^W$ , unfolding is carried out to the full phase-space where the  $E_T^{\text{miss}}$  is defined as the  $p_T$  of the neutrino from the semi-leptonic decay; and in the cases of  $H_T$  and  $S_T$ , unfolding is carried out to particle level where the generated jets have  $p_T \geq 20 \text{ GeV}$ .

Closure tests were carried out to verify the unfolding method using reconstructed simulated events as pseudo-data. A successful closure test results in the unfolded values matching the simulated truth of the same simulation sample, as can be seen in Figure 1.19.

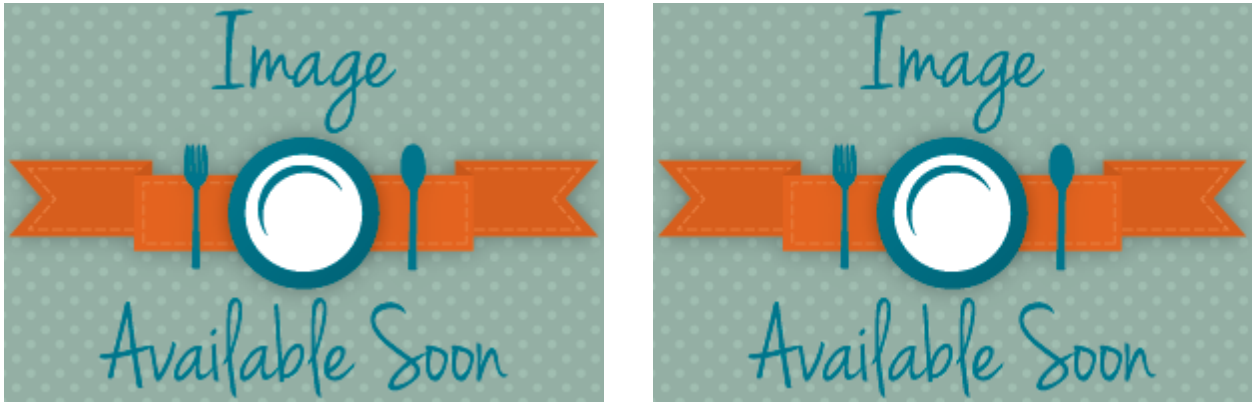


Figure 1.19:  $\log|d_i|$  plots at  $\sqrt{s} = 7 \text{ TeV}$  for the electron+jets channel (left) and the muon+jets channel (right). TODO:  $D_i$  PLOTS

Pull distributions

### 1.4.1 Measurement

TODO: THIS SECTION TAKEN STRAIGHT FROM AN AT THE MOMENT, NEED TO REWRITE.

Once the number of  $t\bar{t}$  events ( $N_{t\bar{t}}$ ) is unfolded (see section 1.4) the normalised differential cross-section is calculated for every bin  $i$  of the measured variable. Firstly the cross-section in each bin is defined as

$$\Delta\sigma_{t\bar{t}}^i = \frac{N_{t\bar{t}}^i}{\text{BR} \times \epsilon \times \mathcal{L}} \quad (1.11)$$

where BR is the branching ratio of the semi-leptonic decay channel calculated using MC,  $\epsilon$  the  $t\bar{t}$  efficiency and  $\mathcal{L}$  the measured luminosity. Since the efficiency is corrected for in the unfolding it is set to 1. Next the average value for the cross-section in each bin is obtained by dividing by the bin width  $\Delta X$ :

$$\frac{d\sigma_{t\bar{t}}^i}{dX} = \frac{\Delta\sigma_{t\bar{t}}^i}{\Delta X} = \frac{N_{t\bar{t}}^i}{\text{BR} \times \mathcal{L} \times \Delta X} \quad (1.12)$$

Finally the average cross-section in each bin is normalised to the total measured cross-section

$$\frac{1}{\sigma_{t\bar{t}}^{\text{tot}}} \frac{d\sigma_{t\bar{t}}^i}{dX} = \frac{1}{\sum_j d\sigma_{t\bar{t}}^j} \frac{d\sigma_{t\bar{t}}^j}{dX} = \frac{\text{BR} \times \mathcal{L}}{\sum_j N_{t\bar{t}}^j} \frac{N_{t\bar{t}}^i}{\text{BR} \times \mathcal{L} \times \Delta X} = \frac{1}{\sum_j N_{t\bar{t}}^j} \frac{N_{t\bar{t}}^i}{\Delta X} \quad (1.13)$$

This normalised cross-section distribution is not normalised to 1 as  $\sigma_{t\bar{t}}^{\text{tot}}$  does not take the bins into account. However, if one was to include the bin widths in the normalisation then the information about the bin-width would be lost in the measurement.

## .1 Binning in muon+jets channel

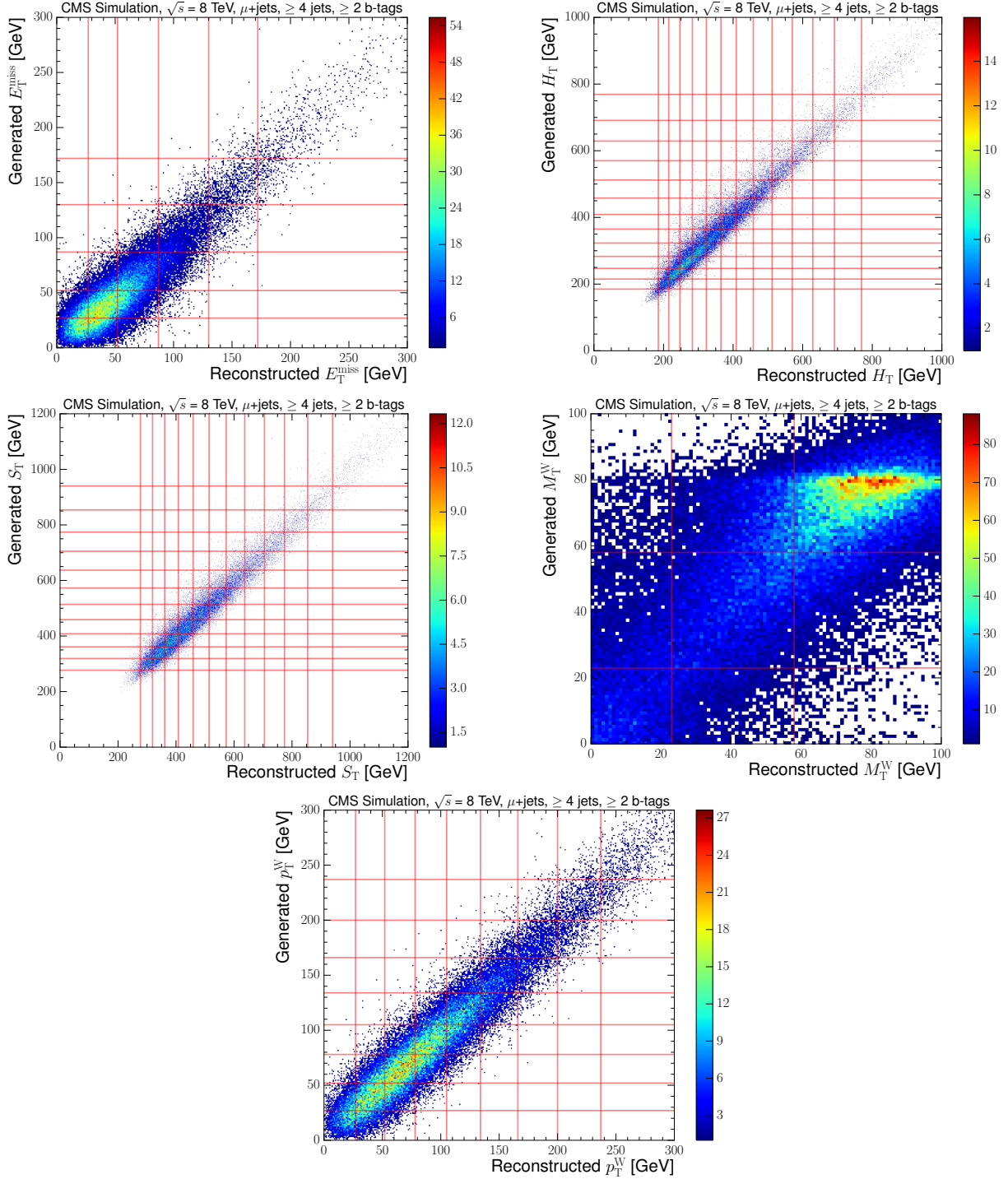


Figure 20: Generated versus reconstructed distributions of the primary variables  $E_T^{\text{miss}}$  (upper left),  $H_T$  (upper right),  $S_T$  (middle left),  $M_T^W$  (middle right) and  $p_T^W$  (lower) with horizontal and vertical lines representing the boundaries of the selected bins at  $\sqrt{s} = 8 \text{ TeV}$  in the muon+jets channel. These distributions are obtained using  $t\bar{t}$  Monte Carlo simulation.

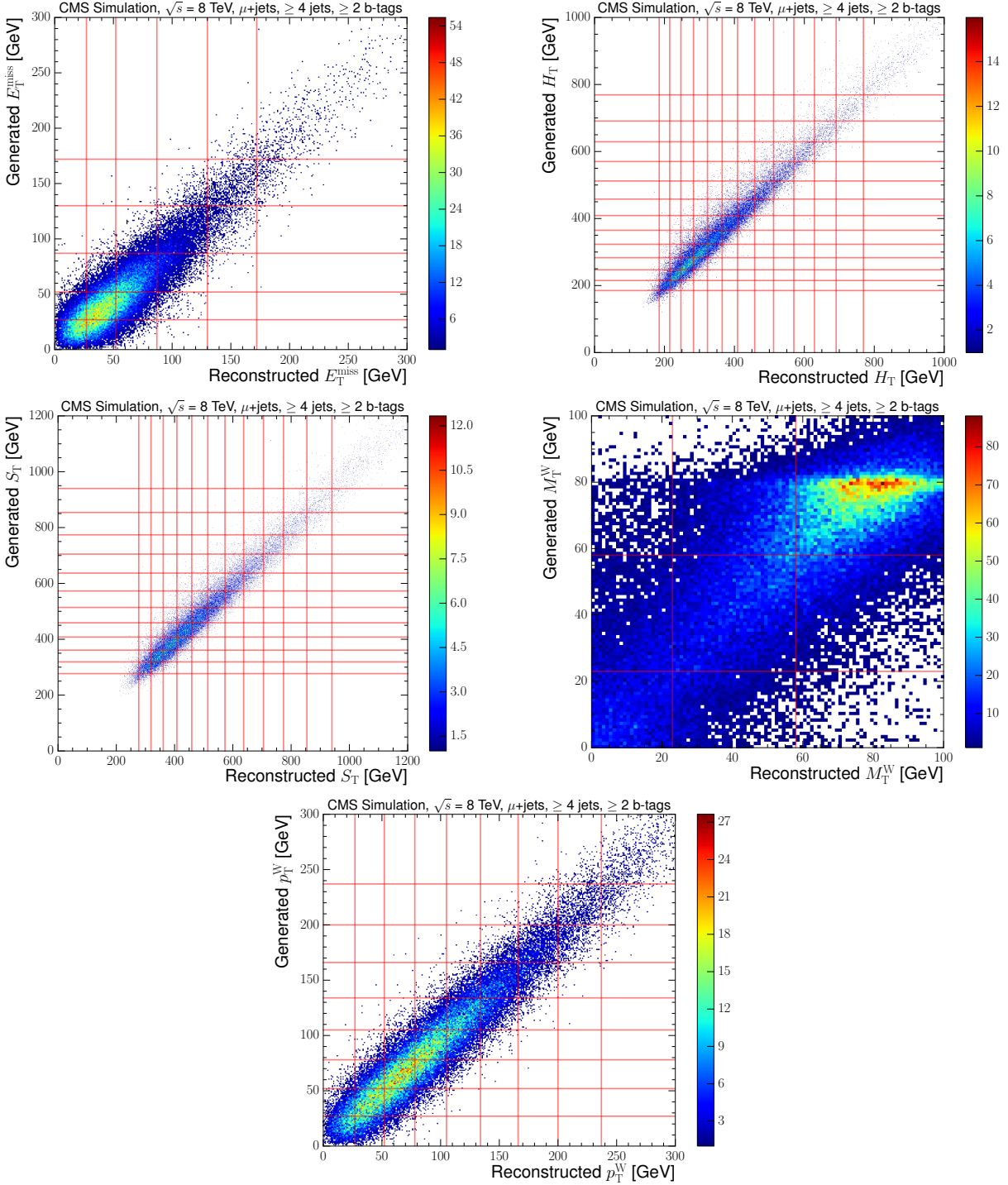


Figure 21: Generated versus reconstructed distributions of the primary variables  $E_T^{\text{miss}}$  (upper left),  $H_T$  (upper right),  $S_T$  (middle left),  $M_T^W$  (middle right) and  $p_T^W$  (lower) with horizontal and vertical lines representing the boundaries of the selected bins at  $\sqrt{s} = 8 \text{ TeV}$  in the muon+jets channel. These distributions are obtained using  $t\bar{t}$  Monte Carlo simulation.

## .2 Binning choice tables

$E_T^{\text{miss}}$ bin ( GeV)	purity	stability	number of events
0 - 27	0.649	0.533	1367
27 - 52	0.588	0.538	2187
52 - 87	0.537	0.636	1691
87 - 130	0.542	0.666	660
130 - 172	0.521	0.624	179
$\geq 172$	0.711	0.824	119
$H_T$ bin ( GeV)	purity	stability	number of events
0 - 186	0.589	0.567	102
186 - 216	0.546	0.565	344
216 - 249	0.542	0.585	676
249 - 286	0.541	0.575	884
286 - 326	0.543	0.556	896
326 - 368	0.536	0.538	765
368 - 412	0.537	0.517	598
412 - 462	0.566	0.538	518
462 - 516	0.573	0.531	375
516 - 574	0.580	0.537	264
574 - 634	0.590	0.529	172
634 - 696	0.581	0.539	113
696 - 781	0.660	0.624	100
$\geq 781$	0.886	0.814	117
$S_T$ bin ( GeV)	purity	stability	number of events
0 - 277	0.565	0.550	108
277 - 319	0.564	0.549	422
319 - 361	0.538	0.543	743
361 - 408	0.530	0.547	939
408 - 459	0.527	0.539	897
459 - 514	0.534	0.536	764
514 - 573	0.539	0.530	601
573 - 637	0.548	0.532	449
637 - 705	0.548	0.534	305
705 - 774	0.540	0.523	194
774 - 854	0.576	0.566	151
854 - 946	0.613	0.580	102
$\geq 946$	0.838	0.837	133
$M_T^W$ bin ( GeV)	purity	stability	number of events
0 - 23	0.528	0.598	659
23 - 58	0.515	0.562	1557
$\geq 58$	0.845	0.786	4518
$p_T^W$ bin ( GeV)	purity	stability	number of events
0 - 27	0.597	0.549	467
27 - 52	0.551	0.526	960
52 - 78	0.550	0.540	1228
78 - 105	0.539	0.538	1107
105 - 134	0.537	0.554	857
134 - 166	0.537	0.568	570
166 - 200	0.524	0.564	314
200 - 237	0.536	0.573	177
$\geq 237$	0.707	0.789	145

Table 6: The selected bins for the measurement in the electron channel at a centre-of-mass energy of 7 TeV. In addition to the bin ranges<sup>32</sup> the purity, stability and number of expected  $t\bar{t}$  events are shown.

$E_T^{\text{miss}}$ bin ( GeV)	purity	stability	number of events
0 - 27	0.641	0.533	1445
27 - 52	0.587	0.536	2374
52 - 87	0.552	0.638	1982
87 - 130	0.550	0.673	770
130 - 172	0.533	0.634	207
$\geq 172$	0.706	0.844	133
$H_T$ bin ( GeV)	purity	stability	number of events
0 - 186	0.595	0.568	121
186 - 216	0.543	0.563	397
216 - 249	0.545	0.583	787
249 - 286	0.541	0.576	1008
286 - 326	0.546	0.559	1010
326 - 368	0.540	0.538	841
368 - 412	0.547	0.529	675
412 - 462	0.569	0.542	558
462 - 516	0.584	0.537	406
516 - 574	0.585	0.547	281
574 - 634	0.590	0.542	181
634 - 696	0.597	0.546	119
696 - 781	0.682	0.623	105
$\geq 781$	0.885	0.818	117
$S_T$ bin ( GeV)	purity	stability	number of events
0 - 277	0.562	0.552	135
277 - 319	0.560	0.542	503
319 - 361	0.536	0.546	866
361 - 408	0.532	0.546	1056
408 - 459	0.530	0.543	1003
459 - 514	0.538	0.540	853
514 - 573	0.543	0.531	645
573 - 637	0.553	0.534	477
637 - 705	0.548	0.539	326
705 - 774	0.542	0.523	200
774 - 854	0.571	0.557	152
854 - 946	0.598	0.585	101
$\geq 946$	0.847	0.832	138
$M_T^W$ bin ( GeV)	purity	stability	number of events
0 - 23	0.535	0.608	742
23 - 58	0.523	0.574	1777
$\geq 58$	0.851	0.789	5093
$p_T^W$ bin ( GeV)	purity	stability	number of events
0 - 27	0.599	0.544	558
27 - 52	0.559	0.529	1141
52 - 78	0.549	0.539	1369
78 - 105	0.531	0.538	1190
105 - 134	0.537	0.557	928
134 - 166	0.537	0.569	610
166 - 200	0.526	0.568	336
200 - 237	0.532	0.575	183
$\geq 237$	0.689	0.794	150

Table 7: The selected bins for the measurement in the muon channel at a centre-of-mass energy of 7 TeV. In addition to the bin ranges<sup>33</sup> the purity, stability and number of expected  $t\bar{t}$  events are shown.

$E_T^{\text{miss}}$ bin ( GeV)	purity	stability	number of events
0 - 27	0.634	0.505	6400
27 - 52	0.557	0.507	9823
52 - 87	0.503	0.606	7792
87 - 130	0.517	0.643	3239
130 - 172	0.500	0.598	904
$\geq 172$	0.700	0.840	670
$H_T$ bin ( GeV)	purity	stability	number of events
0 - 186	0.556	0.514	430
186 - 216	0.511	0.508	1408
216 - 249	0.508	0.540	2878
249 - 286	0.511	0.540	3869
286 - 326	0.502	0.524	3892
326 - 368	0.508	0.511	3463
368 - 412	0.506	0.500	2828
412 - 462	0.532	0.510	2457
462 - 516	0.534	0.509	1857
516 - 574	0.547	0.500	1256
574 - 634	0.557	0.512	902
634 - 696	0.518	0.505	584
696 - 781	0.627	0.551	572
$\geq 781$	0.872	0.815	801
$S_T$ bin ( GeV)	purity	stability	number of events
0 - 277	0.580	0.500	463
277 - 319	0.539	0.500	1769
319 - 361	0.509	0.515	3204
361 - 408	0.505	0.522	4126
408 - 459	0.501	0.514	4035
459 - 514	0.504	0.510	3532
514 - 573	0.503	0.502	2780
573 - 637	0.517	0.510	2179
637 - 705	0.517	0.504	1507
705 - 774	0.506	0.508	1039
774 - 854	0.540	0.504	769
854 - 946	0.552	0.550	551
$\geq 946$	0.842	0.831	909
$M_T^W$ bin ( GeV)	purity	stability	number of events
0 - 23	0.515	0.577	3245
23 - 58	0.507	0.541	7446
$\geq 58$	0.823	0.774	20751
$p_T^W$ bin ( GeV)	purity	stability	number of events
0 - 27	0.556	0.505	1962
27 - 52	0.531	0.507	4354
52 - 78	0.527	0.513	5536
78 - 105	0.515	0.510	5131
105 - 134	0.510	0.533	4051
134 - 166	0.518	0.546	2775
166 - 200	0.502	0.544	1590
200 - 237	0.511	0.545	903
$\geq 237$	0.683	0.790	792

Table 8: The selected bins for the measurement in the electron channel at a centre-of-mass energy of 8 TeV. In addition to the bin ranges<sup>34</sup>the purity, stability and number of expected  $t\bar{t}$  events are shown.

$E_T^{\text{miss}}$ bin ( GeV)	purity	stability	number of events
0 - 27	0.638	0.511	7341
27 - 52	0.563	0.515	11569
52 - 87	0.526	0.610	9865
87 - 130	0.506	0.651	3814
130 - 172	0.504	0.592	1050
$\geq 172$	0.695	0.845	802
$H_T$ bin ( GeV)	purity	stability	number of events
0 - 186	0.559	0.514	527
186 - 216	0.518	0.515	1698
216 - 249	0.518	0.537	3521
249 - 286	0.507	0.548	4735
286 - 326	0.507	0.523	4725
326 - 368	0.500	0.504	4032
368 - 412	0.503	0.501	3297
412 - 462	0.536	0.503	2815
462 - 516	0.529	0.503	2087
516 - 574	0.549	0.520	1551
574 - 634	0.542	0.502	987
634 - 696	0.560	0.504	656
696 - 781	0.644	0.607	641
$\geq 781$	0.886	0.796	842
$S_T$ bin ( GeV)	purity	stability	number of events
0 - 277	0.583	0.523	629
277 - 319	0.548	0.519	2276
319 - 361	0.511	0.508	3895
361 - 408	0.504	0.522	5021
408 - 459	0.502	0.519	4855
459 - 514	0.508	0.512	4170
514 - 573	0.511	0.500	3248
573 - 637	0.502	0.504	2393
637 - 705	0.522	0.517	1766
705 - 774	0.519	0.500	1135
774 - 854	0.546	0.529	884
854 - 946	0.571	0.558	621
$\geq 946$	0.836	0.837	961
$M_T^W$ bin ( GeV)	purity	stability	number of events
0 - 23	0.506	0.589	3712
23 - 58	0.511	0.554	9078
$\geq 58$	0.836	0.774	25227
$p_T^W$ bin ( GeV)	purity	stability	number of events
0 - 27	0.589	0.520	2700
27 - 52	0.535	0.509	5484
52 - 78	0.524	0.509	6644
78 - 105	0.507	0.515	5918
105 - 134	0.509	0.526	4588
134 - 166	0.504	0.544	3012
166 - 200	0.513	0.546	1767
200 - 237	0.506	0.558	994
$\geq 237$	0.676	0.801	894

Table 9: The selected bins for the measurement in the muon channel at a centre-of-mass energy of 8 TeV. In addition to the bin ranges<sup>35</sup> the purity, stability and number of expected  $t\bar{t}$  events are shown.

### .3 Fitting variable QCD background template comparisons

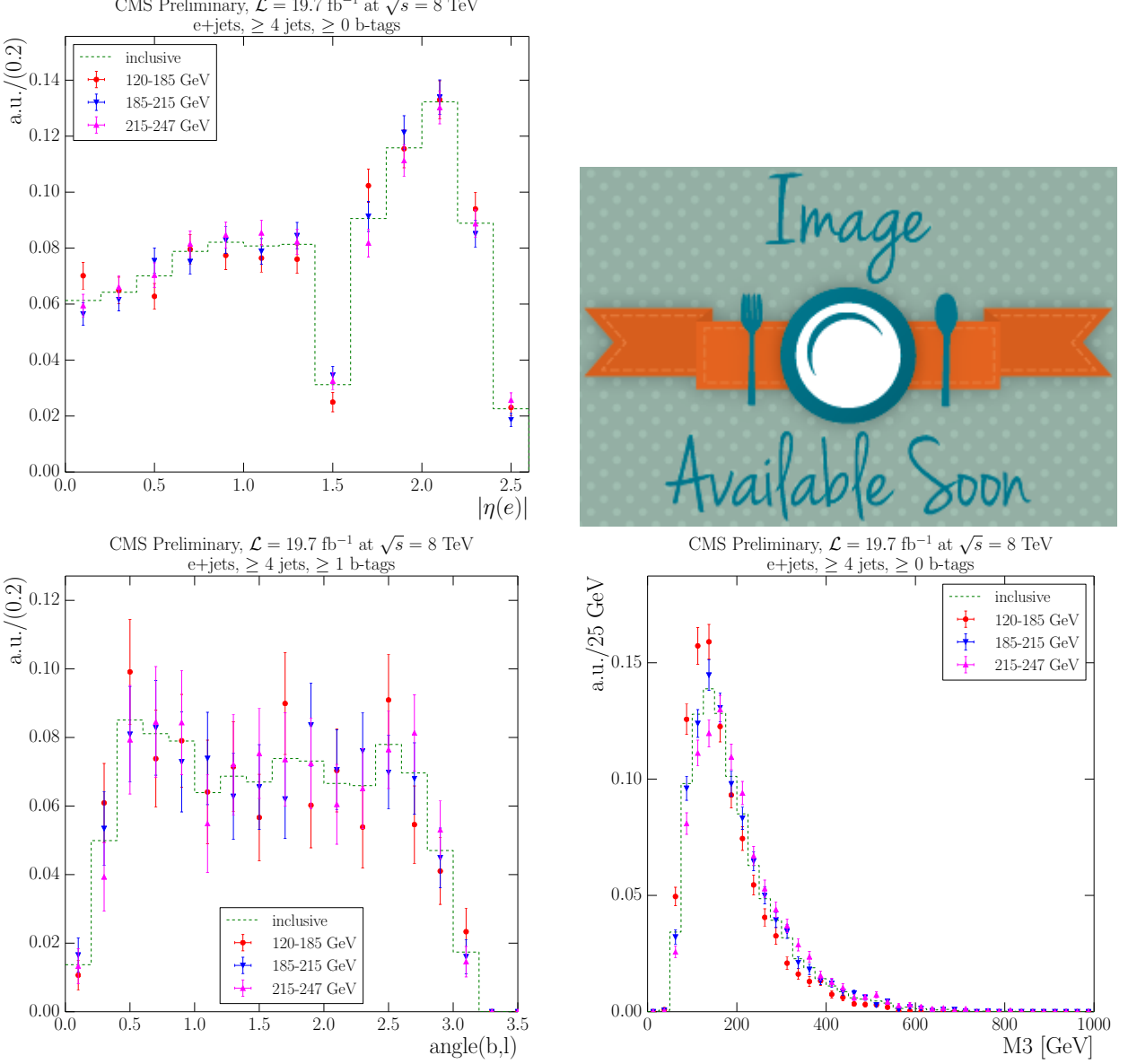


Figure 22: Normalised distributions of the QCD templates for the three fit variables at  $\sqrt{s} = 8 \text{ TeV}$  inclusive across all  $H_T$  bins and for the lowest three  $E_T^{\text{miss}}$  bins: electron  $|\eta|$  (upper left), muon  $|\eta|$  (upper right),  $\alpha$  (lower left) and  $M3$  (lower right).

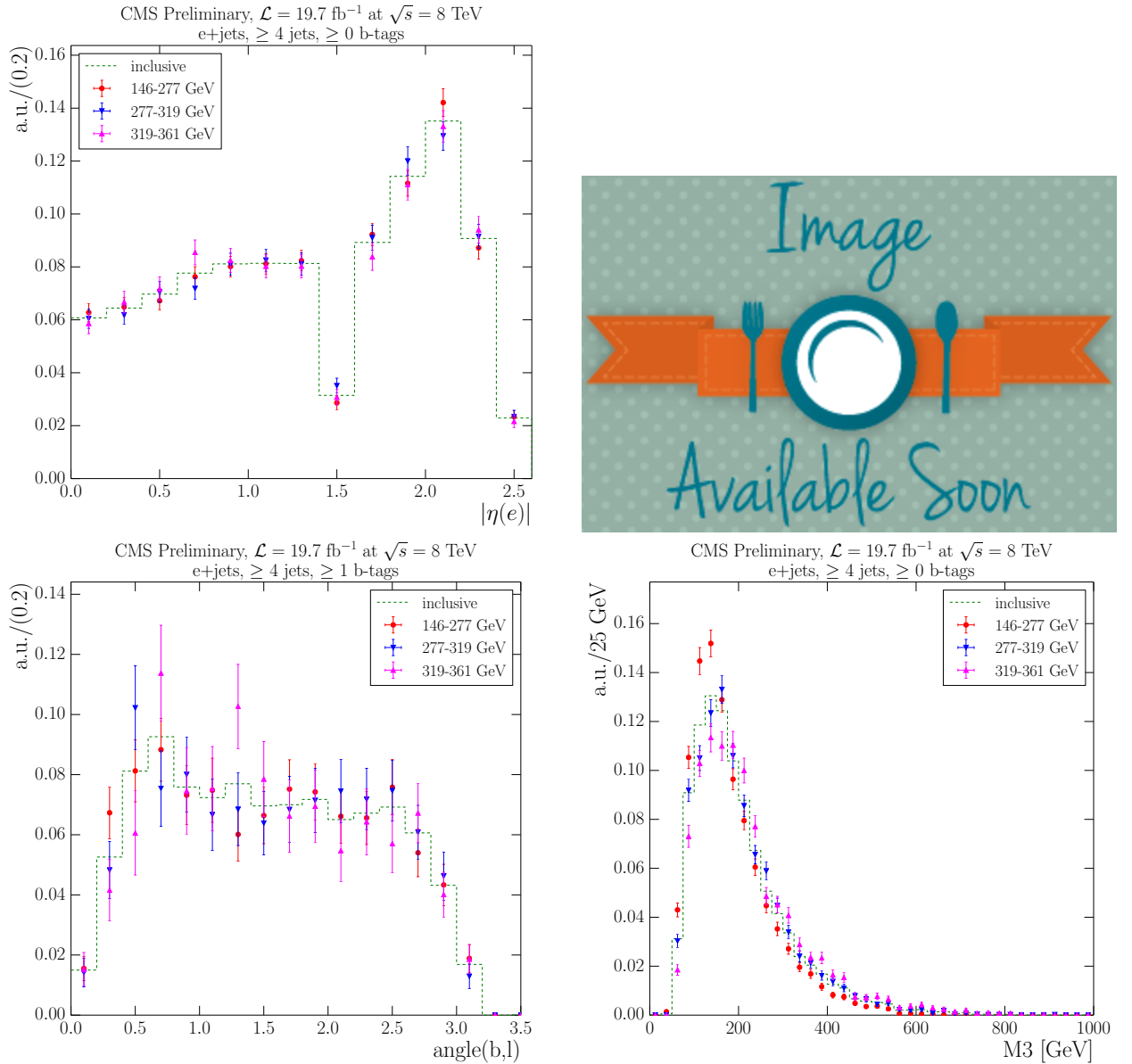


Figure 23: Normalised distributions of the QCD templates for the three fit variables at  $\sqrt{s} = 8 \text{ TeV}$  inclusive across all  $S_T$  bins and for the lowest three  $S_T$  bins: electron  $|\eta|$  (upper left), muon  $|\eta|$  (upper right),  $\alpha$  (lower left) and  $M3$  (lower right).

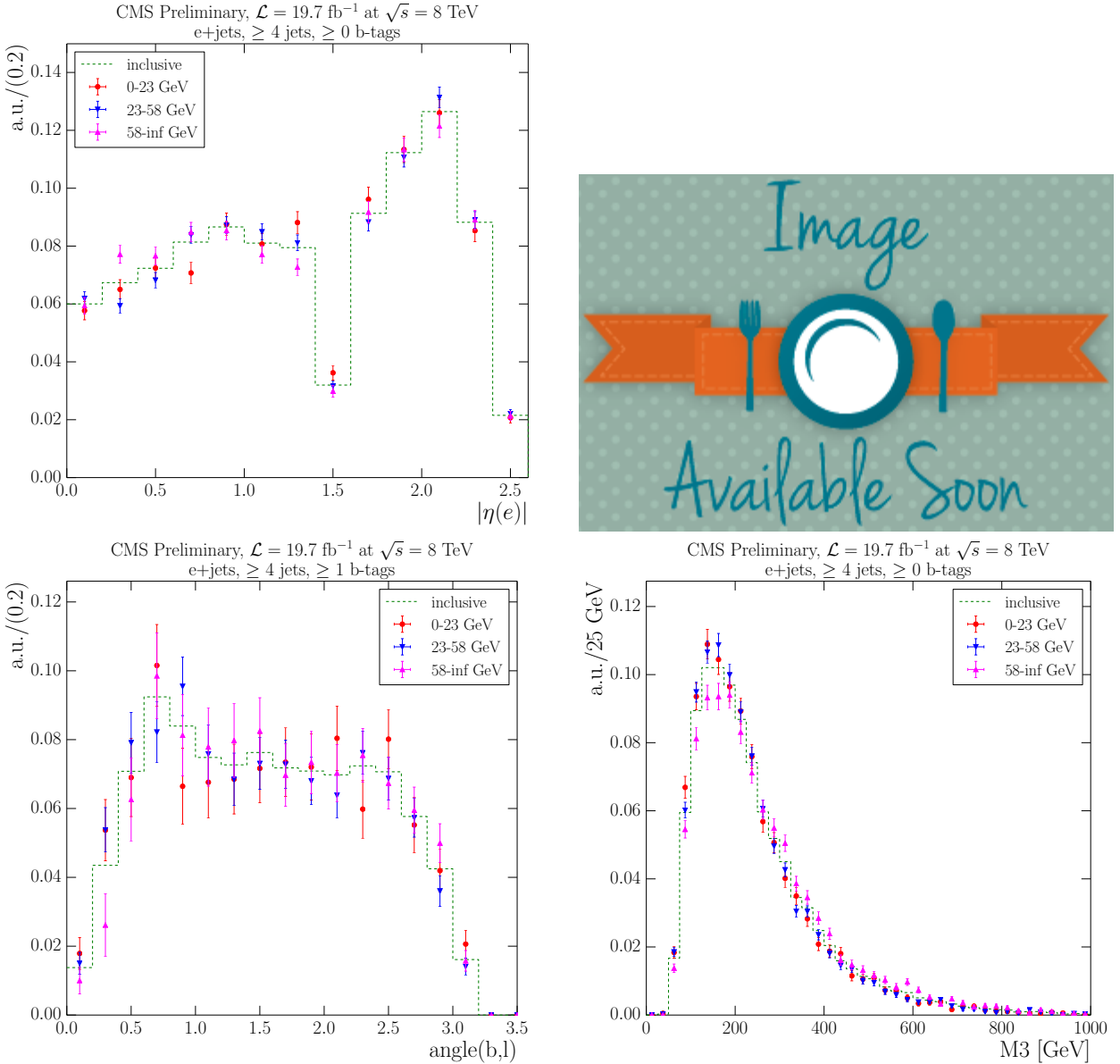


Figure 24: Normalised distributions of the QCD templates for the three fit variables at  $\sqrt{s} = 8 \text{ TeV}$  inclusive across all  $M_T^W$  bins and for the lowest three  $M_T^W$  bins: electron  $|\eta|$  (upper left), muon  $|\eta|$  (upper right),  $\alpha$  (lower left) and  $M_3$  (lower right).

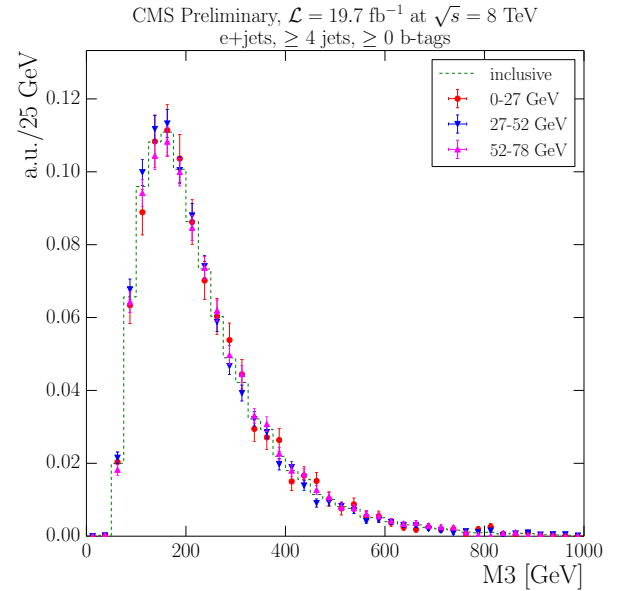
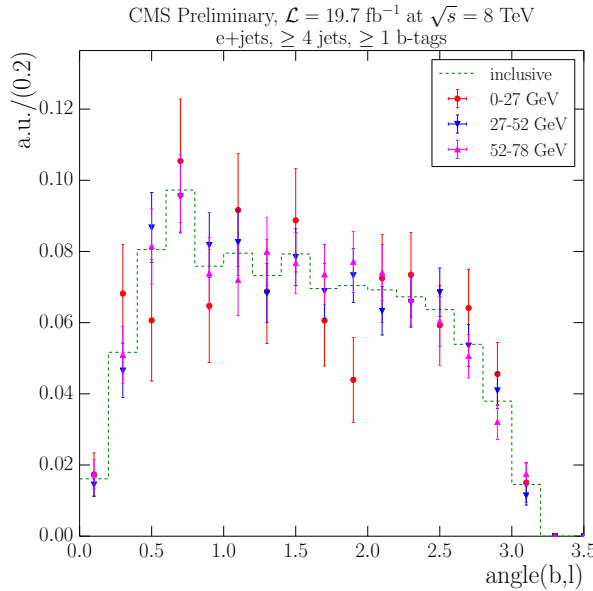
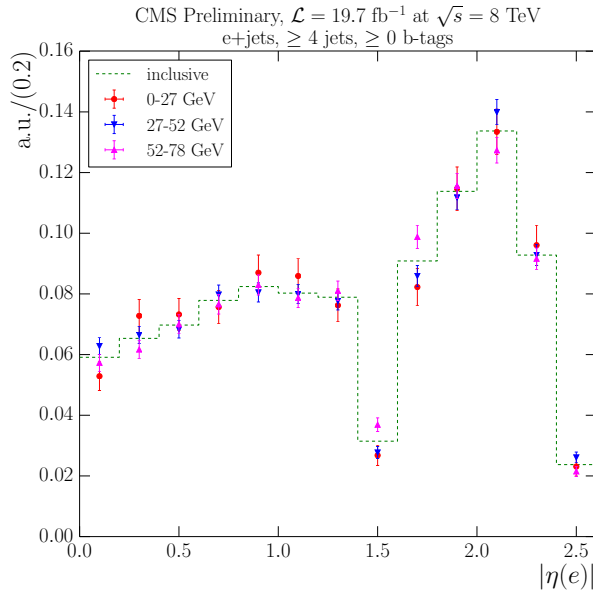


Figure 25: Normalised distributions of the QCD templates for the three fit variables at  $\sqrt{s} = 8 \text{ TeV}$  inclusive across all  $p_T^W$  bins and for the lowest three  $p_T^W$  bins: electron  $|\eta|$  (upper left), muon  $|\eta|$  (upper right),  $\alpha$  (lower left) and  $M3$  (lower right).

## 4 Fitting variable V+jets background template comparisons

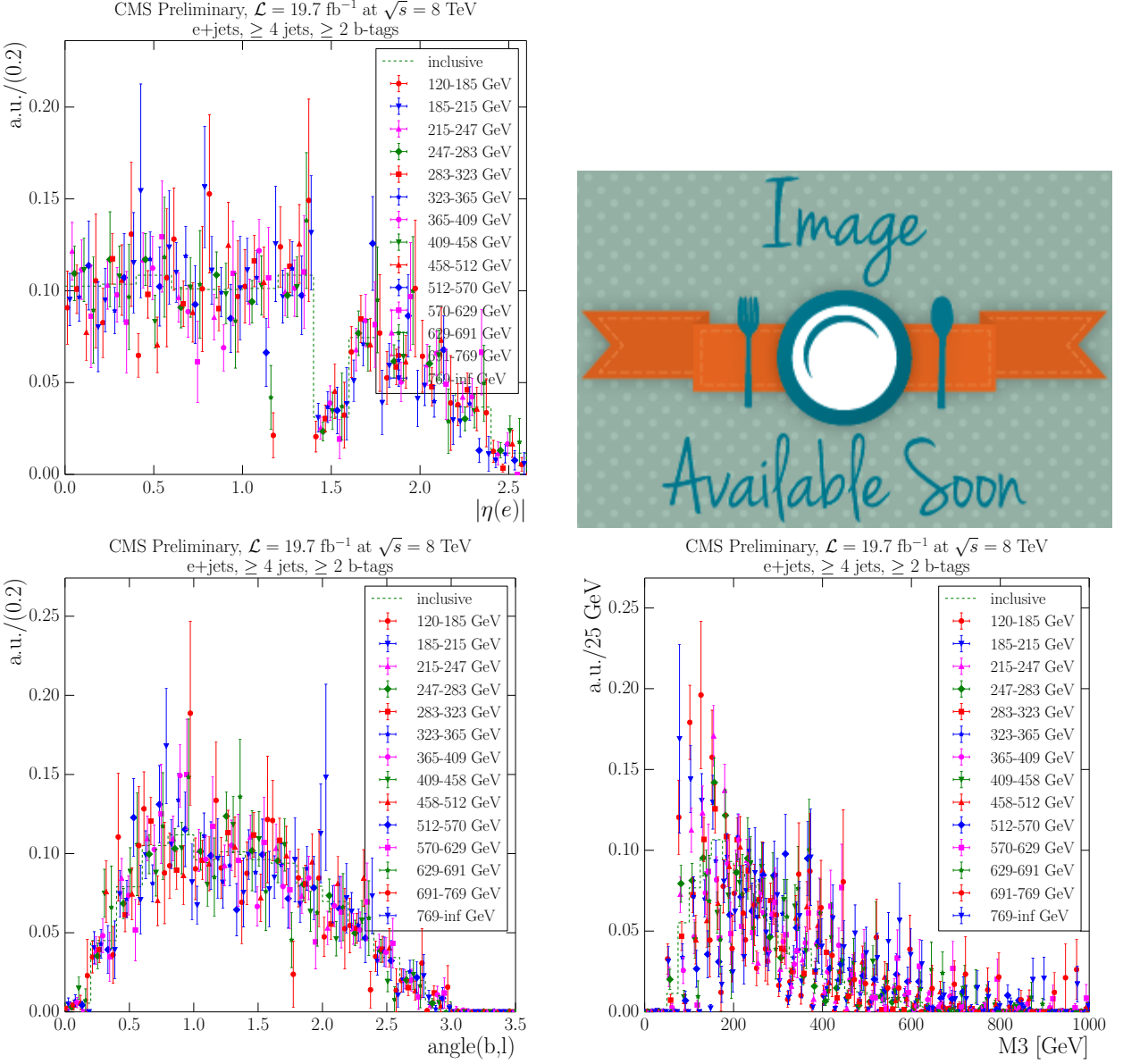


Figure 26: Normalised distributions of the V+jets templates for the three fit variables at  $\sqrt{s} = 8$  TeV inclusive across all  $H_T$  bins and for individual  $H_T$  bins: electron  $|\eta|$  (upper left), muon  $|\eta|$  (upper right),  $\alpha$  (lower left) and  $M_3$  (lower right).

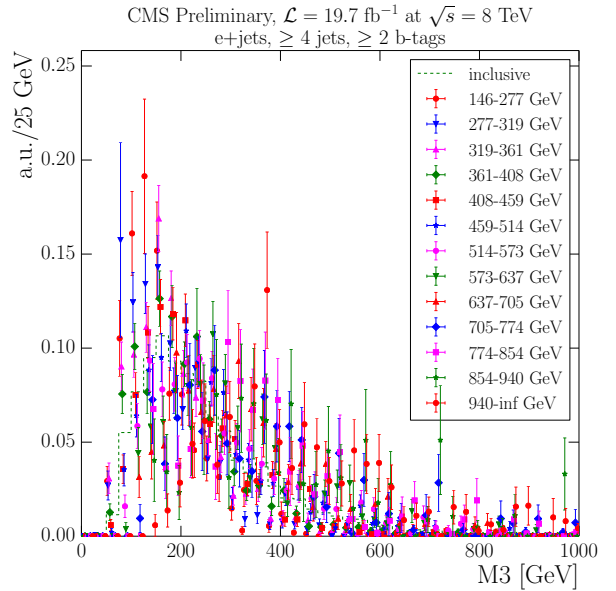
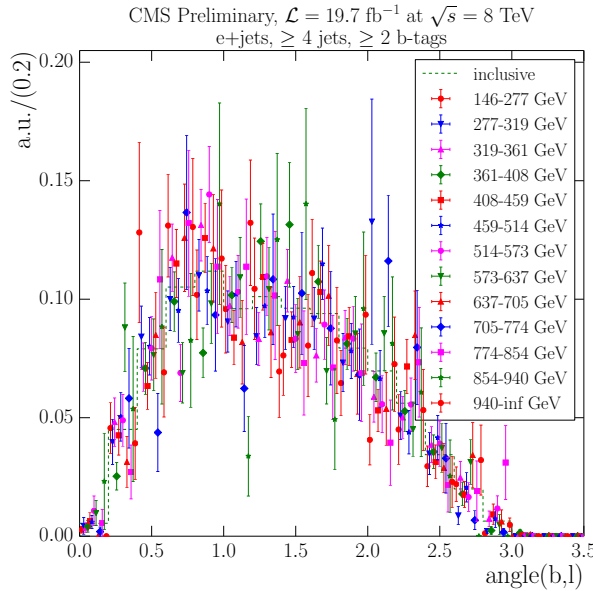
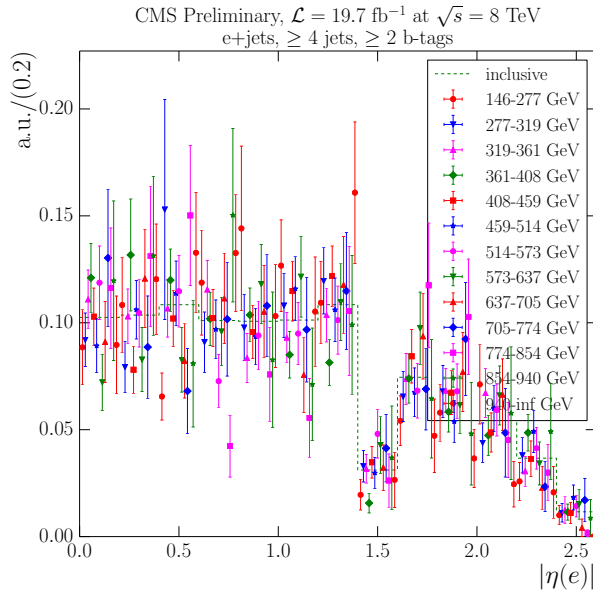


Figure 27: Normalised distributions of the V+jets templates for the three fit variables at  $\sqrt{s} = 8 \text{ TeV}$  inclusive across all  $S_T$  bins and for individual  $S_T$  bins: electron  $|\eta|$  (upper left), muon  $|\eta|$  (upper right),  $\alpha$  (lower left) and  $M3$  (lower right).

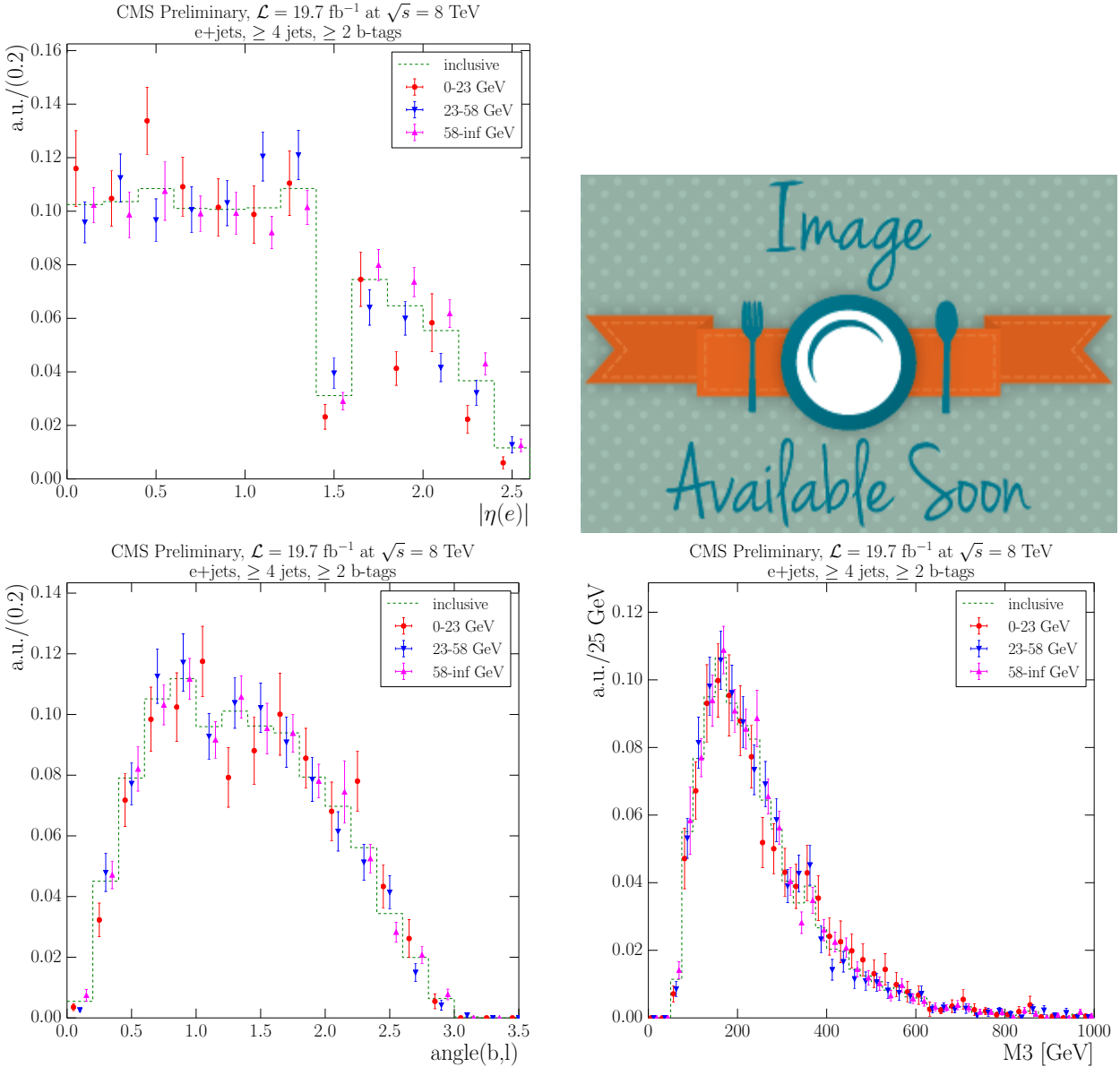


Figure 28: Normalised distributions of the V+jets templates for the three fit variables at  $\sqrt{s} = 8 \text{ TeV}$  inclusive across all  $M_T^W$  bins and for individual  $M_T^W$  bins: electron  $|\eta|$  (upper left), muon  $|\eta|$  (upper right),  $\alpha$  (lower left) and  $M_3$  (lower right).

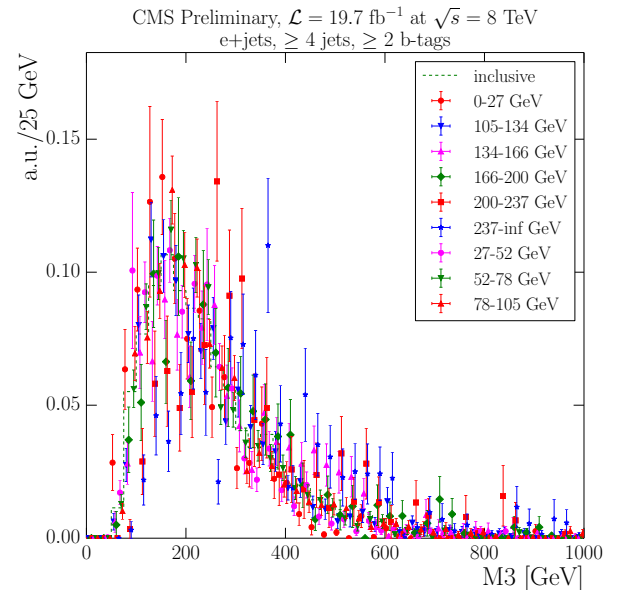
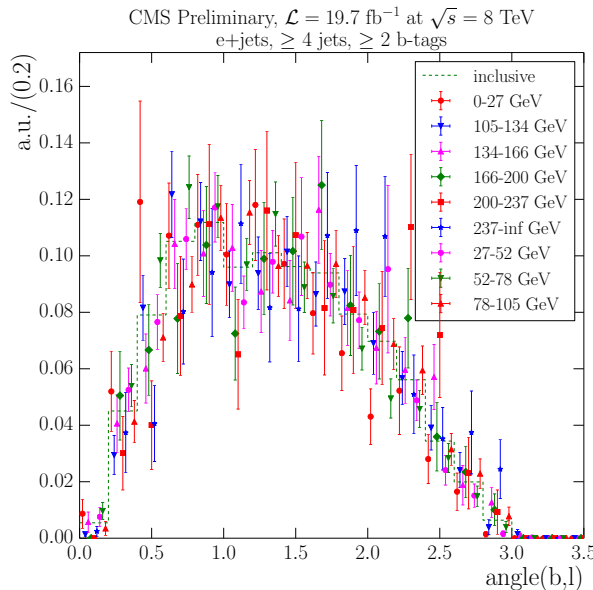
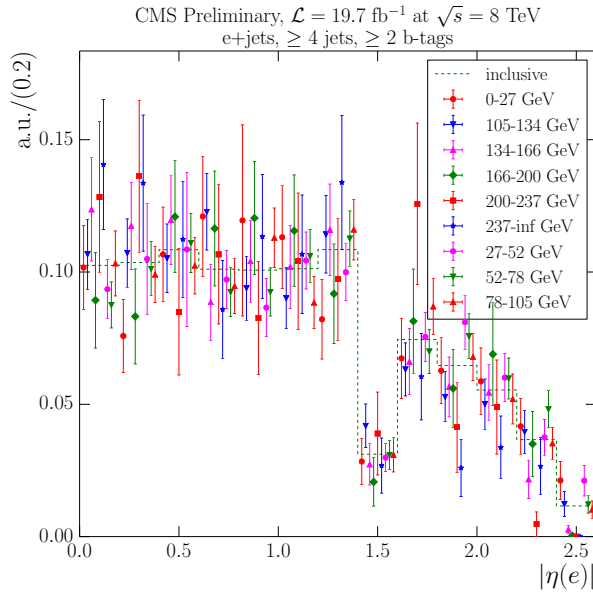


Figure 29: Normalised distributions of the V+jets templates for the three fit variables at  $\sqrt{s} = 8 \text{ TeV}$  inclusive across all  $p_T^W$  bins and for individual  $p_T^W$  bins: electron  $|\eta|$  (upper left), muon  $|\eta|$  (upper right),  $\alpha$  (lower left) and  $M3$  (lower right).

## .5 Fit Results Tables

Table 10: Fit results for the  $E_T^{\text{miss}}$  variable at a centre-of-mass energy of 7 TeV (electron channel).

Process	0–27 GeV	27–52 GeV	52–87 GeV	87–130 GeV	130–172 GeV	$\geq 172$ GeV	Total
t $t$ in	2535.4 $\pm$ 41.2	4519.5 $\pm$ 54.0	4023.3 $\pm$ 55.7	1727.2 $\pm$ 33.3	518.1 $\pm$ 18.5	287.9 $\pm$ 12.2	13611.5 $\pm$ 214.9
t $t$ fit	2383.4 $\pm$ 76.8	3833.7 $\pm$ 159.1	3448.4 $\pm$ 147.2	1445.2 $\pm$ 82.6	352.8 $\pm$ 36.0	207.4 $\pm$ 24.0	11671.0 $\pm$ 525.7
Single-Top in	82.6 $\pm$ 6.6	143.0 $\pm$ 8.9	120.0 $\pm$ 7.7	50.1 $\pm$ 4.9	19.2 $\pm$ 3.1	11.8 $\pm$ 2.0	426.7 $\pm$ 33.2
Single-Top fit	0.0 $\pm$ 3699.1	372.9 $\pm$ 195.9	395.4 $\pm$ 177.5	75.6 $\pm$ 86.8	72.2 $\pm$ 34.8	50.6 $\pm$ 21.5	966.5 $\pm$ 4215.7
W/Z + jets in	121.0 $\pm$ 8.7	139.1 $\pm$ 10.0	82.6 $\pm$ 5.9	31.0 $\pm$ 2.2	12.7 $\pm$ 0.9	9.4 $\pm$ 0.7	395.8 $\pm$ 28.4
W/Z + jets fit	496.6 $\pm$ 70.4	379.4 $\pm$ 109.6	140.2 $\pm$ 101.9	118.2 $\pm$ 57.5	0.0 $\pm$ 109.5	6.0 $\pm$ 13.4	1140.4 $\pm$ 462.4
QCD in	324.8 $\pm$ 15.0	243.5 $\pm$ 11.3	9.0 $\pm$ 0.4	1.3 $\pm$ 0.1	1.0 $\pm$ 0.0	1.0 $\pm$ 0.0	580.7 $\pm$ 26.9
QCD fit	0.0 $\pm$ 435.0	0.0 $\pm$ 18.7	0.0 $\pm$ 66.9	0.0 $\pm$ 13.4	14.0 $\pm$ 11.1	0.0 $\pm$ 24.3	14.0 $\pm$ 569.6
Sum MC in	3063.8 $\pm$ 71.5	5045.1 $\pm$ 84.2	4234.9 $\pm$ 69.7	1809.6 $\pm$ 40.5	551.1 $\pm$ 22.5	310.0 $\pm$ 15.0	15014.6 $\pm$ 303.4
Sum MC fit	2880.0 $\pm$ 4281.4	4586.0 $\pm$ 483.3	3984.0 $\pm$ 493.6	1639.0 $\pm$ 240.3	439.0 $\pm$ 191.4	264.0 $\pm$ 83.3	13792.0 $\pm$ 5773.3
Data	2880.0 $\pm$ 180.1	4586.0 $\pm$ 226.1	3984.0 $\pm$ 207.8	1639.0 $\pm$ 132.0	439.0 $\pm$ 66.7	264.0 $\pm$ 49.6	13792.0 $\pm$ 862.2

Table 11: Fit results for the  $E_T^{\text{miss}}$  variable at a centre-of-mass energy of 7 TeV (muon channel).

Process	0–27 GeV	27–52 GeV	52–87 GeV	87–130 GeV	130–172 GeV	$\geq 172$ GeV	Total
t $t$ in	2708.1 $\pm$ 41.8	4893.4 $\pm$ 58.0	4552.5 $\pm$ 52.2	1984.4 $\pm$ 34.2	594.5 $\pm$ 18.7	321.3 $\pm$ 13.1	15054.1 $\pm$ 217.8
t $t$ fit	1955.0 $\pm$ 116.9	3723.1 $\pm$ 156.2	3628.1 $\pm$ 145.3	1418.5 $\pm$ 86.6	384.1 $\pm$ 39.0	203.4 $\pm$ 24.5	11312.3 $\pm$ 568.4
Single-Top in	88.1 $\pm$ 6.6	151.0 $\pm$ 8.4	137.4 $\pm$ 8.1	58.0 $\pm$ 5.1	20.2 $\pm$ 3.0	14.1 $\pm$ 2.3	468.7 $\pm$ 33.5
Single-Top fit	329.9 $\pm$ 140.4	441.1 $\pm$ 199.9	293.3 $\pm$ 167.2	134.1 $\pm$ 87.1	50.0 $\pm$ 35.1	29.1 $\pm$ 23.4	1277.5 $\pm$ 653.2
W/Z + jets in	105.3 $\pm$ 6.1	144.3 $\pm$ 8.3	100.1 $\pm$ 5.8	39.1 $\pm$ 2.3	11.7 $\pm$ 0.7	10.6 $\pm$ 0.6	411.1 $\pm$ 23.7
W/Z + jets fit	194.0 $\pm$ 81.6	231.8 $\pm$ 119.8	37.6 $\pm$ 105.3	50.3 $\pm$ 61.1	0.0 $\pm$ 759.0	12.5 $\pm$ 15.6	526.4 $\pm$ 1142.4
QCD in	165.6 $\pm$ 6.9	27.0 $\pm$ 1.1	34.9 $\pm$ 1.5	0.1 $\pm$ 0.0	0.1 $\pm$ 0.0	0.1 $\pm$ 0.0	227.8 $\pm$ 9.5
QCD fit	0.0 $\pm$ 203.1	0.0 $\pm$ 322.0	0.0 $\pm$ 274.8	0.0 $\pm$ 170.6	11.9 $\pm$ 21.6	0.0 $\pm$ 18.9	11.9 $\pm$ 1010.9
Sum MC in	3067.2 $\pm$ 61.4	5215.6 $\pm$ 75.8	4824.9 $\pm$ 67.5	2081.6 $\pm$ 41.5	626.4 $\pm$ 22.3	346.1 $\pm$ 16.0	16161.8 $\pm$ 284.5
Sum MC fit	2479.0 $\pm$ 542.0	4396.0 $\pm$ 797.9	3959.1 $\pm$ 692.5	1603.0 $\pm$ 405.5	446.0 $\pm$ 854.6	245.0 $\pm$ 82.4	13128.1 $\pm$ 3374.9
Data	2479.0 $\pm$ 159.2	4396.0 $\pm$ 211.6	3959.0 $\pm$ 200.7	1603.0 $\pm$ 126.7	446.0 $\pm$ 65.9	245.0 $\pm$ 46.9	13128.0 $\pm$ 811.0

Table 12: Fit results for the  $H_T$  variable at a centre-of-mass energy of 7 TeV (electron channel).

Process	120–185 GeV	185–215 GeV	215–247 GeV	247–283 GeV	283–323 GeV	323–365 GeV	365–409 GeV	409–458 GeV	458–512 GeV	512–570 GeV	570–629 GeV	629–691 GeV	691–769 GeV	$\geq 769$ GeV	Total
tt in	222.7 $\pm$ 11.3	786.2 $\pm$ 24.2	1508.2 $\pm$ 32.8	1994.3 $\pm$ 37.6	2109.2 $\pm$ 37.2	1825.2 $\pm$ 37.7	1447.6 $\pm$ 30.9	1169.8 $\pm$ 25.7	866.6 $\pm$ 23.4	602.2 $\pm$ 18.7	381.6 $\pm$ 14.6	257.4 $\pm$ 12.0	192.5 $\pm$ 10.6	247.9 $\pm$ 11.9	13611.5 $\pm$ 328.7
t̄t fit	222.7 $\pm$ 40.9	730.4 $\pm$ 68.9	1409.7 $\pm$ 99.8	1996.7 $\pm$ 200.3	1788.2 $\pm$ 86.2	1502.0 $\pm$ 75.9	1203.0 $\pm$ 67.0	926.3 $\pm$ 66.0	665.2 $\pm$ 53.1	512.6 $\pm$ 45.3	335.0 $\pm$ 35.2	191.3 $\pm$ 23.8	158.6 $\pm$ 21.0	186.6 $\pm$ 28.8	11828.2 $\pm$ 912.3
Single-Top in	13.7 $\pm$ 2.7	31.6 $\pm$ 3.9	50.2 $\pm$ 5.1	58.7 $\pm$ 5.6	63.8 $\pm$ 5.9	52.8 $\pm$ 5.2	41.8 $\pm$ 4.8	33.3 $\pm$ 3.9	26.5 $\pm$ 3.6	18.5 $\pm$ 3.0	12.3 $\pm$ 2.5	8.0 $\pm$ 1.9	6.5 $\pm$ 1.7	9.1 $\pm$ 2.0	426.7 $\pm$ 51.7
Single-Top fit	78.7 $\pm$ 42.4	84.3 $\pm$ 81.3	232.2 $\pm$ 132.9	2.6 $\pm$ 4119.9	74.8 $\pm$ 119.3	78.6 $\pm$ 94.3	91.8 $\pm$ 72.1	134.1 $\pm$ 66.0	86.4 $\pm$ 51.8	48.1 $\pm$ 39.8	33.2 $\pm$ 31.2	16.9 $\pm$ 19.2	5.4 $\pm$ 18.5	47.2 $\pm$ 27.2	1014.5 $\pm$ 4915.9
W/Z + jets in	24.2 $\pm$ 1.7	33.9 $\pm$ 2.4	47.0 $\pm$ 3.4	47.5 $\pm$ 3.4	52.7 $\pm$ 3.8	42.9 $\pm$ 3.1	33.5 $\pm$ 2.4	33.0 $\pm$ 2.4	27.2 $\pm$ 2.0	18.2 $\pm$ 1.3	13.6 $\pm$ 1.0	6.8 $\pm$ 0.5	5.9 $\pm$ 0.4	9.2 $\pm$ 0.7	395.8 $\pm$ 28.4
W/Z + jets fit	0.0 $\pm$ 15.8	30.2 $\pm$ 52.8	7.1 $\pm$ 112.2	193.7 $\pm$ 92.3	247.0 $\pm$ 78.7	176.4 $\pm$ 63.8	28.0 $\pm$ 95.3	62.6 $\pm$ 34.8	52.5 $\pm$ 28.9	18.0 $\pm$ 40.2	9.8 $\pm$ 16.1	29.8 $\pm$ 14.0	0.0 $\pm$ 13.8	0.0 $\pm$ 13.8	855.0 $\pm$ 672.5
QCD in	100.7 $\pm$ 4.7	43.7 $\pm$ 2.0	5.8 $\pm$ 0.3	194.3 $\pm$ 9.0	81.7 $\pm$ 3.8	82.1 $\pm$ 3.8	17.5 $\pm$ 0.8	18.7 $\pm$ 0.9	3.4 $\pm$ 0.2	9.7 $\pm$ 0.4	8.1 $\pm$ 0.4	5.5 $\pm$ 0.3	1.8 $\pm$ 0.1	5.6 $\pm$ 0.3	578.7 $\pm$ 26.8
QCD fit	15.5 $\pm$ 11.4	7.2 $\pm$ 32.7	0.0 $\pm$ 84.0	0.0 $\pm$ 16.6	0.0 $\pm$ 30.6	0.0 $\pm$ 21.2	49.1 $\pm$ 41.9	0.0 $\pm$ 18.1	0.0 $\pm$ 9.8	15.3 $\pm$ 19.0	0.0 $\pm$ 6.2	0.0 $\pm$ 5.1	0.0 $\pm$ 2.0	7.2 $\pm$ 5.8	94.4 $\pm$ 304.2
Sum MC in	361.3 $\pm$ 20.3	895.4 $\pm$ 32.5	1611.1 $\pm$ 41.6	2294.8 $\pm$ 55.6	2307.4 $\pm$ 50.7	2003.0 $\pm$ 49.8	1540.4 $\pm$ 38.9	1254.8 $\pm$ 32.9	923.7 $\pm$ 29.1	648.7 $\pm$ 23.5	415.6 $\pm$ 18.5	277.7 $\pm$ 14.6	206.8 $\pm$ 12.8	271.8 $\pm$ 14.8	15012.6 $\pm$ 435.6
Sum MC fit	317.0 $\pm$ 110.5	852.0 $\pm$ 235.8	1649.0 $\pm$ 428.9	2193.0 $\pm$ 4429.2	2110.0 $\pm$ 314.7	1757.0 $\pm$ 255.1	1372.0 $\pm$ 276.3	1123.0 $\pm$ 184.9	804.0 $\pm$ 143.7	594.0 $\pm$ 144.3	378.0 $\pm$ 88.7	238.0 $\pm$ 62.0	164.0 $\pm$ 55.2	241.0 $\pm$ 75.6	13792.0 $\pm$ 6805.0
Data	317.0 $\pm$ 61.1	852.0 $\pm$ 97.6	1649.0 $\pm$ 135.2	2193.0 $\pm$ 155.3	2110.0 $\pm$ 153.2	1757.0 $\pm$ 139.5	1372.0 $\pm$ 122.7	1123.0 $\pm$ 109.6	804.0 $\pm$ 92.2	594.0 $\pm$ 79.5	378.0 $\pm$ 62.2	238.0 $\pm$ 49.8	164.0 $\pm$ 38.8	241.0 $\pm$ 49.6	13792.0 $\pm$ 1346.4

Table 13: Fit results for the  $H_T$  variable at a centre-of-mass energy of 7 TeV (muon channel).

Process	120–185 GeV	185–215 GeV	215–247 GeV	247–283 GeV	283–323 GeV	323–365 GeV	365–409 GeV	409–458 GeV	458–512 GeV	512–570 GeV	570–629 GeV	629–691 GeV	691–769 GeV	$\geq 769$ GeV	Total
tt in	257.1 $\pm$ 12.1	899.8 $\pm$ 22.6	1741.5 $\pm$ 32.0	2285.3 $\pm$ 37.9	2351.5 $\pm$ 40.6	2015.9 $\pm$ 35.3	1584.3 $\pm$ 34.1	1256.4 $\pm$ 27.8	912.9 $\pm$ 22.2	634.3 $\pm$ 18.5	400.0 $\pm$ 14.8	266.9 $\pm$ 12.9	196.1 $\pm$ 10.4	252.1 $\pm$ 12.4	15054.1 $\pm$ 333.6
t̄t fit	301.2 $\pm$ 43.4	845.8 $\pm$ 94.2	1419.1 $\pm$ 106.4	1844.9 $\pm$ 106.7	1888.1 $\pm$ 77.9	1458.1 $\pm$ 84.8	1063.1 $\pm$ 67.9	929.8 $\pm$ 55.9	569.3 $\pm$ 51.0	447.7 $\pm$ 40.0	258.8 $\pm$ 33.8	140.0 $\pm$ 23.6	111.8 $\pm$ 19.2	129.0 $\pm$ 27.6	11406.6 $\pm$ 832.4
Single-Top in	17.2 $\pm$ 3.1	35.4 $\pm$ 4.0	56.4 $\pm$ 5.2	64.2 $\pm$ 5.6	68.1 $\pm$ 5.7	53.3 $\pm$ 4.9	46.5 $\pm$ 4.6	37.5 $\pm$ 4.2	29.0 $\pm$ 3.6	20.2 $\pm$ 2.9	13.4 $\pm$ 2.3	8.0 $\pm$ 1.8	8.0 $\pm$ 1.9	11.5 $\pm$ 2.2	468.7 $\pm$ 52.2
Single-Top fit	43.8 $\pm$ 41.5	60.8 $\pm$ 104.4	44.0 $\pm$ 144.3	169.8 $\pm$ 136.5	155.7 $\pm$ 94.4	296.2 $\pm$ 96.4	194.9 $\pm$ 70.4	65.1 $\pm$ 55.5	125.7 $\pm$ 48.7	64.9 $\pm$ 36.8	44.2 $\pm$ 33.1	38.5 $\pm$ 20.6	30.9 $\pm$ 17.3	69.0 $\pm$ 27.0	1403.5 $\pm$ 926.7
W/Z + jets in	27.4 $\pm$ 1.6	37.4 $\pm$ 2.2	46.9 $\pm$ 2.7	54.0 $\pm$ 3.1	52.6 $\pm$ 3.0	47.4 $\pm$ 2.7	36.5 $\pm$ 2.1	30.5 $\pm$ 1.8	26.0 $\pm$ 1.5	17.1 $\pm$ 1.0	10.7 $\pm$ 0.6	7.5 $\pm$ 0.4	6.2 $\pm$ 0.4	11.0 $\pm$ 0.6	411.1 $\pm$ 23.7
W/Z + jets fit	0.0 $\pm$ 12.5	15.3 $\pm$ 29.8	48.3 $\pm$ 100.3	26.3 $\pm$ 64.9	28.9 $\pm$ 100.8	22.7 $\pm$ 56.3	0.1 $\pm$ 2443.8	1.1 $\pm$ 339.6	0.0 $\pm$ 46.9	0.0 $\pm$ 23.6	0.9 $\pm$ 63.4	16.5 $\pm$ 30.7	6.3 $\pm$ 9.0	0.0 $\pm$ 4.9	166.4 $\pm$ 3326.3
QCD in	32.8 $\pm$ 1.4	51.7 $\pm$ 2.3	18.0 $\pm$ 0.8	55.2 $\pm$ 2.4	21.5 $\pm$ 0.9	22.0 $\pm$ 1.0	18.4 $\pm$ 0.8	1.8 $\pm$ 0.1	2.3 $\pm$ 0.1	1.8 $\pm$ 0.1	0.8 $\pm$ 0.0	0.1 $\pm$ 0.0	1.1 $\pm$ 0.0	0.2 $\pm$ 0.0	227.7 $\pm$ 9.9
QCD fit	0.0 $\pm$ 22.0	0.0 $\pm$ 34.9	112.6 $\pm$ 84.0	0.0 $\pm$ 106.0	32.3 $\pm$ 71.2	0.0 $\pm$ 52.0	0.0 $\pm$ 149.4	0.0 $\pm$ 26.4	0.0 $\pm$ 11.4	5.4 $\pm$ 12.8	0.0 $\pm$ 12.6	1.1 $\pm$ 27.2	0.0 $\pm$ 244.4	0.0 $\pm$ 3.2	151.4 $\pm$ 1102.5
Sum MC in	334.6 $\pm$ 18.2	1024.3 $\pm$ 31.0	1862.8 $\pm$ 40.7	2458.6 $\pm$ 49.0	2493.7 $\pm$ 50.2	2138.6 $\pm$ 44.0	1685.7 $\pm$ 41.6	1326.1 $\pm$ 33.9	970.3 $\pm$ 27.4	673.4 $\pm$ 22.5	424.8 $\pm$ 17.8	282.5 $\pm$ 15.2	211.4 $\pm$ 12.7	274.9 $\pm$ 15.3	16161.6 $\pm$ 419.4
Sum MC fit	345.0 $\pm$ 119.4	922.0 $\pm$ 263.2	1624.0 $\pm$ 435.0	2041.0 $\pm$ 414.1	2105.0 $\pm$ 344.3	1777.0 $\pm$ 289.5	1258.0 $\pm$ 2731.6	996.0 $\pm$ 477.4	695.0 $\pm$ 157.9	518.0 $\pm$ 113.1	304.0 $\pm$ 142.8	196.0 $\pm$ 347.0	149.0 $\pm$ 290.0	198.0 $\pm$ 62.7	13128.0 $\pm$ 6187.9
Data	345.0 $\pm$ 59.2	922.0 $\pm$ 97.6	1624.0 $\pm$ 129.6	2041.0 $\pm$ 143.7	2105.0 $\pm$ 146.0	1777.0 $\pm$ 133.9	1258.0 $\pm$ 112.8	996.0 $\pm$ 100.5	695.0 $\pm$ 83.3	518.0 $\pm$ 71.0	304.0 $\pm$ 53.8	196.0 $\pm$ 43.3	149.0 $\pm$ 38.4	198.0 $\pm$ 43.6	13128.0 $\pm$ 1256.8

Table 14: Fit results for the  $S_T$  variable at a centre-of-mass energy of 7 TeV (electron channel).

Process	146–277 GeV	277–319 GeV	319–361 GeV	361–408 GeV	408–459 GeV	459–514 GeV	514–573 GeV	573–637 GeV	637–705 GeV	705–774 GeV	774–854 GeV	854–940 GeV	$\geq 940$ GeV	Total
t̄t in	247.4 $\pm$ 12.7	942.7 $\pm$ 23.5	1724.6 $\pm$ 39.1	2205.3 $\pm$ 37.6	2138.3 $\pm$ 36.5	1830.2 $\pm$ 38.5	1435.5 $\pm$ 30.3	1056.5 $\pm$ 25.6	724.8 $\pm$ 20.4	465.8 $\pm$ 15.8	338.8 $\pm$ 14.1	210.6 $\pm$ 10.5	290.9 $\pm$ 12.8	13611.5 $\pm$ 317.4
t̄t fit	234.8 $\pm$ 40.6	899.1 $\pm$ 94.7	1610.4 $\pm$ 101.3	2027.1 $\pm$ 60.7	1907.2 $\pm$ 84.7	1572.8 $\pm$ 79.0	1056.7 $\pm$ 69.4	788.4 $\pm$ 63.4	619.7 $\pm$ 45.7	327.3 $\pm$ 37.0	264.3 $\pm$ 27.1	180.8 $\pm$ 24.1	185.3 $\pm$ 25.6	11674.0 $\pm$ 753.1
Single-Top in	15.1 $\pm$ 2.9	36.5 $\pm$ 4.3	54.5 $\pm$ 5.2	61.0 $\pm$ 5.7	62.4 $\pm$ 5.9	54.3 $\pm$ 5.6	41.0 $\pm$ 4.4	31.5 $\pm$ 3.6	23.8 $\pm$ 3.4	15.8 $\pm$ 2.7	11.2 $\pm$ 2.2	7.6 $\pm$ 1.9	11.9 $\pm$ 2.2	426.7 $\pm$ 50.0
Single-Top fit	85.0 $\pm$ 46.0	152.0 $\pm$ 117.4	152.9 $\pm$ 118.6	0.0 $\pm$ 230.9	143.2 $\pm$ 106.3	66.2 $\pm$ 87.4	197.2 $\pm$ 71.6	163.7 $\pm$ 63.4	71.5 $\pm$ 43.6	57.5 $\pm$ 34.8	55.8 $\pm$ 25.5	30.1 $\pm$ 22.3	63.0 $\pm$ 24.5	1238.1 $\pm$ 992.4
W/Z + jets in	28.2 $\pm$ 2.0	41.9 $\pm$ 3.0	46.5 $\pm$ 3.3	51.7 $\pm$ 3.7	50.9 $\pm$ 3.7	39.9 $\pm$ 2.9	38.8 $\pm$ 2.8	28.0 $\pm$ 2.0	25.1 $\pm$ 1.8	15.3 $\pm$ 1.1	10.4 $\pm$ 0.7	6.9 $\pm$ 0.5	12.0 $\pm$ 0.9	395.8 $\pm$ 28.4
W/Z + jets fit	4.8 $\pm$ 60.9	47.9 $\pm$ 65.6	94.7 $\pm$ 48.7	233.9 $\pm$ 52.8	121.6 $\pm$ 70.1	161.9 $\pm$ 58.7	70.1 $\pm$ 39.9	23.8 $\pm$ 62.9	12.4 $\pm$ 40.9	40.2 $\pm$ 18.7	1.0 $\pm$ 44.7	0.0 $\pm$ 26.0	0.0 $\pm$ 33.5	812.3 $\pm$ 623.4
QCD in	44.3 $\pm$ 2.1	143.2 $\pm$ 6.6	6.6 $\pm$ 0.3	235.3 $\pm$ 10.9	78.7 $\pm$ 3.6	11.3 $\pm$ 0.5	16.2 $\pm$ 0.8	14.4 $\pm$ 0.7	3.9 $\pm$ 0.2	9.5 $\pm$ 0.4	7.1 $\pm$ 0.3	4.0 $\pm$ 0.2	4.1 $\pm$ 0.2	578.7 $\pm$ 26.8
QCD fit	26.3 $\pm$ 22.4	15.0 $\pm$ 33.1	0.0 $\pm$ 39.4	0.0 $\pm$ 32.2	0.0 $\pm$ 21.0	0.0 $\pm$ 28.6	0.0 $\pm$ 22.6	17.1 $\pm$ 28.7	2.5 $\pm$ 27.5	0.0 $\pm$ 92.3	0.0 $\pm$ 4.2	0.0 $\pm$ 5.4	6.7 $\pm$ 5.9	67.6 $\pm$ 363.3
Sum MC in	335.0 $\pm$ 19.7	1164.3 $\pm$ 37.5	1832.2 $\pm$ 48.0	2553.3 $\pm$ 58.0	2330.3 $\pm$ 49.7	1935.8 $\pm$ 47.5	1531.6 $\pm$ 38.2	1130.5 $\pm$ 31.9	777.6 $\pm$ 25.8	506.4 $\pm$ 20.1	367.5 $\pm$ 17.4	229.1 $\pm$ 13.0	318.9 $\pm$ 16.1	15012.6 $\pm$ 422.7
Sum MC fit	351.0 $\pm$ 169.8	1114.0 $\pm$ 310.8	1858.0 $\pm$ 308.1	2261.0 $\pm$ 376.6	2172.0 $\pm$ 282.2	1801.0 $\pm$ 253.8	1324.0 $\pm$ 203.4	993.0 $\pm$ 218.4	706.0 $\pm$ 157.7	425.0 $\pm$ 182.7	321.0 $\pm$ 101.5	211.0 $\pm$ 77.8	255.0 $\pm$ 89.5	13792.0 $\pm$ 2732.2
Data	351.0 $\pm$ 64.6	1114.0 $\pm$ 113.2	1858.0 $\pm$ 143.3	2261.0 $\pm$ 158.2	2172.0 $\pm$ 154.8	1801.0 $\pm$ 141.3	1324.0 $\pm$ 119.1	993.0 $\pm$ 102.0	706.0 $\pm$ 86.0	425.0 $\pm$ 66.6	321.0 $\pm$ 54.5	211.0 $\pm$ 46.3	255.0 $\pm$ 50.2	13792.0 $\pm$ 1300.1

Table 15: Fit results for the  $S_T$  variable at a centre-of-mass energy of 7 TeV (muon channel).

Process	146–277 GeV	277–319 GeV	319–361 GeV	361–408 GeV	408–459 GeV	459–514 GeV	514–573 GeV	573–637 GeV	637–705 GeV	705–774 GeV	774–854 GeV	854–940 GeV	$\geq 940$ GeV	Total
t̄t in	313.0 $\pm$ 13.5	1118.1 $\pm$ 25.9	2000.9 $\pm$ 34.2	2481.7 $\pm$ 38.9	2395.8 $\pm$ 41.7	2008.5 $\pm$ 37.9	1519.0 $\pm$ 30.1	1112.6 $\pm$ 25.2	769.5 $\pm$ 21.2	479.7 $\pm$ 16.0	348.0 $\pm$ 13.7	214.6 $\pm$ 10.6	292.8 $\pm$ 13.3	15054.1 $\pm$ 322.2
t̄t fit	302.8 $\pm$ 55.7	1080.7 $\pm$ 89.6	1752.4 $\pm$ 93.1	1911.4 $\pm$ 103.4	1851.6 $\pm$ 88.0	1334.0 $\pm$ 86.0	1086.3 $\pm$ 66.2	787.9 $\pm$ 54.8	514.2 $\pm$ 44.7	343.6 $\pm$ 29.9	212.2 $\pm$ 27.1	105.3 $\pm$ 21.4	160.3 $\pm$ 24.5	11442.6 $\pm$ 784.2
Single-Top in	18.0 $\pm$ 3.2	42.3 $\pm$ 4.5	58.2 $\pm$ 5.3	71.1 $\pm$ 5.9	64.6 $\pm$ 5.4	58.0 $\pm$ 5.2	46.3 $\pm$ 4.7	34.8 $\pm$ 3.9	24.5 $\pm$ 3.4	16.2 $\pm$ 2.6	12.0 $\pm$ 2.3	8.4 $\pm$ 1.8	14.1 $\pm$ 2.3	468.7 $\pm$ 50.4
Single-Top fit	67.5 $\pm$ 56.7	89.7 $\pm$ 100.6	17.7 $\pm$ 273.3	215.4 $\pm$ 131.8	172.0 $\pm$ 99.3	310.7 $\pm$ 94.8	109.7 $\pm$ 62.2	83.2 $\pm$ 51.4	58.2 $\pm$ 42.9	29.7 $\pm$ 27.3	54.3 $\pm$ 26.6	44.7 $\pm$ 19.7	56.7 $\pm$ 23.3	1309.5 $\pm$ 1009.9
W/Z + jets in	30.9 $\pm$ 1.8	42.5 $\pm$ 2.4	54.0 $\pm$ 3.1	53.6 $\pm$ 3.1	54.8 $\pm$ 3.2	44.9 $\pm$ 2.6	38.8 $\pm$ 2.2	25.0 $\pm$ 1.4	22.1 $\pm$ 1.3	15.4 $\pm$ 0.9	10.0 $\pm$ 0.6	6.1 $\pm$ 0.4	12.9 $\pm$ 0.7	411.1 $\pm$ 23.7
W/Z + jets fit	0.0 $\pm$ 15.1	36.3 $\pm$ 57.3	74.9 $\pm$ 78.2	82.2 $\pm$ 71.5	29.6 $\pm$ 87.0	16.1 $\pm$ 203.3	0.0 $\pm$ 29.3	0.0 $\pm$ 85.8	7.7 $\pm$ 133.2	8.8 $\pm$ 13.8	4.3 $\pm$ 32.3	9.9 $\pm$ 8.8	0.0 $\pm$ 3.8	269.9 $\pm$ 819.4
QCD in	59.4 $\pm$ 2.5	64.5 $\pm$ 2.7	18.8 $\pm$ 0.8	22.5 $\pm$ 0.9	36.7 $\pm$ 1.5	19.5 $\pm$ 0.8	2.3 $\pm$ 0.1	1.9 $\pm$ 0.1	0.8 $\pm$ 0.0	0.1 $\pm$ 0.0	1.0 $\pm$ 0.0	0.1 $\pm$ 0.0	0.3 $\pm$ 0.0	227.7 $\pm$ 9.6
QCD fit	2.7 $\pm$ 24.3	24.4 $\pm$ 62.2	0.0 $\pm$ 112.4	0.0 $\pm$ 78.2	70.8 $\pm$ 58.6	7.2 $\pm$ 249.9	0.0 $\pm$ 15.4	0.0 $\pm$ 15.1	1.0 $\pm$ 890.5	0.0 $\pm$ 13.7	0.2 $\pm$ 466.9	0.0 $\pm$ 54.3	0.0 $\pm$ 2.3	106.2 $\pm$ 2043.7
Sum MC in	421.3 $\pm$ 20.9	1267.4 $\pm$ 35.6	2131.8 $\pm$ 43.4	2628.9 $\pm$ 48.8	2551.9 $\pm$ 51.8	2130.9 $\pm$ 46.4	1606.4 $\pm$ 37.0	1174.3 $\pm$ 30.6	817.0 $\pm$ 25.8	511.5 $\pm$ 19.5	371.0 $\pm$ 16.6	229.3 $\pm$ 12.8	320.1 $\pm$ 16.4	16161.7 $\pm$ 405.8
Sum MC fit	373.0 $\pm$ 151.7	1231.1 $\pm$ 309.6	1845.0 $\pm$ 557.0	2209.0 $\pm$ 384.9	2124.0 $\pm$ 333.0	1668.0 $\pm$ 633.9	1196.0 $\pm$ 173.1	871.0 $\pm$ 207.2	581.0 $\pm$ 1111.3	382.0 $\pm$ 84.6	271.0 $\pm$ 552.9	160.0 $\pm$ 104.2	217.0 $\pm$ 53.9	13128.2 $\pm$ 4657.3
Data	373.0 $\pm$ 62.2	1231.0 $\pm$ 112.7	1845.0 $\pm$ 138.4	2209.0 $\pm$ 149.7	2124.0 $\pm$ 147.1	1668.0 $\pm$ 129.1	1196.0 $\pm$ 109.7	871.0 $\pm$ 92.7	581.0 $\pm$ 75.9	382.0 $\pm$ 60.5	271.0 $\pm$ 51.4	160.0 $\pm$ 38.9	217.0 $\pm$ 45.1	13128.0 $\pm$ 1213.5

Table 16: Fit results for the  $p_T^W$  variable at a centre-of-mass energy of 7 TeV (electron channel).

Process	0--27 GeV	27--52 GeV	52--78 GeV	78--105 GeV	105--134 GeV	134--166 GeV	166--200 GeV	200--237 GeV	$\geq 237$ GeV	Total
t̄t in	953.3 $\pm$ 26.1	2154.4 $\pm$ 35.1	2795.8 $\pm$ 45.6	2627.8 $\pm$ 40.9	2064.5 $\pm$ 37.0	1379.7 $\pm$ 34.1	782.2 $\pm$ 22.0	432.5 $\pm$ 15.5	421.4 $\pm$ 14.8	13611.5 $\pm$ 271.0
t̄t fit	809.7 $\pm$ 61.0	2143.5 $\pm$ 120.7	2486.6 $\pm$ 138.6	2363.0 $\pm$ 124.9	1712.6 $\pm$ 93.0	1103.7 $\pm$ 72.4	531.7 $\pm$ 48.9	287.0 $\pm$ 31.9	274.8 $\pm$ 26.0	11712.7 $\pm$ 717.2
Single-Top in	29.5 $\pm$ 4.0	67.8 $\pm$ 6.1	81.2 $\pm$ 6.8	78.6 $\pm$ 6.4	61.4 $\pm$ 5.5	43.0 $\pm$ 4.6	26.5 $\pm$ 3.3	16.8 $\pm$ 2.6	21.8 $\pm$ 2.8	426.7 $\pm$ 42.2
Single-Top fit	13.0 $\pm$ 92.2	40.0 $\pm$ 138.3	180.0 $\pm$ 200.0	193.1 $\pm$ 144.4	190.6 $\pm$ 106.8	104.9 $\pm$ 78.5	117.5 $\pm$ 52.1	98.1 $\pm$ 30.3	96.2 $\pm$ 24.2	1033.2 $\pm$ 866.8
W/Z + jets in	27.2 $\pm$ 2.0	74.7 $\pm$ 5.4	88.6 $\pm$ 6.4	67.2 $\pm$ 4.8	48.3 $\pm$ 3.5	34.4 $\pm$ 2.5	22.7 $\pm$ 1.6	14.3 $\pm$ 1.0	18.4 $\pm$ 1.3	395.8 $\pm$ 28.4
W/Z + jets fit	157.3 $\pm$ 48.8	281.5 $\pm$ 78.6	178.5 $\pm$ 166.9	136.9 $\pm$ 80.6	103.8 $\pm$ 67.3	111.4 $\pm$ 50.5	62.8 $\pm$ 32.6	0.0 $\pm$ 5.9	0.0 $\pm$ 16.9	1032.2 $\pm$ 548.2
QCD in	6.4 $\pm$ 0.3	137.1 $\pm$ 6.3	55.7 $\pm$ 2.6	268.6 $\pm$ 12.4	85.6 $\pm$ 4.0	15.9 $\pm$ 0.7	3.2 $\pm$ 0.1	2.2 $\pm$ 0.1	4.0 $\pm$ 0.2	578.7 $\pm$ 26.8
QCD fit	0.0 $\pm$ 22.8	0.0 $\pm$ 35.5	14.0 $\pm$ 54.3	0.0 $\pm$ 11.1	0.0 $\pm$ 17.0	0.0 $\pm$ 29.8	0.0 $\pm$ 62.3	0.0 $\pm$ 6.1	0.0 $\pm$ 6.3	14.0 $\pm$ 245.2
Sum MC in	1016.4 $\pm$ 32.4	2434.0 $\pm$ 52.9	3021.3 $\pm$ 61.3	3042.2 $\pm$ 64.6	2259.8 $\pm$ 49.9	1472.9 $\pm$ 41.9	834.5 $\pm$ 27.1	465.7 $\pm$ 19.3	465.7 $\pm$ 19.1	15012.6 $\pm$ 368.5
Sum MC fit	980.0 $\pm$ 224.7	2465.0 $\pm$ 373.0	2859.0 $\pm$ 559.8	2693.0 $\pm$ 361.0	2007.0 $\pm$ 284.1	1320.0 $\pm$ 231.2	712.0 $\pm$ 196.0	385.0 $\pm$ 74.2	371.0 $\pm$ 73.4	13792.2 $\pm$ 2377.4
Data	980.0 $\pm$ 105.9	2465.0 $\pm$ 168.1	2859.0 $\pm$ 177.5	2693.0 $\pm$ 171.1	2007.0 $\pm$ 147.4	1320.0 $\pm$ 118.8	712.0 $\pm$ 86.4	385.0 $\pm$ 60.3	371.0 $\pm$ 58.5	13792.0 $\pm$ 1094.1

Table 17: Fit results for the  $p_T^W$  variable at a centre-of-mass energy of 7 TeV (muon channel).

Process	0–27 GeV	27–52 GeV	52–78 GeV	78–105 GeV	105–134 GeV	134–166 GeV	166–200 GeV	200–237 GeV	$\geq 237$ GeV	Total
t̄t in	$1130.9 \pm 28.2$	$2502.4 \pm 38.9$	$3118.7 \pm 46.3$	$2853.3 \pm 40.6$	$2229.0 \pm 37.9$	$1487.9 \pm 30.3$	$843.9 \pm 21.4$	$457.4 \pm 16.3$	$430.5 \pm 15.4$	$15054.1 \pm 275.5$
t̄t fit	$856.9 \pm 69.3$	$1948.3 \pm 114.1$	$2660.1 \pm 133.9$	$2129.8 \pm 118.4$	$1717.7 \pm 92.4$	$1070.0 \pm 70.0$	$532.5 \pm 51.0$	$272.3 \pm 31.0$	$273.5 \pm 25.9$	$11461.1 \pm 706.1$
Single-Top in	$34.4 \pm 4.1$	$77.8 \pm 6.4$	$91.7 \pm 6.7$	$85.2 \pm 6.4$	$64.6 \pm 5.4$	$47.0 \pm 4.6$	$28.1 \pm 3.4$	$15.9 \pm 2.5$	$24.1 \pm 2.9$	$468.7 \pm 42.3$
Single-Top fit	$29.7 \pm 83.8$	$274.9 \pm 134.3$	$163.2 \pm 154.4$	$266.4 \pm 141.6$	$82.1 \pm 103.2$	$79.3 \pm 66.8$	$97.6 \pm 49.0$	$40.0 \pm 30.1$	$33.3 \pm 25.3$	$1066.6 \pm 788.4$
W/Z + jets in	$39.6 \pm 2.3$	$74.7 \pm 4.3$	$86.5 \pm 5.0$	$67.2 \pm 3.9$	$52.3 \pm 3.0$	$38.2 \pm 2.2$	$20.1 \pm 1.2$	$13.6 \pm 0.8$	$18.8 \pm 1.1$	$411.1 \pm 23.7$
W/Z + jets fit	$73.5 \pm 89.5$	$45.2 \pm 126.9$	$168.0 \pm 148.9$	$93.7 \pm 85.4$	$94.1 \pm 74.9$	$0.0 \pm 256.8$	$0.0 \pm 18.4$	$0.0 \pm 27.9$	$11.1 \pm 14.9$	$485.8 \pm 843.6$
QCD in	$3.8 \pm 0.2$	$118.4 \pm 4.9$	$64.7 \pm 2.7$	$20.3 \pm 0.8$	$1.1 \pm 0.0$	$16.9 \pm 0.7$	$2.4 \pm 0.1$	$0.1 \pm 0.0$	$0.1 \pm 0.0$	$227.8 \pm 9.5$
QCD fit	$56.9 \pm 68.8$	$13.7 \pm 130.3$	$9.7 \pm 279.4$	$0.0 \pm 67.6$	$0.0 \pm 58.8$	$21.7 \pm 35.9$	$7.9 \pm 14.7$	$4.8 \pm 13.9$	$0.0 \pm 9.0$	$114.7 \pm 678.6$
Sum MC in	$1208.7 \pm 34.7$	$2773.4 \pm 54.6$	$3361.6 \pm 60.7$	$3026.0 \pm 51.7$	$2347.0 \pm 46.4$	$1590.1 \pm 37.8$	$894.5 \pm 26.1$	$486.9 \pm 19.6$	$473.6 \pm 19.4$	$16161.7 \pm 350.9$
Sum MC fit	$1017.0 \pm 311.4$	$2282.0 \pm 505.6$	$3001.1 \pm 716.7$	$2490.0 \pm 413.1$	$1894.0 \pm 329.3$	$1171.0 \pm 429.5$	$638.0 \pm 133.2$	$317.0 \pm 102.9$	$318.0 \pm 75.0$	$13128.1 \pm 3016.7$
Data	$1017.0 \pm 102.8$	$2282.0 \pm 152.9$	$3001.0 \pm 175.6$	$2490.0 \pm 159.4$	$1894.0 \pm 138.0$	$1171.0 \pm 107.1$	$638.0 \pm 78.3$	$317.0 \pm 54.8$	$318.0 \pm 54.2$	$13128.0 \pm 1023.1$

Table 18: Fit results for the  $M_T^W$  variable at a centre-of-mass energy of 7 TeV (electron channel).

Process	0--23 GeV	23--58 GeV	$\geq 58$ GeV	Total
t̄t in	$1740.3 \pm 37.6$	$3872.4 \pm 49.2$	$7998.2 \pm 74.2$	$13610.9 \pm 160.9$
t̄t fit	$1325.8 \pm 86.1$	$3308.5 \pm 143.0$	$7001.2 \pm 215.6$	$11635.5 \pm 444.6$
Single-Top in	$52.6 \pm 5.0$	$127.0 \pm 8.3$	$247.1 \pm 11.3$	$426.7 \pm 24.6$
Single-Top fit	$132.8 \pm 103.3$	$283.0 \pm 170.1$	$514.8 \pm 263.2$	$930.6 \pm 536.7$
W/Z + jets in	$58.8 \pm 4.2$	$120.4 \pm 8.7$	$216.5 \pm 15.6$	$395.7 \pm 28.4$
W/Z + jets fit	$229.7 \pm 122.8$	$359.4 \pm 103.3$	$615.1 \pm 143.9$	$1204.2 \pm 369.9$
QCD in	$123.1 \pm 5.7$	$265.4 \pm 12.3$	$190.2 \pm 8.8$	$578.7 \pm 26.8$
QCD fit	$21.7 \pm 45.5$	$0.0 \pm 22.4$	$0.0 \pm 26.9$	$21.7 \pm 94.8$
Sum MC in	$1974.8 \pm 52.6$	$4385.1 \pm 78.4$	$8652.0 \pm 109.9$	$15011.9 \pm 240.8$
Sum MC fit	$1710.0 \pm 357.7$	$3951.0 \pm 438.8$	$8131.0 \pm 649.6$	$13792.0 \pm 1446.0$
Data	$1710.0 \pm 138.3$	$3951.0 \pm 208.3$	$8131.0 \pm 298.4$	$13792.0 \pm 645.0$

Table 19: Fit results for the  $M_T^W$  variable at a centre-of-mass energy of 7 TeV (muon channel).

Process	0--23 GeV	23--58 GeV	$\geq 58$ GeV	Total
t̄t in	$1940.6 \pm 35.5$	$4383.5 \pm 55.1$	$8730.1 \pm 72.2$	$15054.1 \pm 162.9$
t̄t fit	$1541.4 \pm 93.5$	$3322.8 \pm 134.2$	$6497.9 \pm 211.2$	$11362.2 \pm 438.9$
Single-Top in	$63.0 \pm 5.6$	$137.3 \pm 7.9$	$268.4 \pm 11.3$	$468.7 \pm 24.8$
Single-Top fit	$52.1 \pm 110.4$	$211.5 \pm 162.9$	$927.1 \pm 249.5$	$1190.7 \pm 522.9$
W/Z + jets in	$63.8 \pm 3.7$	$117.1 \pm 6.7$	$230.2 \pm 13.3$	$411.1 \pm 23.7$
W/Z + jets fit	$140.5 \pm 80.8$	$260.7 \pm 113.3$	$81.3 \pm 215.1$	$482.4 \pm 409.2$
QCD in	$71.4 \pm 3.0$	$124.7 \pm 5.2$	$31.6 \pm 1.3$	$227.6 \pm 9.5$
QCD fit	$0.0 \pm 61.8$	$0.0 \pm 42.6$	$92.7 \pm 143.1$	$92.7 \pm 247.5$
Sum MC in	$2138.8 \pm 47.7$	$4762.5 \pm 75.0$	$9260.2 \pm 98.1$	$16161.6 \pm 220.8$
Sum MC fit	$1734.0 \pm 346.5$	$3795.0 \pm 453.1$	$7599.0 \pm 818.9$	$13128.0 \pm 1618.5$
Data	$1734.0 \pm 132.8$	$3795.0 \pm 197.7$	$7599.0 \pm 276.5$	$13128.0 \pm 607.0$

Table 20: Fit results for the  $E_T^{\text{miss}}$  variable at a centre-of-mass energy of 8 TeV (electron channel).

Process	0–27 GeV	27–52 GeV	52–87 GeV	87–130 GeV	130–172 GeV	$\geq 172$ GeV	Total
t̄t in	11376.4 ± 297.0	20214.3 ± 396.8	18747.7 ± 379.6	8522.1 ± 253.1	2651.0 ± 141.2	1610.6 ± 108.8	63122.1 ± 1576.6
t̄t fit	10657.8 ± 301.8	19718.4 ± 376.1	17754.5 ± 371.9	7236.2 ± 208.6	2270.0 ± 94.5	1209.1 ± 57.7	58846.0 ± 1410.7
Single-Top in	468.3 ± 44.6	800.5 ± 58.4	721.4 ± 54.7	350.3 ± 39.2	121.3 ± 21.5	89.0 ± 18.4	2550.9 ± 236.9
Single-Top fit	1002.7 ± 411.4	1079.9 ± 469.8	1847.9 ± 426.6	788.9 ± 220.8	208.5 ± 83.2	140.9 ± 50.7	5068.7 ± 1662.4
W/Z + jets in	403.9 ± 22.2	480.8 ± 26.4	297.0 ± 16.3	109.8 ± 6.0	37.7 ± 2.1	36.1 ± 2.0	1365.4 ± 74.9
W/Z + jets fit	2489.5 ± 371.2	3182.8 ± 268.2	1562.5 ± 231.3	511.2 ± 245.6	21.0 ± 106.1	56.0 ± 29.2	7822.9 ± 1251.6
QCD in	2313.7 ± 54.8	207.9 ± 4.9	33.7 ± 0.8	0.8 ± 0.0	1.0 ± 0.0	0.4 ± 0.0	2557.5 ± 60.6
QCD fit	328.9 ± 149.9	0.0 ± 525.4	0.0 ± 106.3	37.7 ± 99.5	71.6 ± 43.6	0.0 ± 30.3	438.2 ± 955.1
Sum MC in	14562.4 ± 418.6	21703.5 ± 486.5	19799.9 ± 451.4	8983.1 ± 298.4	2811.0 ± 164.8	1736.1 ± 129.3	69596.0 ± 1949.0
Sum MC fit	14478.8 ± 1234.3	23981.1 ± 1639.5	21164.9 ± 1136.1	8574.0 ± 774.5	2571.0 ± 327.4	1406.0 ± 167.9	72175.9 ± 5279.8
Data	14479.0 ± 402.7	23981.0 ± 513.6	21165.0 ± 476.2	8574.0 ± 301.0	2571.0 ± 162.1	1406.0 ± 118.1	72176.0 ± 1973.6

Table 21: Fit results for the  $E_T^{\text{miss}}$  variable at a centre-of-mass energy of 8 TeV (muon channel).

Process	0–27 GeV	27–52 GeV	52–87 GeV	87–130 GeV	130–172 GeV	$\geq 172$ GeV	Total
t̄t in	13151.4 ± 318.0	23766.9 ± 427.9	22661.0 ± 416.0	10216.3 ± 278.5	3116.0 ± 152.7	1906.0 ± 117.0	74817.6 ± 1710.2
t̄t fit	12369.1 ± 333.2	22460.8 ± 421.1	20868.1 ± 395.2	9137.2 ± 221.6	2672.1 ± 99.5	1302.9 ± 66.2	68810.3 ± 1536.8
Single-Top in	531.7 ± 47.3	877.6 ± 60.1	878.7 ± 60.4	414.0 ± 41.7	161.9 ± 26.3	120.2 ± 22.7	2984.1 ± 258.4
Single-Top fit	478.2 ± 436.3	1696.9 ± 537.7	1554.6 ± 476.6	622.1 ± 253.5	131.7 ± 92.1	244.3 ± 60.5	4727.8 ± 1856.8
W/Z + jets in	393.0 ± 19.6	547.7 ± 27.4	365.4 ± 18.3	140.5 ± 7.0	62.9 ± 3.1	40.1 ± 2.0	1549.5 ± 77.5
W/Z + jets fit	2096.8 ± 223.8	2340.3 ± 290.4	2013.3 ± 270.5	757.7 ± 169.8	225.2 ± 71.7	75.8 ± 38.2	7509.0 ± 1064.5
QCD in	423.6 ± 5.8	43.0 ± 0.6	14.3 ± 0.2	0.1 ± 0.0	0.5 ± 0.0	0.1 ± 0.0	481.6 ± 6.5
QCD fit	0.0 ± 1497.3	0.1 ± 107.3	0.0 ± 84.4	0.0 ± 211.7	0.0 ± 56.1	0.0 ± 53.4	0.2 ± 2010.1
Sum MC in	14499.7 ± 390.7	25235.3 ± 516.0	23919.3 ± 494.8	10770.9 ± 327.3	3341.4 ± 182.1	2066.3 ± 141.7	79832.9 ± 2052.6
Sum MC fit	14944.1 ± 2490.7	26498.0 ± 1356.6	24436.0 ± 1226.7	10517.0 ± 856.5	3029.0 ± 319.5	1623.0 ± 218.3	81047.2 ± 6468.2
Data	14944.0 ± 392.0	26498.0 ± 520.6	24436.0 ± 499.9	10517.0 ± 325.7	3029.0 ± 174.3	1623.0 ± 125.6	81047.0 ± 2038.2

Table 22: Fit results for the  $H_T$  variable at a centre-of-mass energy of 8 TeV (electron channel).

Process	120–185 GeV	185–215 GeV	215–247 GeV	247–283 GeV	283–323 GeV	323–365 GeV	365–409 GeV	409–458 GeV	458–512 GeV	512–570 GeV	570–629 GeV	629–691 GeV	691–769 GeV	$\geq 769$ GeV	Total
t̄t in	936.8 ± 86.2	3250.2 ± 158.9	6449.2 ± 225.1	8761.8 ± 260.0	9375.4 ± 268.8	8356.3 ± 253.2	6823.8 ± 229.7	5639.2 ± 206.7	4257.9 ± 180.4	2891.6 ± 148.2	2047.8 ± 124.5	1427.6 ± 104.1	1117.7 ± 91.0	1787.0 ± 115.2	63122.1 ± 2452.0
t̄t fit	1104.7 ± 33.5	2984.4 ± 171.0	6508.9 ± 224.9	9461.3 ± 141.7	9319.4 ± 222.7	7879.2 ± 171.6	6106.2 ± 177.1	5140.9 ± 140.1	4028.1 ± 123.4	2790.7 ± 115.6	1769.2 ± 76.8	1299.1 ± 56.7	901.0 ± 46.2	1399.2 ± 70.7	60692.3 ± 1772.1
Single-Top in	68.8 ± 17.1	182.2 ± 28.0	259.3 ± 33.1	351.0 ± 38.6	353.3 ± 38.3	310.6 ± 36.4	265.2 ± 33.5	213.8 ± 29.8	166.3 ± 26.1	124.6 ± 23.1	80.1 ± 18.0	51.1 ± 13.9	46.1 ± 12.9	78.5 ± 17.7	2550.9 ± 366.6
Single-Top fit	0.0 ± 134.8	563.2 ± 214.8	506.8 ± 264.6	0.0 ± 995.3	551.7 ± 296.1	1061.3 ± 240.6	1274.5 ± 196.5	571.6 ± 140.2	411.6 ± 115.6	287.0 ± 112.2	262.6 ± 69.6	50.8 ± 50.1	84.0 ± 39.6	133.0 ± 62.9	5758.0 ± 2932.8
W/Z + jets in	91.0 ± 5.0	119.0 ± 6.5	158.5 ± 8.7	191.5 ± 10.5	159.7 ± 8.8	142.8 ± 7.8	116.6 ± 6.4	106.4 ± 5.8	82.8 ± 4.5	59.7 ± 3.3	38.1 ± 2.1	34.3 ± 1.9	24.2 ± 1.3	40.7 ± 2.2	1365.4 ± 74.9
W/Z + jets fit	0.0 ± 132.4	213.9 ± 134.6	405.3 ± 188.3	959.2 ± 180.6	1128.1 ± 273.9	762.1 ± 280.1	301.7 ± 151.6	447.5 ± 87.5	21.1 ± 189.1	173.1 ± 100.4	74.8 ± 64.3	0.0 ± 123.4	0.0 ± 62.2	58.7 ± 53.2	4545.5 ± 2021.6
QCD in	68.8 ± 1.6	224.8 ± 5.3	1675.7 ± 39.7	214.4 ± 5.1	50.0 ± 1.2	35.1 ± 0.8	52.2 ± 1.2	124.3 ± 2.9	31.9 ± 0.8	11.0 ± 0.3	22.8 ± 0.5	9.7 ± 0.2	18.0 ± 0.4	18.7 ± 0.4	2557.5 ± 60.6
QCD fit	184.3 ± 25.7	264.5 ± 76.5	227.0 ± 103.5	150.5 ± 91.1	85.8 ± 108.0	9.4 ± 276.7	12.5 ± 59.1	0.0 ± 202.7	123.2 ± 65.0	15.2 ± 53.6	3.4 ± 93.4	36.1 ± 14.7	44.0 ± 13.3	24.2 ± 34.9	1180.2 ± 1218.3
Sum MC in	1165.5 ± 109.9	3776.2 ± 198.7	8542.7 ± 306.6	9518.7 ± 314.2	9938.3 ± 317.0	8844.8 ± 298.2	7257.7 ± 270.8	6083.8 ± 245.3	4538.9 ± 211.8	3087.0 ± 174.9	2188.8 ± 145.1	1522.7 ± 120.2	1206.0 ± 105.6	1924.9 ± 135.6	69596.0 ± 2954.0
Sum MC fit	1289.0 ± 326.3	4026.0 ± 597.0	7648.0 ± 781.3	10571.0 ± 1408.7	11085.0 ± 900.7	9712.0 ± 969.1	7695.0 ± 584.2	6160.0 ± 570.6	4584.0 ± 493.1	3266.0 ± 381.9	2110.0 ± 304.1	1386.0 ± 245.0	1029.0 ± 161.4	1615.0 ± 221.7	72176.0 ± 7944.9
Data	1289.0 ± 122.5	4026.0 ± 213.0	7648.0 ± 292.2	10571.0 ± 339.5	11085.0 ± 349.0	9712.0 ± 323.9	7695.0 ± 286.5	6160.0 ± 256.1	4584.0 ± 219.4	3266.0 ± 186.4	2110.0 ± 149.0	1386.0 ± 120.1	1029.0 ± 104.2	1615.0 ± 130.6	72176.0 ± 3092.5

 Table 23: Fit results for the  $H_T$  variable at a centre-of-mass energy of 8 TeV (muon channel).

Process	120–185 GeV	185–215 GeV	215–247 GeV	247–283 GeV	283–323 GeV	323–365 GeV	365–409 GeV	409–458 GeV	458–512 GeV	512–570 GeV	570–629 GeV	629–691 GeV	691–769 GeV	$\geq 769$ GeV	Total
t̄t in	1150.1 ± 94.2	3912.6 ± 173.6	7776.0 ± 243.8	10883.7 ± 289.3	11321.7 ± 295.0	9867.8 ± 274.4	8099.2 ± 249.2	6470.4 ± 221.4	4948.4 ± 193.8	3572.1 ± 164.6	2280.1 ± 131.6	1509.7 ± 106.0	1199.2 ± 95.1	1826.8 ± 116.9	74817.6 ± 2649.0
t̄t fit	1086.6 ± 80.1	3449.5 ± 208.7	7528.7 ± 249.8	10563.5 ± 280.1	10598.9 ± 254.8	9002.1 ± 211.2	7599.3 ± 177.1	5561.2 ± 156.3	4308.3 ± 139.5	2925.7 ± 106.0	1887.3 ± 85.7	1415.0 ± 60.9	940.3 ± 53.4	1415.9 ± 70.4	68282.4 ± 2133.8
Single-Top in	92.3 ± 19.3	196.0 ± 28.2	331.9 ± 37.4	370.9 ± 39.5	417.2 ± 41.9	378.4 ± 39.6	303.9 ± 35.0	251.9 ± 32.4	192.8 ± 28.0	140.0 ± 24.5	99.1 ± 20.4	66.7 ± 16.5	57.1 ± 15.0	85.9 ± 18.4	2984.1 ± 396.1
Single-Top fit	203.4 ± 82.7	884.6 ± 230.6	910.7 ± 318.2	243.1 ± 368.8	1108.2 ± 326.2	1093.1 ± 274.7	563.0 ± 204.7	1099.0 ± 159.8	557.4 ± 138.5	401.8 ± 95.4	219.1 ± 81.8	78.2 ± 52.4	129.9 ± 46.5	147.0 ± 65.4	7638.5 ± 2445.9
W/Z + jets in	96.8 ± 4.8	137.2 ± 6.9	172.4 ± 8.6	189.6 ± 9.5	198.2 ± 9.9	179.1 ± 9.0	141.0 ± 7.0	112.0 ± 5.6	96.6 ± 4.8	65.6 ± 3.3	50.4 ± 2.5	36.2 ± 1.8	26.4 ± 1.3	48.2 ± 2.4	1549.5 ± 77.5
W/Z + jets fit	104.3 ± 85.3	0.0 ± 68.2	359.1 ± 211.6	1205.5 ± 176.4	875.9 ± 175.1	725.9 ± 164.6	561.2 ± 191.6	171.7 ± 93.5	246.3 ± 77.5	163.5 ± 53.7	106.6 ± 38.1	96.3 ± 43.9	56.8 ± 25.2	27.3 ± 56.3	4700.5 ± 1461.0
QCD in	1.0 ± 0.0	408.4 ± 5.7	1.0 ± 0.0	1.7 ± 0.0	1.0 ± 0.0	1.0 ± 0.0	1.0 ± 0.0	12.7 ± 0.2	11.7 ± 0.2	7.5 ± 0.1	14.2 ± 0.2	16.3 ± 0.2	7.7 ± 0.1	1.3 ± 0.0	486.5 ± 6.8
QCD fit	53.7 ± 80.8	231.0 ± 68.3	50.5 ± 149.9	0.0 ± 553.6	0.0 ± 73.0	0.0 ± 145.5	47.5 ± 111.4	0.0 ± 42.4	0.0 ± 48.0	0.0 ± 76.1	0.0 ± 509.2	6.5 ± 25.1	0.0 ± 29.6	36.7 ± 46.2	425.9 ± 1959.0
Sum MC in	1340.2 ± 118.4	4654.2 ± 214.5	8281.4 ± 289.8	11445.8 ± 338.3	11938.1 ± 346.8	10426.3 ± 323.0	8545.1 ± 291.2	6847.0 ± 259.5	5249.6 ± 226.8	3785.1 ± 192.4	2443.7 ± 154.7	1628.9 ± 124.6	1290.4 ± 111.6	1962.1 ± 137.8	79837.8 ± 3129.4
Sum MC fit	1448.0 ± 328.9	4565.0 ± 575.8	8849.0 ± 929.5	12012.1 ± 1378.9	12583.0 ± 829.1	10821.1 ± 796.1	8771.0 ± 684.7	6832.0 ± 452.0	5112.0 ± 403.6	3491.0 ± 331.2	2213.0 ± 714.7	1596.0 ± 182.2	1127.0 ± 154.7	1627.0 ± 238.3	81047.3 ± 7999.7
Data	1448.0 ± 123.2	4565.0 ± 217.3	8849.0 ± 301.6	12012.0 ± 351.4	12583.0 ± 358.7	10821.0 ± 332.3	8771.0 ± 298.7	6832.0 ± 262.3	5112.0 ± 227.2	3491.0 ± 188.2	2213.0 ± 149.1	1596.0 ± 126.2	1127.0 ± 106.7	1627.0 ± 126.2	81047.0 ± 3169.1

Table 24: Fit results for the  $S_T$  variable at a centre-of-mass energy of 8 TeV (electron channel).

Process	146–277 GeV	277–319 GeV	319–361 GeV	361–408 GeV	408–459 GeV	459–514 GeV	514–573 GeV	573–637 GeV	637–705 GeV	705–774 GeV	774–854 GeV	854–940 GeV	$\geq 940$ GeV	Total
t̄t in	963.5 ± 88.0	3882.6 ± 174.3	7352.7 ± 240.3	9659.3 ± 273.7	9678.3 ± 273.4	8473.0 ± 254.4	6742.3 ± 227.2	5139.4 ± 197.6	3618.8 ± 165.6	2544.8 ± 139.2	1824.2 ± 116.6	1213.6 ± 94.1	2029.5 ± 121.5	63122.1 ± 2365.9
t̄t fit	963.8 ± 81.6	3811.9 ± 209.0	7188.8 ± 245.2	10160.7 ± 245.1	9426.5 ± 230.9	7962.6 ± 194.7	6060.0 ± 176.0	4749.3 ± 142.4	3392.6 ± 115.9	2228.0 ± 86.4	1448.3 ± 62.4	906.9 ± 48.7	1588.2 ± 62.0	59887.7 ± 1900.3
Single-Top in	69.1 ± 17.1	186.8 ± 27.8	279.2 ± 34.6	369.1 ± 38.9	357.5 ± 38.7	311.3 ± 36.5	263.6 ± 32.8	216.9 ± 30.3	158.1 ± 26.1	105.5 ± 20.9	80.2 ± 18.2	52.2 ± 14.2	101.4 ± 20.2	2550.9 ± 356.2
Single-Top fit	238.6 ± 89.2	666.4 ± 244.2	915.3 ± 348.8	202.2 ± 343.3	686.3 ± 283.9	1010.5 ± 239.3	968.8 ± 184.5	881.5 ± 145.8	548.0 ± 111.4	207.8 ± 83.8	254.4 ± 57.8	148.3 ± 44.2	192.8 ± 58.0	6921.0 ± 2234.2
W/Z + jets in	101.9 ± 5.6	135.1 ± 7.4	169.1 ± 9.3	191.7 ± 10.5	166.8 ± 9.1	142.9 ± 7.8	117.1 ± 6.4	101.1 ± 5.5	70.9 ± 3.9	45.1 ± 2.5	44.0 ± 2.4	27.7 ± 1.5	52.0 ± 2.9	1365.4 ± 74.9
W/Z + jets fit	9.3 ± 202.4	160.8 ± 147.1	465.8 ± 249.5	1021.7 ± 278.7	1217.2 ± 166.5	690.9 ± 146.1	393.9 ± 156.5	77.3 ± 76.4	0.0 ± 292.3	0.0 ± 128.1	5.7 ± 116.3	49.1 ± 38.7	0.0 ± 38.0	4091.8 ± 2036.6
QCD in	185.5 ± 4.4	1756.0 ± 41.6	235.2 ± 5.6	37.2 ± 0.9	51.9 ± 1.2	39.3 ± 0.9	125.6 ± 3.0	38.3 ± 0.9	17.7 ± 0.4	18.2 ± 0.4	17.6 ± 0.4	19.6 ± 0.5	15.5 ± 0.4	2557.5 ± 60.6
QCD fit	279.2 ± 61.2	313.8 ± 86.1	227.1 ± 108.9	137.4 ± 108.3	0.0 ± 270.7	0.0 ± 172.6	41.2 ± 63.3	0.0 ± 37.2	98.4 ± 29.0	76.2 ± 24.3	36.7 ± 31.1	17.6 ± 25.3	48.0 ± 15.7	1275.7 ± 1033.7
Sum MC in	1319.9 ± 115.1	5960.5 ± 251.1	8036.1 ± 289.7	10257.3 ± 323.9	10254.4 ± 322.4	8966.5 ± 299.7	7248.7 ± 269.5	5495.7 ± 234.4	3865.5 ± 196.0	2713.6 ± 162.9	1966.1 ± 137.6	1313.1 ± 110.3	2198.3 ± 144.9	69596.0 ± 2857.6
Sum MC fit	1491.0 ± 434.4	4953.0 ± 686.4	8797.0 ± 952.4	11522.0 ± 975.3	11330.0 ± 952.0	9664.0 ± 752.7	7463.9 ± 580.4	5708.1 ± 401.8	4039.0 ± 548.7	2512.0 ± 322.6	1745.1 ± 267.6	1122.0 ± 156.9	1829.0 ± 173.6	72176.1 ± 7204.8
Data	1491.0 ± 133.1	4953.0 ± 237.2	8797.0 ± 313.0	11522.0 ± 355.2	11330.0 ± 351.5	9664.0 ± 322.3	7464.0 ± 282.5	5708.0 ± 244.1	4039.0 ± 206.4	2512.0 ± 162.4	1745.0 ± 134.9	1122.0 ± 108.3	1829.0 ± 136.8	72176.0 ± 2987.6

Table 25: Fit results for the  $S_T$  variable at a centre-of-mass energy of 8 TeV (muon channel).

Process	146–277 GeV	277–319 GeV	319–361 GeV	361–408 GeV	408–459 GeV	459–514 GeV	514–573 GeV	573–637 GeV	637–705 GeV	705–774 GeV	774–854 GeV	854–940 GeV	$\geq 940$ GeV	Total
t̄t in	1346.8 ± 103.0	4913.8 ± 194.9	9048.8 ± 264.2	11815.6 ± 301.2	11650.2 ± 299.3	9921.4 ± 275.2	7871.9 ± 245.1	5875.9 ± 210.7	4202.2 ± 177.7	2746.0 ± 143.4	2041.7 ± 123.6	1299.8 ± 99.1	2083.6 ± 123.0	74817.6 ± 2560.3
t̄t fit	1479.5 ± 91.0	4818.1 ± 219.7	8626.5 ± 327.4	11219.1 ± 291.0	10948.2 ± 258.8	9240.2 ± 205.0	7120.4 ± 183.2	5095.0 ± 154.8	3288.8 ± 118.4	2413.4 ± 90.9	1743.6 ± 67.3	1042.3 ± 52.1	1570.4 ± 67.1	68605.5 ± 2126.6
Single-Top in	93.3 ± 19.5	213.9 ± 30.0	351.3 ± 37.9	428.5 ± 42.0	411.7 ± 41.2	364.8 ± 39.1	312.2 ± 36.2	233.4 ± 31.1	179.1 ± 27.2	115.7 ± 21.7	95.6 ± 20.5	69.8 ± 16.7	114.9 ± 21.5	2984.1 ± 384.7
Single-Top fit	215.8 ± 99.3	567.9 ± 273.7	750.6 ± 419.6	948.3 ± 371.2	897.9 ± 327.8	792.7 ± 253.6	911.1 ± 203.8	867.7 ± 159.5	802.8 ± 116.9	155.7 ± 87.0	171.9 ± 64.4	111.3 ± 49.8	156.6 ± 63.4	7350.4 ± 2490.0
W/Z + jets in	106.3 ± 5.3	161.9 ± 8.1	178.5 ± 8.9	212.5 ± 10.6	195.7 ± 9.8	169.4 ± 8.5	140.9 ± 7.0	113.1 ± 5.7	82.8 ± 4.1	60.6 ± 3.0	39.3 ± 2.0	29.9 ± 1.5	58.8 ± 2.9	1549.5 ± 77.5
W/Z + jets fit	92.9 ± 108.9	144.8 ± 145.7	794.8 ± 159.2	856.2 ± 256.2	1039.0 ± 174.2	826.1 ± 164.0	329.5 ± 116.6	89.3 ± 84.1	132.4 ± 58.2	135.9 ± 45.0	30.4 ± 26.1	79.5 ± 24.6	45.3 ± 60.5	4596.1 ± 1423.2
QCD in	408.4 ± 5.6	1.0 ± 0.0	1.7 ± 0.0	1.0 ± 0.0	1.0 ± 0.0	5.4 ± 0.1	12.9 ± 0.2	15.2 ± 0.2	12.5 ± 0.2	16.3 ± 0.2	7.3 ± 0.1	0.4 ± 0.0	1.3 ± 0.0	484.5 ± 6.6
QCD fit	182.8 ± 105.8	156.1 ± 101.6	0.0 ± 169.7	136.3 ± 178.2	0.0 ± 65.9	0.0 ± 61.8	0.0 ± 248.2	0.0 ± 40.0	0.0 ± 74.4	0.0 ± 31.8	0.0 ± 35.1	0.0 ± 135.4	19.7 ± 47.6	495.0 ± 1295.5
Sum MC in	1954.8 ± 133.4	5290.6 ± 233.0	9580.3 ± 311.1	12457.5 ± 353.8	12258.6 ± 350.3	10461.0 ± 322.8	8337.8 ± 288.5	6237.6 ± 247.7	4476.6 ± 209.2	2938.7 ± 168.3	2183.8 ± 146.2	1399.9 ± 117.3	2258.6 ± 147.5	79835.7 ± 3029.1
Sum MC fit	1971.0 ± 405.0	5687.0 ± 740.8	10172.0 ± 1075.8	13160.0 ± 1096.6	12885.0 ± 826.7	10859.0 ± 684.3	8361.0 ± 751.8	6052.0 ± 438.4	4224.0 ± 367.9	2705.0 ± 254.7	1946.0 ± 192.9	1233.0 ± 261.9	1792.0 ± 238.5	81047.1 ± 7335.3
Data	1971.0 ± 144.0	5687.0 ± 243.2	10172.0 ± 324.3	13160.0 ± 367.7	12885.0 ± 363.1	10859.0 ± 332.2	8361.0 ± 290.6	6052.0 ± 246.6	4224.0 ± 206.4	2705.0 ± 165.0	1946.0 ± 138.4	1233.0 ± 110.4	1792.0 ± 131.4	81047.0 ± 3063.1

Table 26: Fit results for the  $p_T^W$  variable at a centre-of-mass energy of 8 TeV (electron channel).

Process	0–27 GeV	27–52 GeV	52–78 GeV	78–105 GeV	105–134 GeV	134–166 GeV	166–200 GeV	200–237 GeV	$\geq 237$ GeV	Total
t̄t in	4089.5 ± 178.7	9543.4 ± 273.9	12426.5 ± 311.1	12045.2 ± 304.2	9702.2 ± 273.3	6739.1 ± 225.5	3946.6 ± 171.4	2289.1 ± 129.4	2340.5 ± 128.6	63122.1 ± 1996.3
t̄t fit	4061.1 ± 176.6	10185.6 ± 278.7	11972.6 ± 300.7	11539.5 ± 303.4	8927.5 ± 241.9	5826.7 ± 181.5	3262.3 ± 123.1	1759.7 ± 77.3	1754.8 ± 61.2	59289.7 ± 1744.2
Single-Top in	143.5 ± 24.5	358.5 ± 38.3	457.7 ± 43.4	434.4 ± 42.9	389.0 ± 40.6	295.3 ± 36.4	183.9 ± 27.3	119.1 ± 22.6	169.5 ± 26.1	2550.9 ± 302.0
Single-Top fit	325.9 ± 179.0	207.9 ± 354.7	934.0 ± 369.6	688.6 ± 360.6	1016.4 ± 261.1	486.9 ± 211.6	396.9 ± 124.1	332.5 ± 78.5	355.0 ± 57.3	4744.1 ± 1996.5
W/Z + jets in	109.8 ± 6.0	240.9 ± 13.2	281.9 ± 15.5	238.1 ± 13.1	179.4 ± 9.8	122.3 ± 6.7	75.1 ± 4.1	46.5 ± 2.6	71.4 ± 3.9	1365.4 ± 74.9
W/Z + jets fit	761.8 ± 171.5	1561.3 ± 296.4	2119.2 ± 301.6	1687.3 ± 281.6	779.1 ± 161.4	663.6 ± 126.0	259.7 ± 135.4	45.6 ± 64.9	0.0 ± 40.1	7877.6 ± 1578.9
QCD in	20.0 ± 0.5	151.0 ± 3.6	1925.7 ± 45.6	340.1 ± 8.1	51.7 ± 1.2	23.0 ± 0.5	16.8 ± 0.4	11.1 ± 0.3	18.0 ± 0.4	2557.5 ± 60.6
QCD fit	18.3 ± 80.9	70.1 ± 109.1	62.2 ± 105.2	35.6 ± 98.3	0.0 ± 1207.4	0.0 ± 74.6	16.0 ± 60.0	23.1 ± 26.7	39.2 ± 17.7	264.6 ± 1780.0
Sum MC in	4362.8 ± 209.8	10293.9 ± 329.0	15091.8 ± 415.6	13057.8 ± 368.2	10322.3 ± 325.0	7179.8 ± 269.1	4222.4 ± 203.2	2465.9 ± 154.8	2599.4 ± 159.1	69596.0 ± 2433.7
Sum MC fit	5167.0 ± 607.9	12025.0 ± 1038.9	15087.9 ± 1077.1	13951.0 ± 1043.9	10723.0 ± 1871.8	6977.1 ± 593.7	3935.0 ± 442.5	2161.0 ± 247.3	2149.0 ± 176.4	72176.1 ± 7099.6
Data	5167.0 ± 241.9	12025.0 ± 365.6	15088.0 ± 408.6	13951.0 ± 389.9	10723.0 ± 337.9	6977.0 ± 271.7	3935.0 ± 201.7	2161.0 ± 147.2	2149.0 ± 144.2	72176.0 ± 2508.7

Table 27: Fit results for the  $p_T^W$  variable at a centre-of-mass energy of 8 TeV (muon channel).

Process	0–27 GeV	27–52 GeV	52–78 GeV	78–105 GeV	105–134 GeV	134–166 GeV	166–200 GeV	200–237 GeV	$\geq 237$ GeV	Total
t̄t in	5340.1 ± 203.7	12050.1 ± 306.7	15101.9 ± 341.3	14152.0 ± 328.7	11151.8 ± 291.0	7532.7 ± 238.4	4360.1 ± 180.8	2488.6 ± 134.5	2640.3 ± 136.2	74817.6 ± 2161.4
t̄t fit	5239.6 ± 182.2	12274.5 ± 332.8	13872.8 ± 351.9	12931.6 ± 326.1	10097.1 ± 252.4	6686.1 ± 201.3	3491.2 ± 117.9	1995.1 ± 78.9	1891.6 ± 69.0	68479.5 ± 1912.4
Single-Top in	199.5 ± 28.1	440.1 ± 42.2	546.9 ± 48.0	530.7 ± 47.0	432.6 ± 42.1	313.3 ± 36.8	189.5 ± 28.2	125.2 ± 23.0	206.4 ± 29.1	2984.1 ± 324.4
Single-Top fit	260.5 ± 194.7	357.9 ± 419.3	1625.0 ± 461.5	1178.4 ± 419.2	560.9 ± 279.0	788.7 ± 248.3	666.4 ± 128.7	143.2 ± 82.8	258.1 ± 67.9	5838.9 ± 2301.5
W/Z + jets in	124.9 ± 6.2	279.3 ± 14.0	321.7 ± 16.1	272.9 ± 13.6	184.8 ± 9.2	153.2 ± 7.7	79.6 ± 4.0	57.9 ± 2.9	75.1 ± 3.8	1549.5 ± 77.5
W/Z + jets fit	598.0 ± 108.5	1342.6 ± 206.9	1550.2 ± 244.2	1320.5 ± 348.1	1113.5 ± 257.2	246.1 ± 230.2	36.9 ± 135.2	163.7 ± 53.8	50.3 ± 36.2	6421.9 ± 1620.2
QCD in	5.7 ± 0.1	424.2 ± 5.8	5.7 ± 0.1	38.9 ± 0.5	0.4 ± 0.0	6.1 ± 0.1	0.5 ± 0.0	0.1 ± 0.0	0.1 ± 0.0	481.6 ± 6.5
QCD fit	0.0 ± 21.3	0.0 ± 125.4	0.0 ± 73.9	61.5 ± 202.0	56.5 ± 170.5	120.2 ± 137.1	68.5 ± 83.5	0.0 ± 14.8	0.0 ± 304.0	306.8 ± 1132.5
Sum MC in	5670.2 ± 238.1	13193.7 ± 368.6	15976.2 ± 405.5	14994.4 ± 389.9	11769.6 ± 342.3	8005.3 ± 282.9	4629.7 ± 213.0	2671.8 ± 160.4	2921.9 ± 169.1	79832.9 ± 2569.9
Sum MC fit	6098.0 ± 506.6	13974.9 ± 1084.4	17048.0 ± 1131.4	15492.0 ± 1295.5	11828.0 ± 959.1	7841.0 ± 816.9	4263.0 ± 465.4	2302.0 ± 230.3	2200.0 ± 477.1	81047.0 ± 6966.7
Data	6098.0 ± 251.0	13975.0 ± 380.4	17048.0 ± 419.8	15492.0 ± 398.0	11828.0 ± 346.0	7841.0 ± 279.4	4263.0 ± 205.4	2302.0 ± 150.2	2200.0 ± 143.1	81047.0 ± 2573.4

Table 28: Fit results for the  $M_T^W$  variable at a centre-of-mass energy of 8 TeV (electron channel).

Process	0--23 GeV	23--58 GeV	$\geq 58$ GeV	Total
t̄t in	$8230.9 \pm 252.4$	$17919.2 \pm 371.6$	$36967.1 \pm 533.1$	$63117.2 \pm 1157.0$
t̄t fit	$7618.7 \pm 204.7$	$16309.1 \pm 335.1$	$35342.5 \pm 546.1$	$59270.3 \pm 1086.0$
Single-Top in	$341.7 \pm 38.8$	$731.6 \pm 55.8$	$1477.7 \pm 78.8$	$2550.9 \pm 173.4$
Single-Top fit	$181.0 \pm 230.8$	$1104.0 \pm 401.3$	$2866.4 \pm 644.5$	$4151.4 \pm 1276.6$
W/Z + jets in	$211.5 \pm 11.6$	$393.0 \pm 21.6$	$760.9 \pm 41.7$	$1365.4 \pm 74.9$
W/Z + jets fit	$1293.1 \pm 259.4$	$2215.7 \pm 347.2$	$4933.1 \pm 332.9$	$8442.0 \pm 939.5$
QCD in	$146.4 \pm 3.5$	$2069.1 \pm 49.0$	$342.0 \pm 8.1$	$2557.5 \pm 60.6$
QCD fit	$76.1 \pm 96.3$	$234.2 \pm 120.6$	$0.1 \pm 178.6$	$310.4 \pm 395.5$
Sum MC in	$8930.5 \pm 306.3$	$21112.8 \pm 497.9$	$39547.7 \pm 661.7$	$69591.0 \pm 1465.9$
Sum MC fit	$9169.0 \pm 791.2$	$19863.0 \pm 1204.2$	$43142.1 \pm 1702.1$	$72174.1 \pm 3697.5$
Data	$9169.0 \pm 316.6$	$19863.0 \pm 465.2$	$43142.0 \pm 684.4$	$72174.0 \pm 1466.2$

Table 29: Fit results for the  $M_T^W$  variable at a centre-of-mass energy of 8 TeV (muon channel).

Process	0--23 GeV	23--58 GeV	$\geq 58$ GeV	Total
t̄t in	$9832.4 \pm 274.7$	$21775.5 \pm 408.9$	$43209.7 \pm 574.0$	$74817.6 \pm 1257.7$
t̄t fit	$8797.8 \pm 239.8$	$20333.9 \pm 378.6$	$40250.1 \pm 543.8$	$69381.8 \pm 1162.1$
Single-Top in	$407.9 \pm 41.6$	$890.3 \pm 61.3$	$1686.0 \pm 83.4$	$2984.1 \pm 186.3$
Single-Top fit	$643.3 \pm 291.4$	$518.2 \pm 461.3$	$2880.2 \pm 684.7$	$4041.6 \pm 1437.4$
W/Z + jets in	$227.7 \pm 11.4$	$473.1 \pm 23.7$	$848.8 \pm 42.4$	$1549.5 \pm 77.5$
W/Z + jets fit	$1277.5 \pm 286.7$	$2661.9 \pm 272.2$	$3617.8 \pm 379.4$	$7557.2 \pm 938.4$
QCD in	$22.3 \pm 0.3$	$458.3 \pm 6.2$	$0.9 \pm 0.0$	$481.5 \pm 6.5$
QCD fit	$66.4 \pm 172.6$	$0.0 \pm 134.9$	$0.1 \pm 69.7$	$66.5 \pm 377.3$
Sum MC in	$10490.2 \pm 328.0$	$23597.2 \pm 500.1$	$45745.4 \pm 699.8$	$79832.7 \pm 1528.0$
Sum MC fit	$10785.0 \pm 990.5$	$23514.0 \pm 1247.0$	$46748.1 \pm 1677.6$	$81047.1 \pm 3915.1$
Data	$10785.0 \pm 333.0$	$23514.0 \pm 491.1$	$46748.0 \pm 689.2$	$81047.0 \pm 1513.3$

# References

- [1] Tim Adye. Unfolding algorithms and tests using RooUnfold. pages 313–318, 2011.
- [2] Andreas Hocker and Vakhtang Kartvelishvili. SVD approach to data unfolding. *Nucl.Instrum.Meth.*, A372:469--481, 1996.